

**Free-flow electrophoresis and impedance  
spectroscopy of small molecular compounds in a  
microfluidic device**

Von der Fakultät für Lebenswissenschaften  
der Universität Leipzig

genehmigte

**DISSERTATION**

zur Erlangung des akademischen Grades

Doctor rerum naturalium

Dr. rer. nat.

vorgelegt von

Master of Science Franziska Dana Zitzmann

geboren am 15.11.1989 in Ilmenau

Dekan: Prof. Dr. Marc Schönwiesner

Gutachter: Prof. Dr. Andrea A. Robitzki

Prof. Dr. Andreas Schober

Tag der Verteidigung: 09. Juli 2021

## **This Thesis is based on the following publications:**

**1. A novel microfluidic microelectrode chip for a significantly enhanced monitoring of NPY-receptor activation in live mode**

Franziska D. Zitzmann\*, Heinz-Georg Jahnke\*, Felix Nitschke, Annette G. Beck-Sickinger, Bernd Abel, Detlev Belder, Andrea A. Robitzki

*Lab on a chip* (2017) 17 (24), S. 4294–4302

**2. Microfluidic Free-Flow Electrophoresis Based Solvent Exchanger for Continuously Operating Lab-on-Chip Applications**

Franziska D. Zitzmann\*, Heinz-Georg Jahnke\*, Ronny Frank, Felix Nitschke, Laura Mauritz, Bernd Abel, Detlev Belder, Andrea A. Robitzki

*Analytical chemistry* (2017) 89 (24), S. 13550–13558

\* shared first authors

# **Panta rhei**

(Altgriechisch: πάντα ῥεῖ , „alles fließt“)

Aphorismus von Heraklit

## Bibliografische Darstellung

Franziska D. Zitzmann

### **Free-flow electrophoresis and impedance spectroscopy of small molecular compounds in a microfluidic device**

Fakultät für Lebenswissenschaften

Universität Leipzig

*Kumulative Dissertation*

131 Seiten, 316 Literaturangaben, 26 Abbildungen, 0 Tabellen

---

The miniaturization of analytical platforms has led to many important developments. Complex laboratory processes on the micro- and nanoscale could be combined in so-called micrototal analysis systems ( $\mu$ TAS) or lab-on-a-chip (LOC) systems. The usage of small dimensions allows the development of parallelized microfluidic devices with high throughput, additionally equipped with integrated analyte detection and process monitoring systems. One of the main challenges of miniaturized devices is the detection method as well as the direct in-line detection of the biological activity of active compounds in a microfluidic system. Non-invasive, label-free, impedimetric analysis of hydrodynamically cultured adherent cell models under microfluidic conditions could be one option for detection in real-time. This thesis aimed to develop a microfluidic module for cell-based detection using electrochemical impedance spectroscopy. Starting from an established static setup, the module was adapted with regard to the optimal electrode configuration for bioelectronic analysis and the realization of cell cultivation in the hydrodynamic system. This resulted in a significant increase of the impedimetric signal for receptor activation in the microfluidic setup. To integrate cell-based impedimetric detection downstream into complex  $\mu$ TAS, a continuously operating module for the separation of organic solvents was additionally developed. Based on the working principle of microfluidic free-flow electrophoresis, the rebuffering into an aqueous buffer system is performed, where the remaining solvent residues have no influence on an adherent cell model in the hydrodynamically cultivated system. The solvent exchanger was further optimized in terms of separation efficiency, reduction of the dilution factor for the compound, and the required supply pumps for an easier integration in LOC. In summary, the developed modules offer a significant contribution to the integration of cell-based, impedimetric inline analysis into complex LOC and  $\mu$ TAS systems.

## Contents

Bibliografische Darstellung .....	I
Contents .....	II
List of Figures.....	VI
Abbreviations.....	VIII
Summary .....	X
Zusammenfassung.....	XV
Aim of the Thesis.....	XX

## Chapter 1

CELL-BASED BIOSENSORS FOR ANALYZING ACTIVE COMPOUNDS, THEIR BASICS AND CONDITIONS FOR MINIATURIZATION AND THE PRINCIPLES OF MINIATURIZED FREE-FLOW ELECTROPHORESIS AS NEW OPPORTUNITIES TO REMOVE SOLVENTS IN CELLULAR DETECTION SYSTEMS.....	1
<b>1.1 Cell-based biosensors for compound analysis using impedance spectroscopy.....</b>	<b>2</b>
1.1.1 Electrochemical impedance spectroscopy.....	3
1.1.2 <i>In vitro</i> microarrays for two-dimensional cell culture and their fabrication techniques.....	5
<b>1.2 Miniaturization of analytical systems.....</b>	<b>9</b>
1.2.1 Physical principles of microfluidic systems and processes .....	10
1.2.2 Methods of manufacturing microfluidic chips.....	13
1.2.3 Cells in microfluidic systems.....	14
1.2.4 Detection methods in microfluidic systems.....	17

<b>1.3 Free-flow electrophoresis as continuous separation technique in microfluidic chip systems .....</b>	<b>20</b>
1.3.1 Theory of electrophoresis .....	21
1.3.2 Common modes of free-flow electrophoresis and their applications .....	24
1.3.3 Fabrication methods, modification approaches and combination techniques for $\mu$ FFE devices .....	27
<b>1.4 Strategy and reference to the thesis project .....</b>	<b>31</b>
<b>1.5 References .....</b>	<b>33</b>

## Chapter 2

A NOVEL MICROFLUIDIC MICROELECTRODE CHIP FOR A SIGNIFICANTLY ENHANCED MONITORING OF NPY-RECEPTOR ACTIVATION IN LIVE MODE .....	54
<b>2.1 Abstract .....</b>	<b>55</b>
<b>2.2 Introduction .....</b>	<b>55</b>
<b>2.3 Materials and Methods .....</b>	<b>56</b>
2.3.1 Fabrication of microelectrode arrays and microfluidic structures .....	56
2.3.2 Cell culture .....	57
2.3.3 Electrochemical impedance spectroscopy .....	57
2.3.4 Finite element method (FEM) simulation .....	58
2.3.5 Statistics .....	58
<b>2.4 Results and Discussion .....</b>	<b>59</b>
2.4.1 Microfluidic systems need optimized microelectrode array design for ..... impedimetric cell monitoring .....	59
2.4.2 FEM simulation based design of an optimized microfluidic MEA .....	61
2.4.3 Impedimetric monitoring of cell attachment under optimized flow conditions .....	64
2.4.4 Microfluidic based cell culturing enhances impedimetric signal for NPY- receptor activation .....	66

---

<b>2.5 Conclusion</b> .....	<b>69</b>
<b>2.6 Acknowledgment</b> .....	<b>70</b>
<b>2.7 References</b> .....	<b>70</b>
<b>2.8 Supplementary Information</b> .....	<b>73</b>
2.8.1 Supplementary Materials and Methods .....	73
2.8.2 Supplementary Figures .....	74
2.8.3 Supplementary Movie.....	78

## **Chapter 3**

---

MICROFLUIDIC FREE-FLOW ELECTROPHORESIS BASED SOLVENT EXCHANGER FOR CONTINUOUSLY OPERATING LAB-ON-CHIP APPLICATIONS.....	79
<b>3.1 Abstract</b> .....	<b>80</b>
<b>3.2 Introduction</b> .....	<b>80</b>
<b>3.3 Experimental Section</b> .....	<b>81</b>
3.3.1 Fabrication of Microfluidic Free-Flow Electrophoresis Chips .....	81
3.3.2 Microfluidic Free-Flow Electrophoresis Device Operation .....	82
3.3.3 Determination of DMSO and Fluorescein Concentration .....	83
3.3.4 Cell Culture and Impedimetric Monitoring.....	83
3.3.5 Finite Element Method (FEM) Simulation .....	84
3.3.6 Software and Statistics.....	84
<b>3.4 Results and Discussion</b> .....	<b>85</b>
3.4.1 Working Principle of the Solvent Exchanger.....	85
3.4.2 Development of the $\mu$ FFE Based Solvent Exchanger Module .....	86
3.4.3 Optimization of the Solvent Removal Performance .....	88
3.4.4 Reduction of $\mu$ -Fluidic Supporting Instrumentation .....	92
3.4.5 Solvent Exchanger Performance for Cell Based Detection Systems.....	93

---

<b>3.5 Conclusions .....</b>	<b>95</b>
<b>3.6 Acknowledgments .....</b>	<b>96</b>
<b>3.7 References .....</b>	<b>96</b>
<b>3.8 Supporting information .....</b>	<b>99</b>

Selbstständigkeitserklärung..... A

Danksagung..... B

Author Contribution Statement I ..... D

Author Contribution Statement II ..... E

Author Contribution Statement III ..... G



## List of Figures

Figure 1-1: Electrochemical impedance spectroscopy for cell-based analysis.....	4
Figure 1-2: Overview of microelectrode array layouts for impedance spectroscopy .....	6
Figure 1-3: Illustration of ' <i>small-volume effects</i> ' in microfluidic cell culture devices.....	15
Figure 1-4: Effects of electroosmotic flow in the microfluidic system .....	22
Figure 1-5: Schematic representation of the FFE separation modes .....	24
Figure 2-1: Microelectrode array based impedimetric monitoring of adherent cells .....	60
Figure 2-2: FEM based optimization of microfluidic microelectrode array .....	62
Figure 2-3: Identification of optimum flow rate and characterization of cells cultured under microfluidic conditions .....	64
Figure 2-4: Enhancement of impedimetric detection for Y1-receptor activation under microfluidic conditions.....	67
Figure 2-5: Analysis of cell morphology and motility . .....	69
Figure S 2.1: Cross-section of FEM simulation derived potential field .....	74
Figure S 2.2: Cross-section of FEM simulation derived current density field.....	75
Figure S 2.3: Influence of the microfluidic structure on the measurement-counter- electrode distance.....	76
Figure S 2.4: Influence of flow rate on shear stress.....	76
Figure S 2.5: Relative impedance trace over time of HEK-Y1 cell cultured under microfluidic conditions.....	77
Figure S 2.6: Influence of the cell height in the microfluidic structure on the impedance magnitude.....	77
Figure S 2.7: Recombinant Y1-receptor expression in HEKA cells under static and microfluidic conditions.....	78
Figure S 2.8: Microscopic images of NPY treated HEK-Y1 cells cultured under microfluidic conditions.....	78
Figure 3-1: Scheme of the solvent exchanger working principle and supporting instrumentation .....	85
Figure 3-2: Quantitative analysis of $\mu$ FFE-based solvent exchange for the model compound fluorescein.....	87

---

Figure 3-3: Optimization of the solvent exchanger module for an enhanced DMSO removal performance and a minimized dilution.....	90
Figure 3-4: Finite element method based simulation of DMSO lateral diffusion .....	91
Figure 3-5: Minimization of supporting instrumentation .....	93
Figure 3-6: Validation of compatibility with cell based downstream applications in a microfluidic setup .....	95
Figure S 3.1: Microelectrode array with integrated microfluidic structures for impedimetric monitoring of cells.....	99
Figure S 3.2: Relative impedance spectra of cells and solvent dilutions.....	100

---

## Abbreviations

$\mu$ TAS	micro Total analysis Systems
$\mu$ FFE	micro free-flow electrophoresis
$\mu$ -fluidic	microfluidic
2D/ 3D	two-dimensional/ three-dimensional
9w42e	nine wells with 42 measurement electrodes each
AC/DC	alternating current/ direct current
CE	counter electrode
CMOS	Complementary metal-oxide-semiconductor
DMEM	Dulbecco's Modified Eagle Medium
DMSO	dimethyl sulfoxide
DNA	deoxyribonucleic acid
doi	digital object identifier system
e.V.	eingetragener Verein
EIS	electrochemical impedance spectroscopy
EOF	electroosmotic flow
ESI	electrospray ionization
FEM	finite element method
FFE	free-flow electrophoresis
FFIEF	free-flow isoelectric focusing
FFSE	free-flow field step electrophoresis
FFZE	free-flow zone electrophoresis
Fig.	figure
FTITP	free-flow isotachopheresis
G <sub>i</sub>	subunit of GPCR
GPCR	G protein-coupled receptor

---

HEK293A	human embryonic kidney 293A cells
HEK-Y1	Y1 expressing HEK293A cells
HPLC	high performance liquid chromatography
IDE	interdigitated electrode
IEF	isoelectric focusing
ITO	indium tin oxide
LOC	lab-on-a-chip
MALDI-TOF	matrix-assisted laser desorption/ionization – time of flight
ME	measurement electrode
MEA	micro electrode array
NPY	neuropeptide Y
opt.	optimized
PDMS	polydimethylsiloxane
PEDOT	poly(3,4-ethylenedioxythiophene)
PEG-DA	poly(ethylene glycol) diacrylate
pI	isoelectric point
pK <sub>a</sub>	acid dissociation constant
SEM	standard error of mean
SiN	silicon nitride
SU-8	photoresist from Microchem
Ti	titanium
TiN	titanium nitride
TPM	3-(Trimethoxysilyl)propyl methacrylate
TPRV1	transient receptor potential cation channel subfamily V member 1
UV	ultraviolet
Y1	neuropeptide Y1

## Summary

The miniaturization of analytical platforms has resulted in many important developments in the past decades and in consequence, it was possible to perform certain studies under hydrodynamic conditions. This rapidly developing field of research combines disciplines such as chemistry, physics, biology, electrical engineering, microsystems technology, medicine, and material sciences and focuses not only on the miniaturization of reactions but also on the combination of complex laboratory processes on the micro and nanoscale. The multidisciplinary field of research is characterized by extraordinary advantages compared to macroscopic systems. The reduced dimensions of miniaturized systems lead to an increase in efficiency, because multiple chemical processes in these systems can be connected seamlessly and many physical-chemical processes are expedited. For example, miniaturization greatly changes parameters of diffusion, which is one of the most important processes in the microfluidic system. In particular, the low sample and reagent consumption makes the miniaturized systems much more economical and sustainable compared to conventional approaches. Due to the reduced dimensions it is possible to develop parallelized microfluidic devices, which additionally feature an integrated detection of the analyte as well as process monitoring with high throughput.

Since the first development of a miniaturized approach, increasing progress has been made with the aim of integrating more complex analysis methods on a chip to form so-called micrototal analysis systems ( $\mu$ TAS) or lab-on-chip (LOC) systems. Although many processes have already been miniaturized, their full potential is far from being realized. In many cases, the analytical and detection method for a specific application has to be developed and highly optimized with regard to sensitivity, compatibility and throughput. One of the greatest challenges in miniaturized devices is the detection process. The generally used absorption measurement method is limited due to the small dimensions in microfluidics, since miniaturization results in a significant reduction of sensitivity. Direct inline detection of the biological activity of active compounds in a microfluidic approach presents an additional challenge.

Every day new chemicals, pesticides, and pharmaceuticals are produced for the growing and ageing population without fully understanding their long-term effects on the human organism. Their risks to physiological and pathological processes in the body can only be identified through long-term and cost-intensive clinical studies. Pharmacological research is limited to animal models or static *in vitro* tests with immortalized cell lines. To increase the success rate of clinical trials and reduce the negative consequences for humans and the environment, efficient and standardized analysis systems for the biological effects of

active substances are required, which simulate the *in vivo* status and are based on human cell lines. One approach is the hydrodynamic cultivation of complex cell models under microfluidic conditions, since the blood flow due to the constant shear stress on the cells can be optimally simulated and the effects of the drugs can be measured more effectively.

To be able to analyze even the smallest changes at the cellular level, high-resolution monitoring in real-time is essential. Non-invasive, label-free electrochemical impedance spectroscopy as a powerful tool for real-time monitoring is ideally suited for this purpose. It has already been widely described for the quantitative analysis of cellular characteristics, changes, and receptor activities in adherent human cells in the static system. The microelectrode array-based bioelectronic analysis technique enables the investigation of capacitive and resistance-related properties of the cell compartments and the identification of complex changes in cellular morphology and structure.

In addition to high-resolution detection, complex, continuously operating systems in LOC devices require possibilities of separation for removing interfering reaction by-products or reaction solvents. One of the first fluidic separation techniques that was miniaturized was the free flow electrophoresis (FFE). The macroscopic method was established as a standard technique in bioanalytics and microbiology for the gentle separation of proteins, peptides, cell organelles, and living cells. Due to its continuous working principle regarding sample introduction, separation and fraction collection, FFE is optimally suitable for integrated  $\mu$ TAS. In addition, the propitious surface-to-volume ratio in microfluidics leads to a better removal of the generated Joule heat during separation, which allows a combination with the sensitive cell-based detection.

The integration of electrochemical impedance spectroscopy in a microfluidic cell culture system for complex human adherent cell models can significantly improve *in vitro* testing of the biological activity of compounds in real-time and obviously facilitate the evaluation of the potential of compounds. Therefore, the aim of this dissertation was to develop a microfluidic module for cell-based detection by impedance spectroscopy. In order to integrate the cell-based detection module downstream into complex  $\mu$ TAS, a further device for the continuous separation of organic solvents was to be developed.

In this context, **chapter 1** is intended to develop an understanding of the relevance of this dissertation and gives background information on developments in the fields of biosensor technology, microfluidics, and continuous on chip analyte separation by free-flow electrophoresis as well as basic manufacturing processes and relevant physical principles.

---

Cell-based biosensors are presented as an innovative method for efficient compound analysis based on electrochemical impedance spectroscopy as an innovative method. The fabrication technique of microelectrode arrays for two-dimensional cell cultures are discussed in detail and a focus will be placed on the diversity of electrode configurations for impedimetric measurements on different human cells. The second section of chapter 1 deals with the miniaturization of analytical systems. Fundamental physical principles, which, compared to macroscopic methods, have a decisive influence on the function of the microfluidic chip. Furthermore, these fundamentals have to be taken into account during the development process and are described and explained. In a short overview proven fabrication methods for microfluidic chips are introduced in the following. The special role of cells in microfluidic platforms are discussed in more detail, explaining the advantages but also the challenges of developing cells in a microfluidic system. Subsequently, the problem of detection in microfluidic systems, which is probably the most challenging part of the development of a  $\mu$ TAS device, is discussed. Free-flow electrophoresis as a continuous separation method in analytical systems is described in detail in the third section of this chapter. In this context, physical principles as preconditions for miniaturization, the four technically different modes of free-flow electrophoresis including their fields of application, and established fabrication methods for free-flow electrophoretic microfluidic chips are presented. At the end of this chapter, the relationship between the presented theory and practice and the following scientific articles are briefly shown.

**Chapter 2** aims to develop a microfluidic microelectrode chip for the cell-based detection of receptor activity in a human cell line using electrochemical impedance spectroscopy. Based on an already described and strongly established microelectrode array consisting of nine individual culture chambers with 42 electrodes each (diameter 100  $\mu$ m) and a semicircular counter electrode, the development of the system is described in detail. The electrode layout of the MEA is adapted from the initial static setup to a microfluidic one. As cellular model HEK293A cells are used, which are already well described for impedimetric monitoring of receptor and ion channel activities. Using FEM based simulations, MEA layout optimization is demonstrated by an optimal distribution of the electric field in the microfluidic structure. Subsequently, the optimization of cell cultivation for the impedimetric monitoring of adherent cells is described in detail, with a focus on the flow rate and the resulting shear stress to supply the cells with the necessary nutrients. The shear stress and time-dependent tests for the distribution of active compounds, each caused by the applied flow rate in the microfluidic structure, are shown by FEM-based analyses.

---

Afterwards the function of the optimized microfluidic chip is tested. First, the simulated analysis spectra for microfluidics, which are actually measured on HEK293A cells, are compared with the static analysis spectra. Furthermore, it is shown how cellular changes in impedimetric analyses can be successfully realized using HEK293A cells expressing Y1 receptors with the developed microfluidic setup. Here the maximum impedimetric signal for receptor activation in the hydrodynamic measurement setup was significantly increased by a factor of 2.8. Finally, in this chapter, detailed studies on cell morphology and motility are presented, which suggest that cultivation under microfluidic conditions could lead to an extended and stabilized cell-electrode interface.

To integrate the solvent-sensitive cell-based detection using electrochemical impedance spectroscopy more effectively as a downstream module in complex integrated lab-on-a-chip systems, a method for the separation of organic solvents was realized. **Chapter 3** presents the development of the micro-fluidic free-flow electrophoresis-based module for solvent exchange for a continuously operating lab-on-a-chip application. At the beginning of the chapter the working principle of the module is explained in detail, which describes the rebuffering of fluorescein dissolved in DMSO into an aqueous buffer as a model system. Subsequently, the detection limits of DMSO determination, the technical design of the module as well as the success of the developed module with regard to quantitative analysis of DMSO separation are presented. To integrate the developed module easier into existing lab-on-a-chip platforms, further optimizations of the module are shown in the following. On the one hand, it is described how the DMSO removal could be increased up to 95 % by reducing the size of the separating bed. On the other hand, it is shown that reducing the separating bed to 0.5 cm results in a significant decrease of the dilution factor of the model substance fluorescein. In a final modification step of the microfluidic module it is considered the reduction of supply pumps with an adapted separating bed layout for better integration does not lead to a significant decrease in DMSO removal. Finally, the compatibility of the developed module for solvent exchange will be tested on HEK293A cells in order to use it for downstream cell-based applications. For this purpose, impedimetric and light microscopic analyses over time are presented, which show the effect of the remaining DMSO residues on cells. These analyses demonstrate the functionality of the developed module.

Finally, this dissertation makes a decisive contribution to the detection methods in microfluidic systems. Using established cell-based detection based on label-free, non-invasive electrochemical impedance spectroscopy, it is possible to analyze the biological



activity of drugs under hydrodynamic culture conditions in real-time. In this context, a resource-saving analysis technique has been developed through the miniaturized approach. Due to the influence of hydrodynamic cultivation, this technique comes much closer to the *in vivo* state than the conventional static setups and increase the detection sensitivity and signal strength. The free-flow electrophoretic based solvent exchanger for the separation of organic solvents is effective method for realization of the inline monitoring of active compounds in cell-based bioanalytical modules. Taken together, the developed modules offer a promising approach for complex LOC and  $\mu$ TAS systems to integrate and combine downstream cell-based detection with other technologies.

## Zusammenfassung

Die Miniaturisierung analytischer Plattformen hat in den vergangenen Jahrzehnten viele bedeutende Entwicklungen hervorgebracht. Erst durch sie konnten überhaupt bestimmte Untersuchungen unter hydrodynamischen Bedingungen stattfinden. Das sich schnell entwickelnde Forschungsfeld verbindet Disziplinen wie Chemie, Physik, Biologie, Elektrotechnik, Mikrosystemtechnik, Medizin und Materialwissenschaften. Außerdem beschäftigt es sich nicht nur mit der Miniaturisierung von Reaktionen, sondern auch mit der Kombination komplexer Laborabläufe im Mikro- bzw. Nanomaßstab. Dieses multidisziplinäre Forschungsgebiet zeichnet sich durch außergewöhnliche Vorteile gegenüber makroskopischen Systemen aus. Die geringeren Dimensionen miniaturisierter Systeme führen zu einer Effizienzsteigerung, da multiple chemische Vorgänge in diesen Systemen nahtlos miteinander verbunden werden können und viele physikalisch-chemische Prozesse beschleunigt werden. Beispielsweise verändert die Miniaturisierung die Parameter der Diffusion, die einer der wichtigsten Prozesse im mikrofluidischen System ist, stark. Insbesondere der geringe Proben- und Reagenzienverbrauch macht die Arbeitsweise der miniaturisierten Systeme wesentlich ökonomischer und nachhaltiger als die herkömmlichen Ansätze. Aufgrund der geringen Dimensionen besteht die Möglichkeit der Entwicklung von parallelisierten mikrofluidischen Geräten, die mit einem hohen Durchsatz zusätzlich über eine integrierte Detektion des Analyten sowie einer Prozessüberwachung verfügen.

Seit der ersten Entwicklung eines miniaturisierten Ansatzes wurden immer größere Fortschritte mit dem Ziel der Integration komplexerer Analysemethoden auf einem Chip zu sogenannten Mikrototalanalysesystemen ( $\mu$ TAS) oder Lab-on-Chip (LOC) Systemen gemacht. Obwohl bereits viele Verfahren miniaturisiert wurden, ist ihr Potential noch längst nicht ausgeschöpft und vielfach muss die analytische Methode und Detektionsart für eine spezifische Anwendung hinsichtlich Sensitivität, Kompatibilität und Durchsatz entwickelt und stark optimiert werden. Eine der Hauptherausforderungen miniaturisierter Geräte liegt in der Detektion. Die sehr universell verbreitete Absorptionmessung kann aufgrund der geringen Dimensionen in der Mikrofluidik nur begrenzt genutzt werden, da die Miniaturisierung eine deutliche Verringerung der Sensitivität zur Folge hat. Die direkte inline-Detektion der biologischen Aktivität von Wirkstoffen in einem mikrofluidischen Ansatz stellt zudem ein Problem dar.

Täglich werden neue Chemikalien, Pestizide und Pharmazeutika für die wachsende und alternde Bevölkerung entwickelt ohne deren Langzeitwirkungen auf den menschlichen Organismus vollständig zu kennen. Erst durch langjährige und kostenintensive klinische

Studien können deren Risiken auf physiologische und pathologische Prozesse im Körper erkannt werden. Die pharmakologische Forschung ist hierbei auf Tiermodelle oder auf statische *in vitro*-Tests mit immortalisierten Zelllinien beschränkt. Um die Erfolgchancen der klinischen Studien zu erhöhen und die negativen Folgen auf Mensch und Umwelt zu reduzieren, bedarf es daher an effizienten und standardisierten Analysesystemen für die biologische Wirkung von Wirkstoffen, die den *in vivo*-Status simulieren und deren Grundlage humane Zelllinien darstellen. Ein Ansatz bietet hierfür die hydrodynamische Kultivierung von komplexen Zellmodellen unter mikrofluidischen Bedingungen, da hierbei der Blutfluss durch den ständig anliegenden Scherstress an den Zellen optimal simuliert werden kann und die Effekte der Wirkstoffe effektiver gemessen werden können.

Um selbst kleinste Veränderungen auf zellulärer Ebene analysieren zu können, ist eine hochauflösende Überwachung in Echtzeit unerlässlich. Die nicht-invasive, markierungsfreie elektrochemische Impedanzspektroskopie als leistungsstarkes Werkzeug für das Echtzeitmonitoring ist dafür bestens geeignet, da sie bereits für die quantitative Analyse von zellulären Charakteristika, Veränderungen und Rezeptoraktivitäten bei adhärenenten humane Zellen im statischen System ausführlich beschrieben ist. Die auf Mikroelektrodenarray-basierte bioelektronische Analysetechnik ermöglicht die Untersuchung von kapazitiven und widerstandsbezogenen Eigenschaften der Zellkompartimente und die Identifizierung von komplexen Änderungen der zellulären Morphologie und Struktur.

Zusätzlich zur hochauflösenden Detektion erfordern komplexe, kontinuierlich arbeitende Systeme in LOC-Geräten Trennmöglichkeiten zur Entfernung störender Reaktionsnebenprodukte oder Reaktionslösungsmittel. Eine der kontinuierlich arbeitenden hydrodynamischen Trenntechniken, die sehr früh miniaturisiert wurde, ist die Freifluss-elektrophorese (FFE). Die makroskopische Variante etablierte sich als Standardtechnik in der Bioanalytik und Mikrobiologie zur schonenden Trennung von Proteine, Peptide, Zellorganellen und lebenden Zellen. Durch ihr kontinuierliches Arbeitsprinzip hinsichtlich Probenaufgabe, Trennung und Fraktionensammlung eignet sie sich optimal für integrierte  $\mu$ TAS. Zusätzlich führt das günstige Oberflächen-zu-Volumen-Verhältnis in der Mikrofluidik zu einer besseren Abführung der entstehenden Jouleschen Wärme während der Trennung, sodass auch eine Kombination mit einer empfindlichen zellbasierten Detektion möglich ist.

Die Integration der elektrochemischen Impedanzspektroskopie in ein mikrofluidisches Zellkultursystem für komplexe humane, adhärenente Zellmodelle kann die *in vitro*-Testung der biologischen Aktivität von Wirkstoffen in Echtzeit deutlich verbessern und die Einschätzung des Potentials von Wirkstoffen deutlich erleichtern. Das Ziel dieser

Dissertation war es daher ein mikrofluidisches Modul für die zellbasierte Detektion mittels Impedanzspektroskopie zu entwickeln. Um die zellbasierte Detektion nachgeschaltet in komplexe  $\mu$ TAS integrieren zu können, sollte zudem ein Modul zur kontinuierlichen Abtrennung organischer Lösungsmittel entwickelt werden.

In **Kapitel 1** wird die Relevanz dieser Dissertation aufgezeigt. Dabei werden zusätzlich Hintergrundinformationen zu hervorgegangenen Entwicklungen in Bereichen der Biosensortechnik, der Mikrofluidik und der Freiflusselektrophorese sowie grundlegende Herstellungsprozesse und relevante physikalische Prinzipien betrachtet. Diesbezüglich erfolgt zunächst die Vorstellung zellbasierte Biosensoren für die effiziente Wirkstoffanalyse basierend auf der elektro-chemischen Impedanzspektroskopie als innovative Methode. Innerhalb der Betrachtung wird auf die Herstellungstechnik der Mikroelektrodenarrays für zweidimensionale Zellkulturen genauer eingegangen und ein Fokus auf die Diversität der Elektrodenkonfigurationen für impedimetrische Messungen an unterschiedlichen humanen Zellen gelegt. Der zweite Abschnitt des Kapitel 1 beschäftigt sich mit der Miniaturisierung von analytischen Systemen. Die Beschreibung und Erklärung physikalischer Grundprinzipien, die verglichen zu makroskopischen Methoden einen entscheidenden Einfluss auf die Funktion des Mikrofluidikchips haben und die bei der Entwicklung berücksichtigt werden müssen, stehen im Fokus. In einem kurzen Überblick erfolgt die Vorstellung erprobter Herstellungsmethoden für Mikrofluidikchips. Weiterhin wird auf die spezielle Rolle von Zellen in Mikrofluidikplattformen näher eingegangen und erläutert, welche Vorteile und Herausforderungen diese in einem abgeschlossenen System bei der Entwicklung mit sich bringen. Anschließend wird die Problematik der Detektion in mikrofluidischen Systemen gezeigt, welche wohl die größte Herausforderung bei der Entwicklung eines  $\mu$ TAS-Gerätes darstellt. Die Freiflusselektrophorese als kontinuierliche Trennmethode in analytischen Systemen wird im dritten Abschnitt dieses Kapitels detailliert beschrieben. Dabei wird auf physikalischen Grundlagen als Voraussetzungen für eine Miniaturisierung, die vier technisch unterschiedlichen Modi der Freiflusselektrophorese inklusive deren Anwendungsgebiete und auf etablierte Herstellungsmethoden für freiflusselektrophoretische Mikrofluidikchips eingegangen. Am Ende des Kapitels wird kurz der Bezug der erörterten Theorie und vorgestellten Praxis zu den nachfolgenden wissenschaftlichen Artikeln aufgezeigt.

**Kapitel 2** hat die Entwicklung eines mikrofluidischen Mikroelektrodenchips für die zellbasierte Detektion der Rezeptoraktivität einer humanen Zelllinie mittels der elektrochemischen Impedanzspektroskopie als Ziel. Ausgehend von einem bereits beschriebenen und stark etablierten Mikroelektrodenarray bestehend aus neun einzelnen Kulturkammern mit je 42 Elektroden (Durchmesser 100  $\mu\text{m}$ ) und einer halbrunden Gegenelektrode wird die Entwicklung des Systems detailliert beschrieben. Dabei erfolgt die Anpassung des Elektrodenlayouts des MEAs aus dem ursprünglichen statischen Setup hin zu einem mikrofluidischen. Als zelluläres Modell werden HEK293A-Zellen, bereits gut beschrieben für impedimetrisches Monitoring von Rezeptor- und Ionenkanalaktivitäten, verwendet. Mit Hilfe von FEM-basierten Simulationen wird durch eine optimale Verteilung des elektrischen Feldes in der mikrofluidischen Struktur die MEA-Layoutoptimierung gezeigt. Anschließend wird die Optimierung der Zellkultivierung für das impedimetrische Monitoring von adhären Zellen detailliert beschrieben, wobei hier für die Versorgung der Zellen mit Nährstoffen Augenmerk auf die Flussrate und dem damit einhergehenden Scherstress gelegt wird. Die Auswirkungen des Scherstress und zeitabhängige Tests zur Wirkstoffverteilung jeweils bedingt durch die angelegte Flussrate in der mikrofluidischen Struktur werden durch FEM-basierte Analysen aufgezeigt. Im Folgenden wird die Funktion des optimierten Mikrofluidikchips getestet. Zunächst werden die simulierten und im Anschluss an HEK293A-Zellen real gemessenen Analysespektren für die Mikrofluidik mit den statischen Analysespektren verglichen. Weiterhin wird gezeigt, wie mit Hilfe von HEK293A-Zellen, welche Y1-Rezeptoren exprimieren, zelluläre Veränderungen in impedimetrischen Analysen mit dem entwickelten mikrofluidischen Setup erfolgreich realisierbar sind. Gezeigt wird hierbei, dass das maximale impedimetrische Signal für die Rezeptoraktivierung im hydrodynamischen Messsetup signifikant um den Faktor 2,8 erhöht war. In diesem Kapitel werden abschließend detaillierte Untersuchungen zur Zellmorphologie und -motilität vorgestellt, die darauf hindeuten, dass die Kultivierung unter mikrofluidischen Bedingungen zu einer verlängerten und stabilisierten Zell-Elektroden-Schnittstelle führt.

Um die lösungsmittelanfällige zellbasierte Detektion mittels elektrochemischer Impedanzspektroskopie effektiver als nachgeschaltetes Modul in komplexen *Lab-on-a-Chip* Systemen integrieren zu können, wurde eine Möglichkeit zur Abtrennung organischer Lösungsmittel realisiert. In **Kapitel 3** wird die Entwicklung des mikrofluidischen Freiflusselektrophorese-basierten Moduls zum Austausch von Lösungsmittel für eine kontinuierlich agierende *Lab-on-a-Chip*-Anwendung vorgestellt. Zu Beginn des Kapitels

wird detailliert das Arbeitsprinzip des Moduls vorgestellt, welches die Umpufferung von Fluoreszein gelöst in DMSO hin in einen wässrigen Puffer als Modellsystem beschreibt. Im Anschluss wird näher auf die Detektionsgrenzen der DMSO-Bestimmung, des technischen Aufbaus des Moduls sowie den Erfolg des entwickelten Moduls hinsichtlich quantitative Analyse der DMSO-Abtrennung eingegangen. Um das entwickelte Modul einfacher in bestehende *Lab-on-a-chip*-Plattformen integrieren zu können, werden nachfolgend weitere Optimierungen des Moduls gezeigt. Zum einen wird beschrieben, wie durch die Reduzierung der Trennbettlänge die DMSO-Entfernung auf bis zu 95 % erhöht werden konnte. Zum anderen wird gezeigt, dass die Verkürzung des Trennbettes auf 0,5 cm eine deutliche Verringerung des Verdünnungsfaktors der Modellsubstanz Fluoreszein zur Folge hat. In einem letzten Modifizierungsschritt des Mikrofluidikmoduls wird gezeigt, dass eine Reduzierung der Versorgungs-pumpen für eine bessere Integrierung mit angepasstem Trennbettlayout zu keiner signifikanten Verschlechterung der DMSO-Abtrennung führt. Abschließend wird die Kompatibilität des entwickelten Moduls zum Austausch von Lösungsmitteln an HEK293A-Zellen getestet, sodass es für nachgeschaltete zellbasierte Anwendungen genutzt werden kann. Hierfür erfolgt die Vorstellung impedimetrischer und lichtmikroskopischer Analysen über die Zeit, die die Wirkung der verbleibenden DMSO-Rückstände auf die Zellen zeigen und somit die Funktionsfähigkeit des entwickelten Moduls demonstrieren.

Schlussendlich liefert diese Dissertation einen entscheidenden Beitrag zu den Detektionsmethoden in mikrofluidischen Systemen. Mit Hilfe der etablierten zellbasierten Detektion basierend auf der markierungsfreien, nicht invasiven elektrochemischen Impedanzspektroskopie ist es möglich die biologische Aktivität von Wirkstoffen unter hydrodynamischen Kulturbedingungen in Echtzeit zu analysieren. Hierbei wurde eine ressourcenschonende Analysetechnik durch den miniaturisierten Ansatz entwickelt, welche durch den Einfluss der hydrodynamischen Kultivierung dem *in vivo*- Zustand deutlich näher kommt als die herkömmlichen statischen Setups und die Nachweisempfindlichkeit sowie Signalstärke erhöht. Der freiflusselektrophoretisch basierende Lösungsmittelaustauscher zur Abtrennung organischer Lösungsmittel ist zudem eine effektive Methode zur Realisierung des *inline*-Monitoring von Wirkstoffen in zellbasierten bioanalytischen Modulen. Zusammengenommen bieten die entwickelten Module einen vielversprechenden Ansatz für komplexe LOC- und  $\mu$ TAS Systeme, um die nachgeschaltete zellbasierte Detektion zu integrieren und mit anderen Modulen zu kombinieren.

## Aim of the Thesis

The aim of the present work was to develop a microfluidic measuring platform for the analysis of the biologic activity of small compounds using human cells as a detection unit. The microfluidic module had to be constructed to enable an optimal integration into microfluidic measuring systems. Electrochemical impedance spectroscopy was used to establish a non-invasive, label-free real-time bioelectronic platform. Therefore, an optimal electrode configuration for the impedimetric measurement of microfluidic analyses including a suitable surface quality for cell-based experiments was determined. The technical engineering was carried out by developing a fabrication process based on a microelectrode array for impedimetric monitoring with microfluidic structures photolithographically made of a polymer for cell cultivation. In parallel, a method for cell cultivation in a microfluidic system using an adherent cell model was established in the cell biological part. Exemplarily for this work the well-characterized and widely applicable cell line HEK293A was used, which is also an excellent transfection model organism. The focus was on optimal culture conditions including practicable flow rates for cell supply, opportunities for cell adhesion, and the reduction of shear stress for a confluent, vital cultivation. To demonstrate the functionality and great advantages of the microfluidic platform, the biological effect of the NPY cell model, which is already well characterized in static experiments, was investigated impedimetrically. By analyzing cell adhesion, the effect of hydrodynamic cultivation was shown.

Synthesis of active compounds is usually only feasible in organic solvents, whereby a direct inline analysis of the biological activity of the active compounds is not possible with the developed cell-based microfluidic detection platform. Residues of organic solvents in active substances can also falsify the analysis of their effect on human cells. To make this possible, an integratable microfluidic module was developed, which efficiently removes organic solvents and performs a rebuffering. The efficiency of the solvent removal was tested on the microfluidic microelectrode chip using impedimetric analysis. The photolithographic process was also used for the fabrication in order to guarantee the integration into a microfluidic platform. The technical challenge for the development was to generate a process that on the one hand allows a continuous separation. On the other hand, it permits an efficient removal even on a small area of the microfluidic chip with a simplified layout that reduced the technical equipment.

# Chapter 1

## Introduction

---

**CELL-BASED BIOSENSORS FOR ANALYZING ACTIVE COMPOUNDS,  
THEIR BASICS AND CONDITIONS FOR MINIATURIZATION AND  
THE PRINCIPLES OF MINIATURIZED FREE-FLOW ELECTROPHORESIS  
AS NEW OPPORTUNITIES TO REMOVE SOLVENTS IN  
CELLULAR DETECTION SYSTEMS**

---

Unpublished.

Franziska D. Zitzmann



## 1.1 Cell-based biosensors for compound analysis using impedance spectroscopy

Since the 1970s, living cells have been used at the interface between biology and electronics as bio-recognition elements in biosensors. Due to the flexibility in the design of biosensors, they allow different sensor strategies and have enabled the emergence of such a diverse range of applications. Advances in the fields of synthetic biology, microfluidics, and lithography have led to many technically complex innovations in cell-based biosensors in recent years.<sup>1</sup>

Depending on the requirements, parameters such as response time, sensitivity, and specificity are decisive for the selection of the type of bioreceptor used in a biosensor. Living cells are an attractive option as a bioreceptor in addition to biomolecules such as enzymes, antibodies, and DNA, because they express a wide variety of molecules in different properties. In this case, they can not only react quantitatively to a specific stimulus, but also react to various analytes. Furthermore, they have already been convincing with a relatively easy and cost-effective production since the first studies and are many times cheaper than purified enzymes and antibodies.<sup>2</sup> Target biomolecules are present in their native environment with their optimal activity and specify against their analytes and this allows for example studies on drug-ligand interactions, effect of bioactive agents or environmental toxicity in a more physiologically relevant way. Cell-based biosensors have developed from pure electrodes to powerful bioelectronic systems that are not only able to detect specific analytes, but can also provide physiologically relevant information even on the single cell level.<sup>3-5</sup> Especially biosensors are used in many fields of study such as cancer research<sup>6, 7</sup>, clinical diagnosis<sup>8, 9</sup>, food safety and food technology<sup>10, 11</sup>, pharmaceutical<sup>1</sup>, and environmental monitoring<sup>12</sup>.

In contrast to simple organisms, more advanced techniques such as light addressable potentiometric sensor (LAPS) or electrochemical impedance spectroscopy (EIS) are preferred as detection method for higher eukaryotic cells.<sup>13</sup> Fluorescence imaging and amperometry are also among the most commonly used techniques.<sup>1, 10, 14</sup> Microelectrode based impedimetric analysis of cells, which was already developed in 1993 for cells by Giaver and Keese using gold interdigital electrodes for monitoring changes in cell density<sup>15</sup>, offers the great advantage of being label-free, noninvasive, and allowing real-time detection capabilities.

However, despite the progress achieved in the development of biosensors, challenges such as faster and more sensitive detection even in high-throughput screening,

regeneration and storability, high interference and high costs due to manufacturing, and accessory instruments need to be addressed. These challenges need to be overcome before the full potential of cell-based biosensors can be realised and they can be used as a complete alternative to living organisms in research. With increasing industrial development and social progress, the number of new chemically synthetically produced active substances will probably also rise in the coming decades and their biological effects will vary in a wide range of ways. Hence, it will be essential to be able to better estimate long-term effects on humans and the environment of active substances and toxins by improving biosensors. Today, cell-based *in vitro* analyses have already become standard methods to reduce animal testing.<sup>16</sup> Now, one of the tasks is to develop biosensors for complex cell systems and, above all, to include further parameters of the *in vivo* state, for example the effect of laminar flow on the detection systems.

### 1.1.1 Electrochemical impedance spectroscopy

Impedance spectroscopy is a suitable real-time detection method for biosensors to determine the biological activity of active substances on living systems like tissue or cell structures.<sup>17-19</sup> The principle of electrochemical impedance spectroscopy (EIS) for the detecting of cells and tissues was first introduced in the 1980s<sup>15</sup> and ever since it has been used in several electrochemical measurement techniques<sup>17, 20-23</sup>. With this method, studies of various cellular effects such as apoptotic morphological changes<sup>24, 25</sup>, detection of receptor activities<sup>17</sup>, degenerative and cytotoxic effects<sup>26-28</sup> or migration of cells<sup>23</sup>, could be carried out label-free and non-invasively.

In general, the EIS measures the time-dependent impedance of a system.<sup>29, 30</sup> The measured impedance indicates the ratio of voltage and current in an AC circuit at the investigated system. The impedance can be described by two parameters. On the one hand, the ratio of the amplitudes of sinusoidal alternating voltage and sinusoidal alternating current and, on the other hand, the difference in phase angle between voltage  $U$  and current  $I$ . By combining the two quantities, impedance can be described as a complex quantity and in the two equations.

$$Z \in \mathbb{C} \quad Z = |Z| \cdot e^{i\varphi} = R + iX \quad (1.1.1)$$

The values  $|Z|$  and  $\varphi$  represent in this case the description of AC in polar coordinates. The impedance is equal to the magnitude  $|Z|$  of  $\underline{Z}$  in the vector diagram. Parameter  $\varphi$  describes the angle between the vector  $\underline{Z}$  and the real axis and is equivalent to the phase shift between current and voltage.

The real part  $R$  describes the part of the impedance without phase shift, the ohmic resistance. The imaginary part  $iX$  is equivalent to the impedance with  $90^\circ$  phase shift, where  $X$  represents the reactance. Ideal ohmic resistances do not have a reactance even in an AC circuit, because there is no phase shift between current and voltage. This is different for capacitors and coils. On an ideal capacitor, the current  $I$  precedes the voltage  $U$  by  $90^\circ$ , on an ideal coil it is the reverse.<sup>30</sup> Therefore, both components have an impedance, which is composed of resistance and reactance. The reactance is frequency-dependent, therefore the impedance spectra of the respective components also show a frequency dependence.

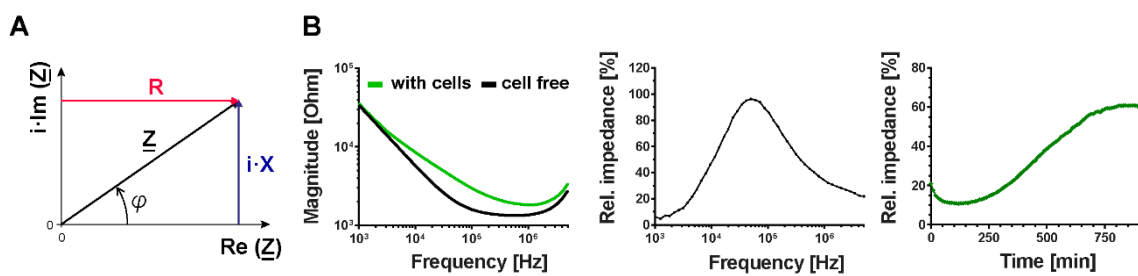


**Figure 1-1: Electrochemical impedance spectroscopy for cell-based analysis.** (A) Impedance  $\underline{Z}$  as a complex value in the vector diagram.  $\underline{Z}$  is a vector in the Gaussian number plane and can be described by the polar coordinates or as the sum of the real ( $R$ ) and imaginary ( $i \cdot X$ ) parts. (B) Data processing of recorded raw impedance data. The impedance magnitude spectra shows the frequency-dependent signals with cells and cell free (left) and the relative impedance results from their difference (middle). The frequency-dependent maximum can be followed in a time trace (right), created according to<sup>29</sup>.

Biological systems, such as cell structures, can be described by equivalent circuit diagrams of ohmic resistance and capacitance components of the alternating current circuit.<sup>31</sup> The cytoplasm of cells or the enclosing medium can be described by an ohmic resistance, while the cell membranes act like capacitors with respect to the isolated lipid bilayer. Charges inside and outside the cell are isolated by a non-conducting, lipophilic layer. This results in the formation of the impedance, which can be shown in an equivalent circuit diagram and can be determined with the help of the complex alternating current calculation. Due to the fact that the impedance of such biological systems contains capacitor-like elements, it is frequency-dependent. The impedance can be influenced by various factors such as temperature, pH value and cell medium. Therefore, in biological impedance spectroscopy measurements of cell-covered electrodes are compared to measurements taken with free electrodes. The resulting difference is plotted against frequency and the frequency is determined where the highest impedance differences occur. The temporal course of the impedance difference between cells and cell-free measuring system is observed at this frequency (Figure 1-1).

Due to its non-invasive and sensitive nature, EIS is particularly suitable for real-time analysis of cells and tissues<sup>17, 23, 32-34</sup> and consequently EIS has a high potential for cellular

microfluidic analysis systems. First studies already demonstrate that impedance spectroscopy offers considerable advantages in microfluidic applications. With the help of EIS, Lee et al. could detect the formation of carbon nanomaterials in a microfluidic platform<sup>35</sup> and Cheng et al. developed a cell detection and counting microfluidic device for cell lysates<sup>36</sup>. A microfluidic application has already been developed for the identification and characterization of cells in suspension.<sup>37</sup> The microfluidic chip was fabricated in glass, equipped with two electrodes for impedance measurement and used the capillary force to get the cell suspension into the micro channels for short analysis. Taken together, a biosensor for the direct impedimetric long-term analysis of two-dimensional adherent cells to detect cellular effects on a microfluidic scale was not previously developed. To overcome this gap, this dissertation focused on the development of a microfluidic module for cell-based detection, for further details see chapters 2 and 3.

### **1.1.2 *In vitro* microarrays for two-dimensional cell culture and their fabrication techniques**

Microelectrode arrays (MEAs) have the great potential as analysis tools, because measurements can be carried out independently on each electrode in the array. As a result, EIS can be used to study changes in cell morphology and structure, electrode-cell coverage and cell-cell and cell-substrate interaction in real-time. In this way, various physiological and pathological phenomena such as proliferation and viability, adhesion, cell cycle, migration and invasion, and cytotoxicity can be analyzed.<sup>38</sup>

Since the 1980s, different types of MEAs for the impedimetric analysis of cells have been developed and various companies offer commercially available MEA-based devices for the analysis of *in vitro* cell systems. Applied BioPhysics supplies different systems in 16, 24 or 96 well format for static impedimetric analyses on 2D cultures. The associated MEAs have either single measuring electrodes with an electrode diameter of 250  $\mu\text{m}$  or interdigital electrodes (IDE).<sup>39</sup> The chip manufacturer ibidi offers various MEAs for flow experiments which are compatible with Applied BioPhysics' measurement system. These MEAs have a maximum number of 8 measuring electrodes distributed in the microfluidic channel with a channel height of 0.66 mm and a total electrode area of 0.49  $\text{mm}^2$ .<sup>40</sup> A further system for static impedimetric analysis is Agilent's RTCAiCELLience™, which is mainly available in 96 well plate format.<sup>41</sup> Roche's® MEA system in 96 well format has one gold microelectrode per well in contrast, which can be used to monitor cell vitality by EIS.<sup>42</sup> The screening platform CardioExcyte 96 from Nanion® is a hybrid system for both extracellular potential and impedance recording of cardiac cells.<sup>43</sup>

An important drawback of all commercially available devices is that they are fully configured systems with limited parameter readout possibilities. Furthermore, they can not be easily integrated and adapted to specially developed microfluidic setups. Most of the systems were mainly developed for static analysis of 2D cultures with a fixed electrode design. To analyze for example small effects of drugs on cells, individual electrode designs with a suitable electrode size and electrode density of the MEAs as well as modified parameters of the monitoring systems are necessary for the real-time analysis of different cell models.

Therefore, different research groups developed adjusted electrode setups to measure specific effects of individual cell systems. Figure 1-2 gives an overview of different designed electrode layouts of MEAs for the impedimetric analysis of various cell models.

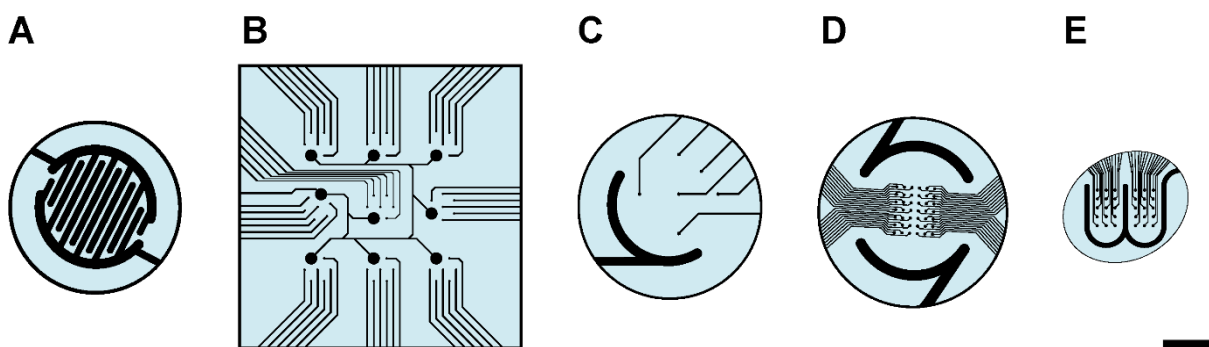


**Figure 1-2: Overview of microelectrode array layouts for impedance spectroscopy.** (A) Interdigitated electrode comprising symmetric fingers (100  $\mu\text{m}$  wide, electrode area 8.6  $\text{mm}^2$ ). (B) Electrode layout for neuronal detection consisting of 54 working and 9 reference electrodes (working electrode diameter: 50 $\mu\text{m}$ ). (C) MEA layout for cardiomyocyte detection (6 working electrodes with diameter: 100 $\mu\text{m}$  and 1 reference electrode). (D) 42-electrode MEA layout for migration analysis of melanoma cells. (E) Electrode layout for microfluidic detection with 30 electrodes and a W-shaped reference electrode (working electrode diameter 100  $\mu\text{m}$ ). Scale bar: 1mm, modified from <sup>22, 23, 34, 45, 46</sup>

Cellular changes of monocultures such as toxic compound effects or receptor activities, which occur over a whole cell layer, can be optimally detected with IDE electrodes. <sup>34, 44</sup> The IDE electrode covers nearly the entire bottom of the measuring area and therefore generates low noise signals (Figure 1-2A). Due to their size IDE electrodes are not designed for the analysis of single cells. In contrast, analyses of neurons and neuronal networks require an electrode layout with many separate electrodes of small size because individual cells can generate different signals (Figure 1-2B). <sup>45</sup> Cardiomyocytes form a strongly connected network, often by the formation of a syncytium. To analyse effects on this cell type with several beating areas, MEAs with less small electrodes distributed over a larger area are appropriate (Figure 1-2C). <sup>46</sup> MEAs with small electrodes that have a high number of electrodes over a small area are particularly suitable for migration studies of

tumor cells to detect even the slightest cell migration (Figure 1-2D).<sup>23</sup> A special electrode layout had to be developed for the impedimetric detection of cells under microfluidic conditions. To compensate the small distance between the cover plates of the micro fluidic MEA, it was shown that the distance between the measuring and the counter electrode (W-shape form electrode, Figure 1-2E) must be very small in contrast to static MEA applications<sup>22</sup>, further details see chapter 2.

However, the more precisely the electrode layout is adapted to the cell model, the more sensitive the biosensor is and even small effects of active substances can be detected. In addition to a special electrode layout adaptation, the development of MEAs in 96 well format for high-throughput applications is currently in focus to be able to perform a large number of analyses simultaneously.<sup>26, 33, 47</sup> The continuous improvement of the MEA technology is a challenge for the measurement hardware, the detection and analysis software, but also for the fabrication techniques of the MEAs.

A common process for the production of MEAs is the lift-off technique, in which metallic microstructures are added additively to surfaces. The size of the producible structures is thereby in the micrometer range. Typical electrode materials used for MEA are platinum<sup>48</sup>, gold<sup>33, 34, 49</sup>, titanium nitride<sup>47</sup>, but also transparent materials such as indium tin oxide (ITO)<sup>50</sup> or PEDOT (poly(3,4-ethylenedioxythiophene))<sup>51</sup>, which have all different impedances due to their material properties. In addition, the impedance of an electrode depends on the electrode area and the layer thickness of the electrode material.<sup>52</sup> Silicon nitride or the resist SU-8 is mainly used to define the free electrode area and to isolate the remaining area (including conductor paths). Especially SU-8 is a widely used material for lab-on-a-chip systems, because processing allows a large variability of layer thicknesses, it is transparent, can be applied by lift-off technique and is biocompatible. Furthermore, SU-8 can be used for plasma post-treatments, which have been shown to increase cell adhesion.<sup>53</sup>

A new method has also been developed besides the classical fabrication methods, in which the electrodes and the passivation layer are in one plane and therefore the surface of the MEA is completely planar.<sup>54</sup> This offers the advantage that a homogeneous contact between the MEA surface and a second layer such as microstructures can be achieved. In order to reduce the impedance of the electrodes, the researchers around Zaid Aqrave used conductive polymers as electrode coatings for neuronal MEAs.<sup>55</sup> Besides reducing the impedance, they were also able to increase the long-term stability of the electrodes. A significantly better resolution in both impedimetric and electrophysiological analyses could be obtained by CMOS-based high-density microelectrode arrays, which have a large

number of electrodes with integrated readout and stimulation circuits compactly integrated on chip.<sup>48, 56</sup> Consequently, these arrays are particularly useful for the analysis of single cells and neurons, where a high electrode density is required on a small area. The method is primarily used for electrophysiological monitoring<sup>56-59</sup>, but can also be applied for impedimetric analyses<sup>56, 60</sup>. Electrodes with very small measuring areas can be fabricated in this process, which results in a good signal-to-noise ratio. However, one disadvantage of the measurement methodology is the very time-consuming and costly chip development, which is comparable to the development of a CPU (central processing unit) and can take at least one to two years. Due to the immense development effort, CMOS-based microelectrode arrays are not designed for small quantities but for large mass production and therefore unsuitable for basic research questions. Electrodes of CMOS-based microelectrodes are limited to the material silicon, resulting in an opaque surface that makes optical detection impossible.

## 1.2 Miniaturization of analytical systems

Miniaturization of systems describes the transfer of as many chemical process steps as possible from laboratory scale to a system with a smaller size. Taking into account the miniaturization of electrical engineering to microelectronics, the term microfluidic systems was introduced. The research field of microfluidics, which includes systems with a width/height scale between 100 nm and 100  $\mu\text{m}$ <sup>61</sup>, is a widely studied area that has its origins in the 1950s with the basic research of today's inkjet technology. Research at that time focused on the precise dosing of small quantities of liquid in the nano- and subnanoliter range.<sup>62</sup> The year 1979 marked a milestone in analytical miniaturization with the development of a gas chromatographic method on a silicon carrier.<sup>63</sup> Manz et al. published the development of the first high-pressure liquid chromatography column in a microfluidic system in 1990.<sup>64</sup> Numerous techniques based on liquid phases have been established since then, with many instruments now able to exceed their classical precursors, as well as the development of new devices that have enabled novel functions and the study of phenomena that were impossible for instruments on a macro scale.

Andreas Manz is regarded as the founder of the research field of micrototal analysis systems ( $\mu\text{TAS}$ ).<sup>65</sup> The term Lab-on-a-Chip (LOC) systems, which have the function of combining and integrating complex laboratory operations on one chip, has also been established as equivalent to this. Many pioneering efforts have been made since the introduction to develop new microfluidic components for fluid transport, fluid metering, fluid mixing, valving, or concentration and separation of molecules within miniaturized quantities of fluids in the last two decades.

Miniaturized synthesis and analysis methods enable, among other things, significantly faster processes, require only a fraction of the resources of macroscopic representatives and have excellent heat transport properties due to the greatly increased surface to volume ratio.<sup>66, 67</sup>

Thanks to their clear benefits, microfluidic systems have found applications in many areas of science and, as mentioned below, have become indispensable in some areas. The small sample volume available makes the devices ideal for use in medical technology, particularly in the health sector for diagnostics and drug research<sup>68</sup>, especially for microfluidic based point-of-care diagnostics<sup>8</sup>. However, miniaturized devices are also successfully used in areas such as basic research, biotechnology, process engineering, sensor technology, drug and pollutant testing, genome, and proteome analysis and metabolism studies, to name only the most important examples.<sup>69-73</sup>



In addition to their advantages, however, miniaturized approaches also have disadvantages and thus present challenges for development. The fabrication and development process is often very complex and associated with increased costs. Capillary forces, surface properties and chemical interactions of the chip materials influence miniaturized systems and must always be taken into account during development. Probably the greatest challenge is the detection due to the smallest volumes in the systems. In this chapter, first, the physical characteristics are examined and afterwards the manufacturing processes, the special aspects of cell cultivation that the system entails and possible detection methods, are discussed.

### 1.2.1 Physical principles of microfluidic systems and processes

To develop miniaturized systems, it is important to understand the physics of fluids on this scale and to understand which physical forces play a crucial role in microfluidics. Substances that continuously deform under the influence of shear forces are defined as fluids. The shear modulus of ideal fluids can be considered to zero. A fluid can be characterized by the three important parameters: density,  $\rho$ , pressure,  $p$  and viscosity,  $\eta$ . Pressure in liquids is only dependent on depth and therefore pressure differences due to different depths can be ignored in planar microsystems with channel depths in the micrometer range. The density is defined as mass per unit volume. Viscosity of a fluid is the resistance of the fluid to shear and describes the internal friction inside the fluid during movement. The coefficient of viscosity can be defined as the ratio of shear stress to shear rate and can be given by the following equation. <sup>74</sup>

$$\eta = \frac{F/A}{v/l} \quad (1.2.1)$$

$F$ - force acting on the liquid surface       $A$  - liquid surface

$v$  - velocity       $l$ - thickness of the liquid films

In case of very thin fluid layers, the velocity curve is linear and liquids that follow this relationship are called Newtonian fluids. They can be described by the Navier-Stokes equations and there is a dependence by laminar flow, temperature, and pressure. <sup>75</sup> In contrast, if there is a dependency between  $\eta$  and  $v$ , the fluids are non-Newtonian fluids. For the development of microfluidic devices, the usage of non-Newtonian fluids has been shown to be more promising, but their behavior is more complex. <sup>74, 75</sup>



The Peclet number, which is a dimensionless value, also provides information on the mass transport of a fluid. In transport processes, this number represents the ratio of advective to diffusive fluxes over a characteristic length. <sup>71</sup>

$$Pe = \frac{v \cdot L}{D} \quad (1.2.4)$$

*D*- diffusion coefficient

As already with the Reynolds number, a reduction in the dimensions of a system leads to a reduction in the Peclet number, which results in simpler, more predictable kinetics. If the Peclet number is much smaller than 1, then diffusion dominates the microfluidic flow. The crucial variable that determines the Peclet number is the channel length. If a microfluidic channel is correspondingly long, the Peclet number is greater than 1 and a directed mass transport occurs in the channel. For the design of a microfluidic system, the Peclet and Reynolds numbers are extremely important because they can be used to simulate hydrodynamic effects and help to find the optimal geometric dimensions of microfluidic layouts. <sup>74</sup>

A further aspect, which clearly differs between the macro and micro scale, is the behavior of a fluid on the surface. The surface tension and interfacial tension are decisive for this. The former describes the affinity of a fluid to keep its interface between surface and air as small as possible in order to reduce its free energy. The interfacial tension describes the same phenomena, but in two immiscible liquids, which is mainly used in the field of droplet microfluidics. <sup>77</sup> Both forces dominate in microfluidic systems, with the result that gravity, unlike in macroscopic systems, has little influence. Only the two forces alone can be used to transport liquids, which makes the use of pumps unnecessary.

The central role in a microfluidic device is given to the microchannels in which all reactions take place. Therefore, the surface properties of the channels have a significant effect on the behavior of the fluids. In a microfluidic channel the capillary force determines the flow of the liquid (1.2.5) and is thus the dominating force in relation to the gravitational force.

$$h = \frac{2 \cdot \sigma \cdot \cos\theta}{\rho \cdot g \cdot r} \quad (1.2.5)$$

*h*- height of a liquid column

$\sigma$ - surface tension

$\theta$ - contact angle

$\rho$ - density

*g*- gravity acceleration

*r*- radius of tube

The capillary force is mainly influenced by the described surface tension of the liquid and by the surface energy of the channel walls. The surface free energy can be easily determined by contact angle measurements. <sup>74, 78</sup>

A final major difference to common devices is the much faster reaction time in microfluidic systems, which offers an enormous advantage and has significantly accelerated the development of  $\mu$ TAS. The reason behind the reduced reaction times is the small size of the systems, which leads to a shorter diffusion time for a given molecule. Equation 1.2.6 shows an approximation for the diffusion time,  $t$ .

$$t \approx \frac{x^2}{2D} \quad (1.2.6)$$

$x$ - distance of travelled by one molecule of solute along one axis after time

$D$ - diffusion coefficient of the solute

The equation demonstrates that the diffusion time is reduced with the decrease of the dimensions of a system, which leads to faster reaction times in microfluidic systems. <sup>71</sup> In summary, the changed physical conditions in microfluidic systems have a significant influence and have to be observed during the development process. However, flow behavior and other parameters within a microfluidic system can be determined much more easily and there are many advantages compared to macroscopic devices.

### 1.2.2 Methods of manufacturing microfluidic chips

The fabrication of microfluidic structures can be performed by different methods. Which method is finally used, depends on the intended chip material, the application, and the quantity. In recent years, the methods for the production of microfluidic chips have developed considerably, resulting in a wide range of materials. For example, glass, silicon, elastomers, plastics, thermosets, and paper can be used. <sup>72</sup>

Flexible microfluidic devices, often used only one time, have the great advantage of being mass produced with simple and cost-effective production tools in a resource-constrained environment. Those are usually made from paper or plastic, have an integrated detection tool, and the user requires minimal skills for their operation. Typical types for their fabrication are cutting or printing processes e.g. wax-printing, screen printing, and inkjet printing. <sup>79</sup>

In contrast, more complex microfluidic devices, e.g. for analytical methods or chemical syntheses, require properties such as thermostability, chemical and pressure resistance,

biocompatibility, and good optical properties for detection. To meet these requirements, microfluidic chips are often fabricated from several technically more complex materials for reusable application. The fabrication processes can be divided into the following three categories and for an overview they are only mentioned or briefly explained in this chapter (1. Molding methods, 2. Ablative methods, 3. Photolithography). Detailed information on specific methods used in this thesis can be found in the corresponding chapters.

Molding methods include soft lithography, hot embossing and injection moulding.<sup>72</sup> PDMS is probably the most common material used in soft lithography to create biocompatible microfluidic structures. Materials such as polymethyl methacrylate (PMMA), cycloolefin polymer (COP) or polytetrafluoroethylene (PTFE) are processed by hot embossing.<sup>80</sup> Thermoplastic polymer chips are made by injection moulding.<sup>81</sup>

Ablative methods comprise the wet-etching of glass or silicon using strong acids such as hydrofluoric acid<sup>82</sup>, sandblasting<sup>83</sup>, laser cutting<sup>84</sup> or milling<sup>83</sup>. Especially glass etching has proven to be an established method of fabrication in the past. Compared to polymer chips, more effort, and higher costs were necessary. Nevertheless, glass offers significant advantages such as thermal and mechanical resistance, significantly better optical properties when using quartz glass, and high chemical stability against common solvents. Thanks to this fabrication process, many methods could be established on a miniaturized scale. In addition to the named advantages, the method requires further technically complex methods such as glass bonding for the fabrication of pure glass chips. Moreover, the process is limited in the depth of the microfluidic structures.

Photolithography is a low-cost and relatively simple method of fabricating microfluidic structures and represents the last category of fabrication processes. Biocompatible photoresists like SU-8, polymers like PEG-DA or other UV- curable materials like NOA (Norland optical adhesive) can be used for photostructuring.<sup>85-88</sup> Using this method, various designs of microfluidic chips can be quickly and easily developed and tested in a research setting.

### **1.2.3 Cells in microfluidic systems**

Since the earliest developments of miniaturized applications, chip systems for cell biological experiments have also been devised, which has become a separate, steadily growing research field in recent years. Especially the cell cultivation in a microfluidic system with the aim to create an *in vivo* like system represents a fundamental change in cell culture technology. The basic methods of cell cultivation have not changed significantly

since their introduction in 1912.<sup>89</sup> The research focused only on the optimization of the cell culture medium and the identification of suitable materials for the cell culture dishes including surface coating. The composition of the cell culture media was modified to prevent contamination with bacteria, molds or yeast and to achieve an optimal expansion, differentiation and de-differentiation of cells.<sup>73</sup> However, the shape of the cell culture dishes and the cell supply have remained almost identical ever since and was only fundamentally changed with the development of microfluidic systems (Figure 1-3).

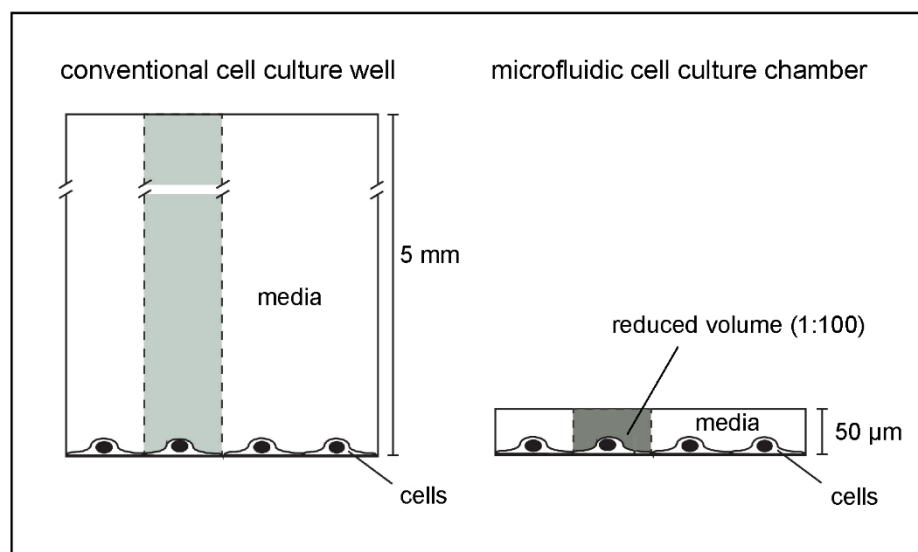


**Figure 1-3: Illustration of 'small-volume effects' in microfluidic cell culture devices.** Smaller culture media volume for a given cell results in faster consumption of nutrients and increased concentration of metabolites or secreted molecules, modified from<sup>73</sup>.

A major advantage of microfluidic cell cultivation is the ability to control the cellular environment on the microscale and control culture parameters such as temperature, pressure and nutrient concentrations.<sup>90, 91</sup> Given the small geometric dimensions in the micro and nanorange, dosing of liquid volumes in the nL-range, pL-range and even in the fL-range is possible. Here, a laminar flow is present.<sup>92</sup> Based on this technology, manipulations and analyses of cells in one cell reservoir can take place simultaneously. In recent years, a large number of studies have been carried out to demonstrate the revolutionary change in cell cultivation with microfluidic systems. The first examples include the control of glucose<sup>93</sup> and oxygen concentrations<sup>94</sup> with the potential to characterize cellular responses of individual cells to these changes. Thus,  $\mu$ TAS provides researchers with tools to study key biological processes caused by the microenvironment, including inter alia cell migration<sup>95, 96</sup>, chemotaxis<sup>97</sup>, adhesion and cell-to-cell signaling<sup>98</sup>. The local microenvironment can be constantly maintained in microchannels, which makes microfluidic systems very easy to mimic the *in vivo* environment. Therefore, researchers

also attempted to make 3D cell cultures in a microfluidic system with cellular confinement in narrow micro-chambers.<sup>99</sup> However, for a well imitated *in vivo* like 3D microarchitecture it was shown that 3D scaffolds are essential and with the controlled fluidic environment dynamic studies on 3D cell cultures are feasible.<sup>100</sup>

Furthermore, the use of microfluidic cell culture devices allows precise control of cell number and density in a given area or volume. It also enables the placement of cells in complex geometries, their monitoring with high spatial and temporal resolution and their individual collection during or after experiments.<sup>73</sup> As a result, a lower number of cells is required compared to macroscopic approaches, as well as a reduced use of cell medium and additives.<sup>101</sup> Moreover, dynamic cultivation offers the enormous advantage that toxic metabolic end products and dead cells are continuously removed from the cell layer and the cells are supplied with fresh nutrients and oxygen.

Microfluidic approaches have a high potential to be automated. Automation offers the opportunity to cultivate, manipulate, monitor, and analyze cells under precisely defined and controlled conditions for several weeks without manual intervention.<sup>92, 102</sup> Thus, dynamic processes can be characterized in short time intervals and an improved efficiency of cell culture by controlling carbon dioxide and oxygen levels, temperature, and cell density has been achieved.<sup>103, 104</sup> The development of new and improved devices has been driven by less consumption of fluids, low sample volumes, rapid incubation times, automation, and more quantitative results.<sup>72, 105-107</sup> Various cell types, adherent and non-adherent cells, have been cultivated in microfluidic systems<sup>70, 90, 108, 109</sup> and have been used in a wide range of applications in recent years. In the following a few examples of applications are shown: Cell culture systems are indispensable tools used in a variety of basic and clinical *in vitro* research studies. In this context, microfluidic platforms have already been successfully established for heterogeneous cell models such as tumor cells<sup>110-112</sup>, cell models that are difficult to cultivate such as stem cells<sup>113-116</sup>, and for many other cell types<sup>117-119</sup>. In the meantime, microfluidic applications have been developed for cell trapping<sup>120, 121</sup>, filtration<sup>122, 123</sup>, cell sorting<sup>124</sup>, detection of biomarkers<sup>125, 126</sup>, drug screening and discovery<sup>127-132</sup>, cryopreservation of cells<sup>133</sup>, cell metabolism<sup>134</sup>, genome-<sup>135</sup>, and proteome studies<sup>136-138</sup>. A recent study shows that even in the development of peptide coatings for bio-implant surfaces, microfluidic flow tests provide more significant results than static tests.<sup>139</sup>

Based on the shown advantages and possible applications, it is not surprising that the field of cells-on-a-chip research has already been further developed to highly complex technologies such as organ-on-a-chip or organism-on-a-chip. The  $\mu$ TAS are becoming

more and more an image of the *in vivo* microenvironments and are already able to model for example the interaction of several organs named organ-on-one-chip<sup>140-144</sup> or in body-on-a-chip applications<sup>145-147</sup>. In addition to the analysis of very heterogeneously composed structures such as tissues, there is also a major development in the analysis of single cells<sup>148-151</sup>, often also using droplet microfluidic based systems<sup>152, 153</sup>. Microfluidic systems will be the future of research, especially in drug screening, but they still need to be optimized with regard to their short lifetime. Admittedly, more and more microfluidic systems are gaining attention when it comes to control of the microenvironment, high throughput systems and integrated functionality. Nevertheless, during the development of such systems, their challenges and limitations must always be kept in mind. Due to their size, the integration of common monitoring systems cannot easily be transferred from macro to micro scale and new methods with a longer planned development time definitely have to be created. Furthermore, the sample volumes of such systems are very small, which limits the use of existing laboratory techniques.

#### 1.2.4 Detection methods in microfluidic systems

One challenge in microfluidic systems is the detection for example of chemical synthesis products with possible residues of educts, chemical reaction processes or cellular effects. Miniaturization primarily describes the reduction of the sample quantity to be analyzed or the available sample volume, which must be sensitively recorded. Detection methods, which are used on a macroscopic laboratory scale, can not easily be miniaturized and the choice of methods is therefore limited.<sup>154</sup> Optical methods such as UV absorption, whose sensitivity depends on the thickness of the layer being irradiated, reach their limits in microfluidic systems.<sup>155</sup> Although there are approaches to increase the sensitivity of this method in  $\mu$ TAS<sup>156, 157</sup>, other detection methods are more convincing and it is thus rarely used in miniaturized systems.

Light microscopic imaging is one of the most popular analytical techniques in microfluidics.<sup>70, 158-160</sup> Fluorescence detection in particular, a light microscope method, is frequently used due to its high sensitivity even with small sample volumes.<sup>161-163</sup> The only condition for this method is the presence of a fluorophore in the analyte. Fluorophores can be divided into intrinsic and extrinsic ones. The former have a natural fluorescence, such as tryptophan with its indole group. Peptides and proteins that contain the amino acid tryptophan therefore fluorescence in the UV wavelength range without external labeling.<sup>164</sup> Extrinsic fluorophores are fluorescent substances that are added to a non-fluorescent sample to make it optically visible. For example, diphenylhexatriene can be



used to stain cell membranes.<sup>165</sup> Xanthenes are an important substance class of fluorophores, which also include fluorescein and rhodamine. Substances of this class have an aromatic system with delocalized electrons and are particularly characterized by a high quantum yield (e.g. structure of Rhodamine B and Fluorescein, see Figure 3-1). The labelling of an analyte with a fluorescent dye can lead to changes in the chemical properties of the analyte. For example, the labeling of proteins or peptides causes a change in the isoelectric point<sup>166, 167</sup>, which must be kept in mind during an electrophoretic separation. Fluorescence, like phosphorescence, is part of luminescence and describes the emission of light by a substance. The basis for both phenomena is described in the Jablonski thermal scheme.<sup>168</sup>

In addition to light spectroscopic methods, a common detection method in LOC systems is the MALDI-TOF as well as the ESI mass spectrometry, which were further developed for detection downstream of electrophoretic separations.<sup>169-172</sup> Electrochemical detection methods, in which the chemical signal is directly converted into an electrical signal by means of simple electrodes, offer another classical method for  $\mu$ TAS.<sup>173, 174</sup> These are based on amperometric<sup>175</sup>, conductometric<sup>176</sup>, or potentiometric methods<sup>177</sup>. However, the disadvantages of this method are the following: Electroactive analytes can be used and the electrodes are exposed to a stronger aging process and consequently have a shorter lifetime.

The already adapted analytical methods for microfluidic systems such as Raman spectroscopy, liquid chromatography, surface plasmon resonance, or mass spectrometry have one important feature in common: They are not able to determine the biological activity of the analytes. At this point, a detection method based on living cell systems is appropriate, because cells as biosensors detect even the smallest concentrations of active substances and react by cellular changes.<sup>17, 34, 178</sup> However, this represents a major challenge in  $\mu$ TAS because, among other things, a defined, site-bound cell growth has to be available. Further details are explained in section 2.4.3 (page 64).

Optical imaging in microscopic systems has been significantly improved by optofluidics and integratable elements for microfluidic platforms have been developed.<sup>143, 162</sup> With plasmonic nanodimers<sup>179</sup> and optical tweezers<sup>121</sup>, extremely high-quality signals could be obtained during cell analyses. Above all, metallic nanodimers represent an optimal instrument for the analysis of a single cell at the subcellular level such as the cell membrane and the cytoplasm. By coupling and probing with an external Raman spectrometer, they can significantly improve the results of vibrational spectroscopy. Being powerful optical sensors, they enable fast and multiparametric analysis of individual

cells.<sup>70, 179</sup> Both optofluidic methods are limited to the treatment and analysis of single living cells, but are not suitable for the analysis of multicellular models or even tissues.

To investigate the biological activity of substances and consequently their effect or toxicity on whole cell groups in two-dimensional cell cultures under fluidic conditions, the impedance spectroscopy offers a suitable method. As already described in section 1.1, it is a very sensitive method that provides compatibility for a miniaturized approach and can theoretically be scaled down. Their advantages of label-free real-time detection are especially important for lab-on-a-chip systems and offer new possibilities, which are described in chapter 3.

### 1.3 Free-flow electrophoresis as continuous separation technique in microfluidic chip systems

Free-flow electrophoresis (FFE) is a method of electrophoretic separation techniques. The analytes in FFE are continuously separated by a perpendicularly applied electric field driven by a pressure of a thin electrolyte flow between two isolating glasses. The sample mixture is injected into the carrier electrolyte flow and with increasing residence time the differently charged components split up and can be collected at different outlets.<sup>180</sup>

In contrast to common types such as gel electrophoresis or capillary electrophoresis, FFE is a matrix-free method of electrophoresis. The quantitative separation of samples is carried out according to charge differences or isoelectric points. The greatest advantage of this method is the unique continuity of the separation compared to HPLC and capillary electrophoresis. Due to the continuous mode of working and the high volume throughput, this technique allows a very fast (semi-)preparative separation with high resolution.<sup>161</sup> During separation the analytes do not interact with carrier or matrix structures, therefore the FFE has a very high recovery rate of about 95%.<sup>181</sup> In addition to the advantage of continuity, FFE is a very gentle separation technique that is carried out under native or denaturing conditions and is therefore particularly attractive for biological samples. Since the development of FFE by Kurt Harting in the 1960s at the Max Planck Institute in Germany<sup>182</sup>, in recent years the method has been continuously improved, further developed and optimized for various applications. Originally, FFE was developed for the gentle purification of amino acids, peptides and proteins and later also for cells, organelles as well as inorganic and organic compounds.<sup>180</sup> Due to its versatility, it is mainly used for sensitive analytes to be fractionated in their native state.

Raymond et al. developed the first miniature scale FFE device ( $\mu$ FFE) in 1994 and achieved a significant reduction of Joule heating with their device while simultaneously detecting the analyte current in real-time on the device.<sup>183</sup> Since the first successful  $\mu$ FFE the optimization of the miniaturized FFE has been continued by improved manufacturing methods and increased performance of the separation. In contrast to their large-scale analogues, microfluidic FFE ( $\mu$ FFE) systems offer new possibilities for very fast separation within several seconds or less and the demand for sample volumes in the microliter range. In addition, they show enhanced separation efficiencies and sensitivities, and a better thermal control with a simpler possibility for automation and portability. Consequently, these  $\mu$ FFE systems have great potential to find applications in lab-on-a-chip devices for real-time monitoring and separation applications.

### 1.3.1 Theory of electrophoresis

All different modes of FFE are based on the principle of electrophoresis, the migration of charged colloidal particles or dissolved molecules in an electric field. The term electrophoresis is derived from the ancient Greek word "electro-", which meant that the method is operated by applying an electrical voltage. The word part "-phor" also comes from ancient Greek and means "to carry". The migration of the particles and thus the separation principle of electrophoresis is founded on the electrophoretic mobility ( $\mu_{ep}$ ) of the analytes and their interaction with the chemical environment. It is mainly determined by the size and charge state of the analytes. Thereby, the accelerating force ( $F_B$ ) is decisive, which has an effect on the charge of the ion or charged particles ( $q$ ). This force can be described as the product of the net charge of the particles ( $z$ ) of the elementary charge in SI-unit Coulomb ( $e$ ) and the applied electric field strength ( $E$ ).

$$F_B = q \cdot E = z \cdot e \quad (1.3.1)$$

The frictional force ( $F_R$ ) counteracts the accelerated force and thus leads to a slow-down of the analytes. This is dependent on the hydrodynamic radius of the particles ( $r$ ), the viscosity of the separation medium ( $\eta$ ), and the migration velocity of the particles ( $v_{ep}$ ) and can be calculated according to Stokes' law.

$$F_R = 6 \cdot \pi \cdot r \cdot \eta \cdot v_{ep} \quad (1.3.2)$$

If the brake and frictional forces are in equilibrium, the ions migrate in the electric field at a constant speed.

$$F_B = F_R \quad (1.3.3)$$

The following equation results by rearranging to  $v_{ep}$ :

$$v_{ep} = \frac{z \cdot e}{6 \cdot \pi \cdot \eta \cdot r} \quad (1.3.4)$$

Electrophoretic mobility ( $\mu_{ep}$ ) of the charged particle in this separation medium results from the combination of all constants depending on the applied electric field ( $E$ ).

$$\mu_{ep} = v_{ep} \cdot E \quad (1.3.5)$$

Equation 1.3.5 demonstrates that smaller ions show higher mobility compared to larger ones as well as multiple charged ions show higher mobility compared to single charged ones. Consequently, neutral analytes such as organic solvents are not deflected by the electric field. <sup>184-186</sup>

Besides electrophoretic mobility, electroosmotic flow (EOF) plays an important role in all electrophoretic separation processes as another electro kinetic factor (Figure 1-4). EOF occurs whenever a voltage is applied to a liquid system in contact with a charged solid surface. This interface phenomenon is explained by the principle of the two-phase system described by Helmholtz and Stern (Figure 1-4).<sup>187-192</sup>

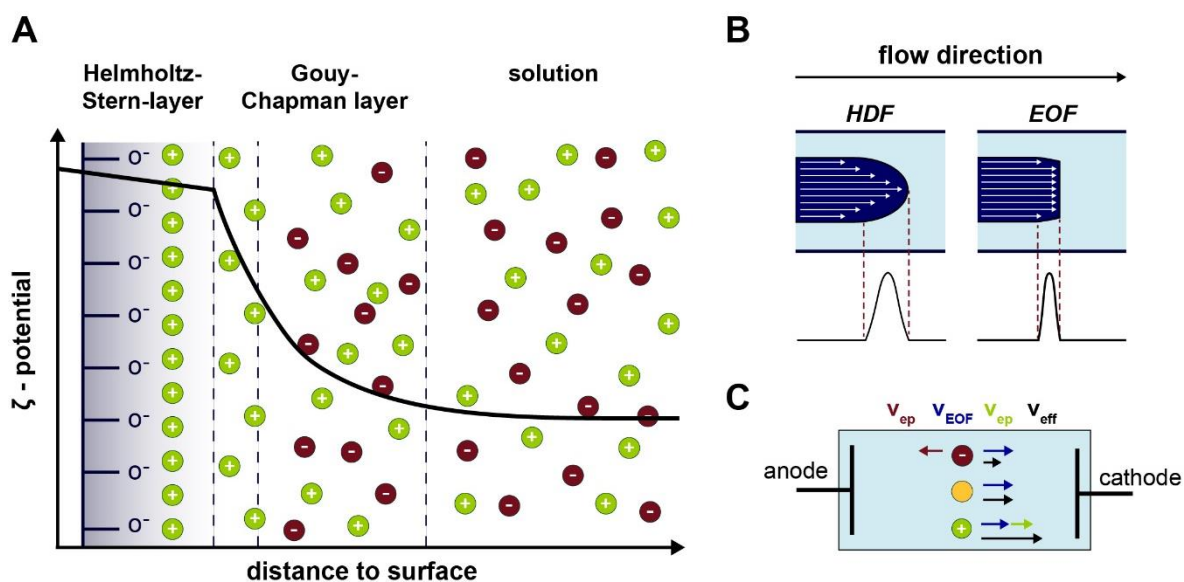


**Figure 1-4: Effects of electroosmotic flow in the microfluidic system.** A: Schematic overview of the electroosmotic flow through the Helmholtz- Stern and Gouy- Chapman double layer formation. The potential in the individual layers is indicated. B: Flow profile with resulting signal width for hydrodynamic flow (HDF) and electroosmotic flow (EOF). C: Overview of the behavior of charged and neutral particles in the electric field, created according to<sup>193</sup>.

Materials like glass and quartz have under dry conditions uncharged silanol groups (SiOH). Due to electrolytic buffer solutions from a pH value of 4, hydrogen ions are split off at the silanol groups and a negatively charged surface layer is formed. As a result, positive charge particles from the aqueous solution are attracted to the surface by electrostatic forces, are captured, and a rigid layer (Helmholtz-Stern-layer) is formed. At a slightly larger distance from this rigid layer, a diffuse double layer consisting of freely moving counterions forms, the so-called Gouy-Chapman layer. Between the two layers there is a potential difference ( $\zeta$ -potential), which is the characteristic parameter of EOF. In the Helmholtz-Stern layer the potential is linear, whereas it decreases exponentially in the Gouy-Chapman layer. As soon as an electric field is applied, the cations of the diffuse layer migrate with their hydrate shell towards the cathode. In this process, the complete solvent molecules are taken along due to hydrogen bridge bonds between the water molecules in the solution, resulting in the formation of a steady flow, the EOF. Depending on the

dielectric constant ( $\varepsilon$ ), the  $\zeta$  -potential, the applied electric field (E) and the viscosity ( $\eta$ ) of the separation medium, the velocity of the EOF ( $v_{EOF}$ ) can be calculated as follows <sup>194, 195</sup>

$$v_{EOF} = \frac{\varepsilon \cdot \zeta \cdot E}{4 \cdot \pi \cdot \eta} \quad (1.3.6)$$

The electroosmotic velocity ( $v_{EOF}$ ) is also proportional to the electroosmotic mobility ( $\mu_{EOF}$ ) and the electric field strength (E) analogous to the electrophoretic velocity.

$$v_{EOF} = \mu_{EOF} \cdot E \quad (1.3.7)$$

In contrast, the potential depends on the surface charge of the material ( $\sigma$ ), the thickness of the diffuse layer ( $\delta$ ) and the dielectric constant ( $\varepsilon_r, \varepsilon_0$ ).

$$\zeta = \frac{4 \cdot \pi \cdot \sigma \cdot \delta}{\varepsilon_0 - \varepsilon_r} \quad (1.3.8)$$

EOF can influence the electrophoretic migration of the ions in such a way that anions are also directed towards the cathode, if the influence of EOF is strong. Especially, the EOF has a positive effect on capillary electrophoresis (CE). The rather hyperbolic flow profile of the laminar flow is a flat flow profile due to the EOF, which leads to a reduction of band widening in the CE (Figure 1-4B).

The EOF is strongly dependent on the pH value of the electrolyte solution, which is caused by the dissociation equilibrium of the silanol groups of the glass surface. At low pH values the silanol groups are mostly protonated and the EOF is very low. With rising pH value and increasing deprotonation, the influence of EOF is increased. In contrast, an increasing concentration of electrolytes and organic solvents leads to a lower EOF. In electrophoretic separation, the migration velocity of the separation medium is included in the total velocity of the analytes due to the effect of the EOF towards the cathode. Due to the sum of the electrophoretic velocity ( $v_{ep}$ ) and the electroosmotic velocity ( $v_{EOF}$ ), cations migrate with a higher total velocity ( $v_{eff}$ ) and thus faster through the electric field. The anions, on the other hand, migrated more slowly, since the EOF counteracts the electrophoretic velocity here. Neutral charged particles (like organic solvents) migrate with the EOF to the cathode. Because EOF has a rather negative effect on FFE, chemical modifications of the glass surface can be applied to suppress or reduce the EOF. In this case, dynamic or permanent coatings of the surface are possible. In dynamic coating, a surface-active substance (e.g. HPMC) is added to the electrolyte solution, which attaches itself to the charged surface in a dynamic equilibrium. <sup>185, 186, 196, 197</sup>

### 1.3.2 Common modes of free-flow electrophoresis and their applications

Recently, four main methods of FFE have been developed, derived from standard capillary electrophoresis modes and applied to micro-scale FFE devices as well. These modes are free-flow zone electrophoresis (FFZE), free-flow isoelectric focusing (FFIEF), free-flow isotachopheresis (FFITP), and free-flow field step electrophoresis (FFFSE, see Figure 1-5). The FFZE was applied in the present study (see Chapter 3, Research Paper II), only this mode will be described in detail in the following. The other three modes are only briefly explained.

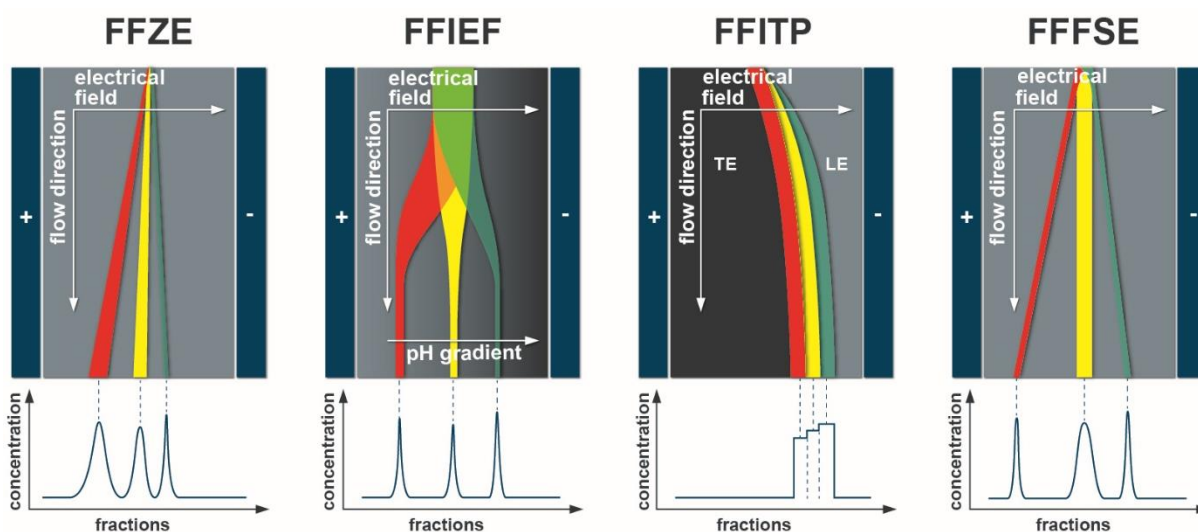


**Figure 1-5: Schematic representation of the FFE separation modes.** FFZE: free-flow zone electrophoresis. FFIEF: free-flow isoelectric focusing. FFIEP: free-flow isotachopheresis, TE: terminating buffer, LE: leading buffer. FFFSE: free-flow field step electrophoresis, created according to <sup>180</sup>.

The first mode is the FFZE, in which a carrier electrolyte flow with a constant composition of pH and electrical conductivity is used. The components are separated according to their mobility. The deflection of the separated analyte is linear at a constant angle, which is determined by the electric field strength, the mobility of the analyte and the flow velocity. The following context applies to the migration distance ( $d$ ) of the analyte moving through the electrical field <sup>183</sup>:

$$d = \mu_p \cdot E_t \quad (1.3.9)$$

$\mu_p$ - apparent electrophoretic mobility

$E$ - electrical field strength

$t$ - residence time of molecules in separation chamber

To achieve high resolution in FFZE, the aim is to focus the analytes into small zones with sharp boundaries. However, several phenomena have a negative influence on the separation quality of the FFZE and a band widening occurs. Negative effects include the width of the injected sample stream, diffuse broadening, hydrodynamic broadening, electrodynamic broadening, Joule heating and electro migration dispersion. <sup>198, 199</sup>

Inside the separation chamber, the parabolic flow profile caused by the pressure-driven flow leads to unequal velocity ranges. The analytes moving close to the external sides of the chip spend more time in the electric field and are therefore more deflected than those moving close to the centre of the chip. This hydrodynamic broadening results in a crescent-shaped deformation of the sample. To reduce this effect considerably, it is recommended to use flatter separation chambers as shown in the following equation. <sup>200</sup>

$$\sigma_{HD}^2 = \frac{h^2 t}{105D} E^2 \mu_p^2 \quad (1.3.10)$$

$\sigma_{HD}^2$ - hydrodynamic broadening

$D$ - analyte diffusion coefficient

$h$ - chamber height

Negative effects on separation and band broadening are of course also caused by EOF inside the separation chamber at FFE, as explained in detail in the previous section.

The electrolyte solution is heated by the electric current inside the FFE chip (Joule heating), whereby a temperature gradient is created between the two cover plates and the maximum is located in the middle. This change in temperature leads to a decrease in viscosity in the center, which has a local effect on the analyte mobility and thus leads to a broadening of the band. Conventional large-scale FFE systems must therefore be actively cooled. But the flat separation regions of  $\mu$ FFE devices favour a fast heat dissipation, which reduces this kind of sample distortion and usually also involves much lower electrical currents. In the past it was shown that  $\mu$ FFE separations can be performed without significant influence of Joule heating at electrical field strengths up to 60 V/mm. <sup>200, 201</sup> Areas with different electrical conductivity in the analyte and the electrolyte lead to an electromigration dispersion. <sup>198, 199</sup> This type of distortion results from different migration rates of the analytes in zones with different electric field strengths. To minimize this effect, the analyte can be dissolved in the same or similar buffer system with corresponding conductivities or, in addition, a lower concentration of the analyte in the same buffer system is chosen. In addition to band broadening, the dilution of the separated compounds is a major disadvantage of the method. In order to improve this, no modification of the FFZE in this aspect is known in the literature up to now. Only a new FFE mode with different



separation conditions, the FFFSE, has been developed, which is briefly explained at the end of the chapter.

FFZE has been used in many publications for separations of fluorescent dyes or fluorescence-labelled molecules.<sup>178, 183, 202</sup> The first FFZE chips developed were already used to separate fluorescently labelled amino acids.<sup>183</sup> Using a PDMS chip developed by Zhang and Manz, fluorescein and rhodamine 110 and labelled amino acids could be separated.<sup>203</sup> Also, in multi-step chip designs such as those of Fonslow et al., fluorescent dyes were used as standard compounds to investigate separation conditions.<sup>200, 203, 204</sup> Kohlheyer et al. also used fluorescent dyes to validate their  $\mu$ FFE chip.<sup>205</sup> The fluorescein and rhodamine B were separated and the current positions within the chip were controlled by changing the flow rates at the buffer inlets.

In the application of the FFZE, three disadvantages have a considerable effect on the separation: Joule Heating, the EOF and the formation of gas bubbles by electrolysis of water at the electrodes. These three phenomena are important in every device development.

Whereas FFZE is often used for the fractionation of particles such as cells and cell organelles, IEF is suitable for the separation of amphoteric compounds such as proteins and peptides. In the FFIEF (Figure 1-5b), the used carrier electrolyte consists of an ampholyte mixture, which leads to the formation of an alinear pH gradient perpendicular to the flow direction at an applied voltage and a natural pH gradient.<sup>206, 207</sup> The FFIEF separates molecules on the basis of their isoelectric point (pI). Components of the analytes migrate within this pH gradient due to the electric field until they reach the point where their pI is equal to the local pH of the buffer, where they become neutrally charged and become focused and concentrated. A great advantage of this method is the high resolution with a fast focusing time. In the literature it has been successfully used in many applications, including miniaturization<sup>208</sup>, especially for peptide and protein separations<sup>201, 206, 209</sup>. The low solubility of the analytes at their pI and the resulting precipitation often leads to a non-ideal and distorted focusing. In addition, ampholyte mixtures usually consist of non-biocompatible substances. Therefore, the method is not suitable as a cell-based detection method. The fact that the ampholytes can have a disturbing effect on subsequent detection methods has already been shown in the literature. For example, they are not suitable for following mass spectrometric techniques and the established pH gradient in the IEF is negative in preserving the biological activity of proteins. To overcome these problems, IEF techniques without carrier ampholytes were developed.<sup>198, 210, 211</sup>

The third mode of FFE is FFITP (Figure 1-5c), in which the sample is introduced into a discontinuous electrolyte system consisting of a leading and a trailing electrolyte. The leading electrolyte is selected to contain ions with a higher mobility than the target analytes, while the trailing electrolyte contains ions with a lower mobility than the target analytes. During separation, the individual components of the analytes arrange themselves according to their descending electrophoretic mobility ( $\mu$ ) and their charge ( $z_i$ ) in adjacent regions at the boundary zone of both electrolytes, forming zones with permanently sharp boundaries next to each other. The concentrations of the different components are readjusted according to the lead ions in order to keep them constant during separation. The principle of this method allows to separate and concentrate certain components of the analyte during the separation process.<sup>212, 213</sup> Isotachopheresis is mainly used to separate and concentrate large amounts of samples and only a few  $\mu$ FFITP applications are available in the literature.<sup>214</sup>

The last type of FFE is the FFFSE (Figure 1-5d), in which a gradient in the electric field is generated by differently concentrated buffer solutions. Highly conductive buffers are used along the sides of the separation area, whereas less conductive buffers are used in the middle of the separation area. The analytes move through the middle zone relatively fast with high electric field strength until they reach the boundary with the high ion buffer concentration and the low electric field strength. This field step leads to a drastic reduction in the electric mobility of the analyte, causing the bands to concentrate and focus.<sup>180, 209</sup>

### **1.3.3 Fabrication methods, modification approaches and combination techniques for $\mu$ FFE devices**

A variety of materials can be used to fabricate  $\mu$ FFE devices, including glass<sup>203-205, 215</sup>, PDMS (poly(dimethylsiloxan))<sup>206, 208, 216, 217</sup>, silicon<sup>183, 218</sup>, plexiglas<sup>219</sup> or polyester films<sup>220</sup>. However, classic materials of  $\mu$ TAS applications are PDMS, glass and silicon. The first  $\mu$ FFE devices were produced using the rigid material silicon, which was compatible with many common micro-processing techniques. However, silicon has a low breakdown voltage, so that the voltage that could be applied to the  $\mu$ FFE devices is limited and other materials replaced silicon as  $\mu$ FFE material.<sup>183, 218</sup>

Glass is likewise a rigid material, but can tolerate much higher voltages.<sup>203, 221</sup> For the production of glass  $\mu$ FFE devices several methods have to be used such as photolithography, wet etching techniques with hydrofluoric acid<sup>222</sup>, thermomechanical

structuring<sup>223</sup> and glass-glass bonding<sup>203, 224</sup>. Metal electrodes can be placed in the FFE devices in this way, among others. However, this is a very significant machine effort: The structuring can only be done from the surface, the structuring of glass often shows a low resolution and it is a very cost-intensive manufacturing method, e.g. due to very pure glass wafers.

Since the production of  $\mu$ FFE devices made of glass is very cost-intensive, a new material has become established in miniaturization devices in recent years, the soft deformable polymer PDMS. It offers many advantages, including: It is isolating, transparent to light above 280 nm, biocompatible and can be reversibly bonded to itself or glass.<sup>225</sup> The hydrophobic surface of PDMS can also be modified to be hydrophilic, which influences the EOF.<sup>225</sup> A big disadvantage of this easily processable material is on the one hand its elasticity, which means that supporting structures have to be inserted into the  $\mu$ FFE devices.<sup>208</sup> On the other hand it is gas permeable, thus it cannot tolerate higher pressures in the microfluidic chip system. In the fabrication process, PDMS is placed in a pre-structured negative form and the positive is subsequently bonded to a glass substrate.

In addition to PDMS, PEG-DA (poly (ethylene glycol) diacrylate) with its manufacturing process offers an attractive application for  $\mu$ FFE devices. The liquid prepolymer PEG-DA is changed into a solid form by a photoinitiator-controlled, light-induced, radical polymerization process and microfluidic structures can be created in the material by using a structuring mask<sup>85</sup>. As a biocompatible polymer, it has already been used for years for sensitive microfluidic applications.<sup>226-229</sup> It is a fast, simple and cost-effective method to produce microfluidic chips.

Anciaux et al. also presented the fabrication of a  $\mu$ FFE device by additive manufacturing (3D-printing)<sup>230</sup>, where microfluidic ridged with dimensions as small as 20  $\mu$ m high x 640  $\mu$ m wide could be manufactured and the minimum valley dimensions were 30  $\mu$ m wide 130  $\mu$ m wide. Although the separation efficiency of the 3D printed  $\mu$ FFE chip was comparable to the efficiency of a chip made of glass, the detection limit of the 3D printed chip was about ten times worse.

Decisive for the decision on the material of a microfluidic chip in research and development is not only the material quality, it is also the fast production of small numbers of pieces with a low unit price. This concept, known as rapid prototyping, therefore plays a key role during the development phase.<sup>231, 232</sup>

To overcome the disadvantages of FFE miniaturization, various modifications of the  $\mu$ FFE chips have been developed. The most challenging part is the isolation of the electrolysis

bubbles, which are created by the application of an electric field and which interfere with the separation within the separation channel by distorting the analyte current and the electric field. The use of ion exchange membranes to separate the electrodes, as used on a macro scale, is difficult to integrate in the  $\mu$ FFE devices with their low channel heights.<sup>219</sup> Therefore, different approaches to reduce bubble formation in  $\mu$ FFE chips have been developed over time. In the first  $\mu$ FFE devices, the channels were arranged in a membrane-like manner, which isolated the electrodes from the separation channel.<sup>183, 203, 206, 218, 233</sup> As a result, bubbles were prevented from entering the separation zone by a high flow resistance. Although, high electrical resistance was also formed and a low voltage efficiency was achieved. Only about 5 % of the applied electric field reached the separation zone.<sup>208</sup> In order to compensate for this, a higher voltage had to be applied, which also resulted in higher bubble formation. A further modification to reduce bubble formation was achieved by the fact that the electrodes were not isolated from the separation channel and were in direct contact with the separation channel. Consequently, low voltages (less than 2V) were necessary for the separations, which prevented bubble formation but also increased the separation times.<sup>205, 206</sup> Another method of reducing bubble formation was the usage of palladium as electrode material.<sup>234</sup> To prevent contamination with electrode reaction products in the case of electrodes that have direct contact with the separation channel, platinum electrodes are often chosen.<sup>202, 235, 236</sup>

In order to isolate the electrodes from the separation area, different types of membranes were developed to isolate both parts.<sup>201, 203, 205, 206, 214, 217</sup> However, as with the first modifications, the major disadvantage remained that a large part of the electric field outside the separation area was used by a voltage decrease across the membrane.

Using different depths of the separation channel and the electrode channel, Fonslow et al. developed a  $\mu$ FFE chip which resulted in an isolated electrode channel.<sup>204</sup> The electrode area was four times deeper than the separation channel. As a result, the linear velocity of the electrode buffer was significantly higher than in the separation channel and the formed bubbles could be flushed out of the device without disturbing the separation. About 91% of the applied voltage in the separation channel could be localized, which led to a high separation efficiency and only above 589 V cm<sup>-1</sup> did the occurring Joule heating significantly disturb the separation. This chip modification was used as a basis for further studies and further developed.<sup>237, 238</sup>

In addition to the technical modifications, electrochemical tools were also used to reduce bubble formation<sup>235</sup>. Kohlheyer et al. used the oxidation reduction of hydroquinone and p-benzoquinone near the electrodes and achieved a 2.5-fold improvement in resolution, but

there was also a considerable pH change within the separation channel near the electrodes resulting in a limited effective range of the separation channel.

To sum up, since the development of  $\mu$ FFE devices, many different approaches have been developed to solve the main problem, suppression of bubble formation. Further problems of  $\mu$ FFE can be solved technically easier. The heating of the chip can be regulated by a cooling system or due to the small size of the  $\mu$ FFE chip an improved heat removal is given to avoid additional cooling.<sup>239</sup> On the other hand, the negative effect of EOF can be reduced by covalent modifications or by dynamic coatings.

To improve the efficiency of the separation, it was shown that the shape of the separating bed also has an influence. By default, a rectangular separating bed is selected for both FFE and  $\mu$ FFE devices, where there are several inlets for samples and separating buffers at the input and many outlets for the individual fractions at the output.<sup>240,241</sup> For preparative devices, FFE instruments were developed with a trapezoidal separating area, where the narrow side served as the inlet for separating buffer and sample solution and the wide side had outlets for the various fractions.<sup>211,242-244</sup> Here, the advantage of the trapezoidal shape was that a stable wattage could be achieved in the separation area, with a low voltage at the input and a high voltage at the output.<sup>245</sup> This leads to a faster focusing speed and thus to a reduction of the analysis time. Decisive for the separation efficiency is, besides the shape of the separating zone, the length of the separating area in which the electric field is built up and the sample is separated. The longer the separating bed, the greater the migration time and, in the case of FFZE, the angle of deflection increases. However, a longer separating bed leads to a larger band broadening and also to a larger dilution of the individual samples.

The fact that continuous  $\mu$ FFE is a method which can be well integrated with subsequent detection methods, has been demonstrated in the last years of development. Thus, many different approaches to detect and quantify the separated analytes directly online have emerged. Up to now, the only subsequent online analysis method is mass spectrometry (MS). Here the  $\mu$ FFE was analyzed by electro spray ionization-MS<sup>246-248</sup> and quadrupole-time-of-flight liquid chromatography /MS (Q-TOF LC/MS)<sup>249</sup>. Various modifications of the  $\mu$ FFE devices have significantly improved the voltage efficiency and the separation resolution of the  $\mu$ FFE. However, the development also has its limits. Until now no online combination with cell-based detection methods has been reported, because the used separation buffers are not biocompatible in their pure form.

## 1.4 Strategy and reference to the thesis project

Detection methods in miniaturized systems often present a challenge because conventional systems cannot simply be scaled down. Especially the inline monitoring of the biological activity of synthesis products or active compounds (e.g. resulting from chemical synthesis on a microfluidic chip) offers many possibilities for lab-on-a-chip applications. For this reason, first a microfluidic chip has been developed which can sensitively analyze cellular changes in the hydrodynamic flow based on electrochemical impedance spectroscopy <sup>22</sup>. To fabricate the microfluidic microelectrode chip, a fluidic structure of the polymer PEG-DA was applied to a microelectrode array by using photolithography. Due to its pressure stability and gas impermeability, PEG-DA was selected to enable confluent cell cultivation in a system with slight overpressure. The combination of an MEA with the transparent PEG-DA also allows, in addition to the impedimetric monitoring, an optical detection of the cells. The impedance as a real-time, non-invasive, and label-free analysis method is perfectly suited for lab-on-a-chip approaches. As practical experiments and theoretical FEM simulations have shown, the electrode layout had to be adapted to miniaturization due to the small dimensions. Using the well characterized cell-drug model of the NPY receptor <sup>17</sup>, it was demonstrated that the new microelectrode microfluidic chip is significantly more sensitive compared to static measurements. One may find more details about the newly developed detection method for microfluidic applications in chapter 2 of this study.

Organic solvents such as ethanol or DMSO are typical solvents in synthesis of organic, bioactive drugs. In multistep synthesis with different solvents or in sensitive analysis systems (e.g. based on cell systems) even small residues of these solvents can interfere. For this reason, a free-flow electrophoresis based microfluidic chip device were developed in a second step to continuously remove organic solvents from bioactive compounds <sup>178</sup>. The solvent exchanger was developed for miscible organic and aqueous fluids and the working principle was demonstrated by the component fluorescein as a model drug solved in DMSO for exchange in an aqueous buffer. Fluorescence was chosen as the detection method, because it is a very sensitive method that can be easily integrated into microfluidic systems and has a high degree of significance. Furthermore, it was shown that the exchange is sufficient for cell based tests, such as impedimetric monitoring of HEK293A cells. Moreover, the developed solvent exchanger offers the opportunity of a combination with further in-line microfluidic modules. Further details on the solvent exchanger can be found in chapter 3 of this study.

---

A miniaturized FFE was used for the development of the solvent exchanger, because only small amounts are often necessary for the detection of active substances. In addition, the advantages of miniaturization, such as faster reaction times, smaller sample volumes, higher sensitivity, and lower Joule heating, were significant for the FFE. The method developed for the removal of organic solvents should be as simple as possible to apply and technically feasible to integrate it in LOC. On the basis that organic solvents in FFE will not be deflected, but charged molecules are, the mode FFZE could be used, which could be realized in this case with a low conducting phosphate buffer. The photopolymer PEG-DA was used for the fabrication and in order to keep the setup simple, the development was focused on creating an application that does not require membranes or cooling systems. To overcome the negative influence of EOF, a hydrodynamic coating was applied to the solvent exchanger for FFE. The study also demonstrated a key result: By reducing the length of the separating bed, the dilution of the sample can be minimized significantly.

---

## 1.5 References

1. Gupta, N., Renugopalakrishnan, V., Liepmann, D., Paulmurugan, R. and Malhotra, B.D. Cell-based biosensors: Recent trends, challenges and future perspectives. *Biosens Bioelectron* 141, 111435 (2019).
2. Corcoran, C.A. & Rechnitz, G.A. Cell-based biosensors. *Trends in Biotechnology* 3, 92-96 (1985).
3. Shear, J.B. et al. Single cells as biosensors for chemical separations. *Science (New York, N.Y.)* 267, 74-77 (1995).
4. Hazama, A., Hayashi, S. & Okada, Y. Cell surface measurements of ATP release from single pancreatic  $\beta$  cells using a novel biosensor technique. *Pflügers Archiv* 437, 31-35 (1998).
5. Wu, C. et al. A novel biomimetic olfactory-based biosensor for single olfactory sensory neuron monitoring. *Biosensors and Bioelectronics* 24, 1498-1502 (2009).
6. Erdmann, S. et al. Induced cross-resistance of BRAF(V600E) melanoma cells to standard chemotherapeutic dacarbazine after chronic PLX4032 treatment. *Sci Rep* 9, 30 (2019).
7. Seidel, D. et al. A multidimensional impedance platform for the real-time analysis of single and combination drug pharmacology in patient-derived viable melanoma models. *Biosens Bioelectron* 123, 185-194 (2019).
8. Pandey, C.M. et al. Microfluidics Based Point-of-Care Diagnostics. *Biotechnology journal* 13 (2018).
9. Jiang, Y. et al. Enhancing the response of microbial fuel cell based toxicity sensors to Cu(II) with the applying of flow-through electrodes and controlled anode potentials. *Bioresource technology* 190, 367-372 (2015).
10. Jiang, D. et al. Fluorescent magnetic bead-based mast cell biosensor for electrochemical detection of allergens in foodstuffs. *Biosens Bioelectron* 70, 482-490 (2015).
11. Zou, L. et al. Detection of diarrhetic shellfish poisoning toxins using high-sensitivity human cancer cell-based impedance biosensor. *Sensors and Actuators B: Chemical* 222, 205-212 (2016).



12. Cai, S. et al. Engineering highly sensitive whole-cell mercury biosensors based on positive feedback loops from quorum-sensing systems. *Analyst* 143, 630-634 (2018).
13. Liu, Q. et al. Cell-based biosensors and their application in biomedicine. *Chemical reviews* 114, 6423-6461 (2014).
14. Cevenini, L., Calabretta, M.M., Tarantino, G., Michelini, E. & Roda, A. Smartphone-interfaced 3D printed toxicity biosensor integrating bioluminescent “sentinel cells”. *Sensors and Actuators B: Chemical* 225, 249-257 (2016).
15. Giaever, I. & Keese, C.R. Monitoring fibroblast behavior in tissue culture with an applied electric field. *Proceedings of the National Academy of Sciences of the United States of America* 81, 3761-3764 (1984).
16. Wu, M.H., Huang, S.B. and Lee, G.B. Microfluidic cell culture systems for drug research. *Lab Chip* 10, 939-956 (2010).
17. te Kamp, V. et al. Quantitative impedimetric NPY-receptor activation monitoring and signal pathway profiling in living cells. *Biosens Bioelectron* 67, 386-393 (2015).
18. Jahnke, H.G. et al. An impedimetric microelectrode-based array sensor for label-free detection of tau hyperphosphorylation in human cells. *Lab Chip* 9, 1422-1428 (2009).
19. Asami, K. Characterization of biological cells by dielectric spectroscopy. *Journal of Non-Crystalline Solids* 305, 268-277 (2002).
20. Lundstrom, K. Cell-impedance-based label-free technology for the identification of new drugs. *Expert opinion on drug discovery* 12, 335-343 (2017).
21. Gharooni, M. & Abdolahad, M. Bioelectrical impedimetric sensor for single cell analysis based on nanoroughened quartz substrate; suitable for cancer therapeutic purposes. *Journal of pharmaceutical and biomedical analysis* 142, 315-323 (2017).
22. Zitzmann, F.D. and Jahnke, H.-G. et al. A novel microfluidic microelectrode chip for a significantly enhanced monitoring of NPY-receptor activation in live mode. *Lab Chip* 17, 4294-4302 (2017).
23. Jahnke, H.G. et al. Electrochemical live monitoring of tumor cell migration out of micro-tumors on an innovative multiwell high-dense microelectrode array. *Sci Rep* 9, 13875 (2019).

24. Shamsipur, M., Pashabadi, A., Molaabasi, F. & Hosseinkhani, S. Impedimetric monitoring of apoptosis using cytochrome-aptamer bioconjugated silver nanocluster. *Biosens Bioelectron* 90, 195-202 (2017).
25. Arndt, S., Seebach, J., Psathaki, K., Galla, H.J. & Wegener, J. Bioelectrical impedance assay to monitor changes in cell shape during apoptosis. *Biosens Bioelectron* 19, 583-594 (2004).
26. Eichler, M. et al. A novel 96-well multielectrode array based impedimetric monitoring platform for comparative drug efficacy analysis on 2D and 3D brain tumor cultures. *Biosens Bioelectron* 67, 582-589 (2015).
27. Yoo, Y.K. et al. A highly sensitive plasma-based amyloid- $\beta$  detection system through medium-changing and noise cancellation system for early diagnosis of the Alzheimer's disease. *Scientific Reports* 7, 8882 (2017).
28. Huynh, D.T.N., Kim, A.-Y. & Kim, Y.-R. Identification of Pathogenic Factors in *Klebsiella pneumoniae* using Impedimetric Sensor Equipped with Biomimetic Surfaces. *Sensors (Basel)* 17, 1406 (2017).
29. Lvovich, V.F. Impedance spectroscopy: applications to electrochemical and dielectric phenomena. (Wiley, Hoboken; 2012).
30. Pänke, O., Balkenhohl, T., Kafka, J., Schafer, D. & Lisdat, F. Impedance spectroscopy and biosensing. *Advances in biochemical engineering/biotechnology* 109, 195-237 (2008).
31. Lisdat, F. & Schafer, D. The use of electrochemical impedance spectroscopy for biosensing. *Anal Bioanal Chem* 391, 1555-1567 (2008).
32. Pänke, O., Weigel, W., Schmidt, S., Steude, A. and Robitzki, A.A. A cell-based impedance assay for monitoring transient receptor potential (TRP) ion channel activity. *Biosens Bioelectron* 26, 2376-2382 (2011).
33. Jahnke, H.G. et al. A novel 384-multiwell microelectrode array for the impedimetric monitoring of Tau protein induced neurodegenerative processes. *Biosens Bioelectron* 88, 78-84 (2017).
34. Weyer, M. and Jahnke, H.-G. et al. Quantitative characterization of capsaicin-induced TRPV1 ion channel activation in HEK293 cells by impedance spectroscopy. *Anal Bioanal Chem* 408, 8529-8538 (2016).

35. Jung Lee, H., Bai, S.-J. & Seok Song, Y. Microfluidic Electrochemical Impedance Spectroscopy of Carbon Composite Nanofluids. *Scientific Reports* 7, 722 (2017).
36. Cheng, X. et al. Cell detection and counting through cell lysate impedance spectroscopy in microfluidic devices. *Lab on a Chip* 7, 746-755 (2007).
37. Iliescu, C., Poenar, D.P., Carp, M. and Loe, F.C. A microfluidic device for impedance spectroscopy analysis of biological samples. *Sensors and Actuators B: Chemical* 123, 168-176 (2007).
38. Xu, Y. et al. A review of impedance measurements of whole cells. *Biosens Bioelectron* 77, 824-836 (2016).
39. Online contribution from Applied BioPhysics: ECIS, the label free, non-invasive method to electronically monitor cells grown in tissue culture, at: <https://www.biophysics.com>. Last access of webpage: 01.09.2020.
40. Online contribution from ibidi: Impedance Measurement. Non-invasive, label-free cell-based assays to measure cell behavior in culture medium, at: <https://ibidi.com/32-impedance-measurement>. Last access of webpage: 02.09.2020.
41. Online contribution from Agilent: xCELLigence Real-Time Cell Analysis, at: <https://www.agilent.com/en/product/cell-analysis/real-time-cell-analysis/rtca-analyzers>. Last access of webpage: 02.09.2020.
42. Ke, N., Wang, X., Xu, X. & Abassi, Y.A. The xCELLigence system for real-time and label-free monitoring of cell viability. *Methods in molecular biology (Clifton, N.J.)* 740, 33-43 (2011).
43. Doerr, L. et al. New easy-to-use hybrid system for extracellular potential and impedance recordings. *Journal of laboratory automation* 20, 175-188 (2015).
44. Sonnendecker, C. et al. Large-Ring Cyclodextrins as Chiral Selectors for Enantiomeric Pharmaceuticals. *Angewandte Chemie (International ed. in English)* 58, 6411-6414 (2019).
45. Seidel, D., Jahnke, H.G., Englich, B., Girard, M. and Robitzki, A.A. In vitro field potential monitoring on a multi-microelectrode array for the electrophysiological long-term screening of neural stem cell maturation. *Analyst* 142, 1929-1937 (2017).

46. Fleischer, S., Jahnke, H.-G., Fritsche, E., Girard, M. and Robitzki, A.A. Comprehensive human stem cell differentiation in a 2D and 3D mode to cardiomyocytes for long-term cultivation and multiparametric monitoring on a multimodal microelectrode array setup. *Biosensors and Bioelectronics* 126, 624-631 (2019).
47. Online contribution from Multichannel Systems: *In Vitro* MEA-Systems, at: <https://www.multichannelsystems.com/products/vitro-mea-systems>. Last access of webpage: 04.08.2020.48. Viswam, V. et al. Impedance Spectroscopy and Electrophysiological Imaging of Cells With a High-Density CMOS Microelectrode Array System. *IEEE transactions on biomedical circuits and systems* 12, 1356-1368 (2018).
49. Seidel, D. et al. Impedimetric real-time monitoring of neural pluripotent stem cell differentiation process on microelectrode arrays. *Biosens Bioelectron* 86, 277-286 (2016).
50. Jahnke, H.G. et al. FEM-based design of optical transparent indium tin oxide multielectrode arrays for multiparametric, high sensitive cell based assays. *Biosens Bioelectron* 129, 208-215 (2019).
51. Bartsch, H. et al. Functionalized Thick Film Impedance Sensors for Use in In Vitro Cell Culture. *Biosensors* 8 (2018).
52. Zhou, W. et al. Characterization of impedance properties of metal dry bioelectrodes with surface microstructure arrays. *Sensors and Actuators A: Physical* 263, 252-258 (2017).
53. Hennemeyer, M. et al. Cell proliferation assays on plasma activated SU-8. *Microelectronic Engineering* 85, 1298-1301 (2008).
54. Slavik, J., Skopalik, J., Provaznik, I. and Hubalek, J. Multi-Electrode Array with a Planar Surface for Cell Patterning by Microprinting. *Sensors (Basel)* 19 (2019).
55. Aqrawe, Z., Montgomery, J., Travas-Sejdic, J. and Svirskis, D. Conducting Polymers as Electrode Coatings for Neuronal Multi-electrode Arrays. *Trends Biotechnol* 35, 93-95 (2017).
56. Miccoli, B. et al. High-Density Electrical Recording and Impedance Imaging With a Multi-Modal CMOS Multi-Electrode Array Chip. *Frontiers in Neuroscience* 13 (2019).

57. Berdondini, L. et al. Active pixel sensor array for high spatio-temporal resolution electrophysiological recordings from single cell to large scale neuronal networks. *Lab on a Chip* 9, 2644-2651 (2009).
58. Hafizovic, S. et al. A CMOS-based microelectrode array for interaction with neuronal cultures. *Journal of Neuroscience Methods* 164, 93-106 (2007).
59. Ballini, M. et al. A 1024-Channel CMOS Microelectrode Array With 26,400 Electrodes for Recording and Stimulation of Electrogenic Cells In Vitro. *IEEE journal of solid-state circuits* 49, 2705-2719 (2014).
60. Vijay, V. et al. High-density CMOS Microelectrode Array System for Impedance Spectroscopy and Imaging of Biological Cells. *Proceedings of IEEE Sensors. IEEE International Conference on Sensors* 2016, 1-3 (2017).
61. D. Qin, Y.X., J.A. Rogers, R.J. Jackman, X.-M. Zhao, G.M. Whitesides in *Microsystem Technology in Chemistry and Life Sciences*. (ed. H.B. A. Manz) 1-20 (Springer, Heidelberg; 1999).
62. Le, H.P. Progress and Trends in Ink-jet Printing Technology. *Journal of Imaging Science and Technology* 42, 49-62 (1998).
63. Terry, S., Jerman, J.H. & Angell, J. A gas chromatographic air analyzer fabricated on a silicon wafer. *IEEE Transactions on Electron Devices* 26, 1880-1886 (1979).
64. Manz, A. et al. Design of an open-tubular column liquid chromatograph using silicon chip technology. *Sensors and Actuators B: Chemical* 1, 249-255 (1990).
65. Harrison, D.J., Manz, A., Fan, Z., Luedi, H. & Widmer, H.M. Capillary electrophoresis and sample injection systems integrated on a planar glass chip. *Analytical Chemistry* 64, 1926-1932 (1992).
66. Janasek, D., Franzke, J. and Manz, A. Scaling and the design of miniaturized chemical-analysis systems. *Nature* 442, 374-380 (2006).
67. Hardt, S. & Baier, T. Mean-field model for heat transfer in multichannel microreactors. *AIChE Journal* 53, 1006-1016 (2007).
68. Cui, P. and Wang, S. Application of microfluidic chip technology in pharmaceutical analysis: A review. *Journal of pharmaceutical analysis* 9, 238-247 (2019).
69. Fiorini, G.S. & Chiu, D.T. Disposable microfluidic devices: fabrication, function, and application. *BioTechniques* 38, 429-446 (2005).

70. Coluccio, M.L. et al. Microfluidic platforms for cell cultures and investigations. *Microelectronic Engineering* 208, 14-28 (2019).
71. Convery, N. and Gadegaard, N. 30 years of microfluidics. *Micro and Nano Engineering* 2, 76-91 (2019).
72. Kovarik, M.L. et al. Micro total analysis systems: fundamental advances and applications in the laboratory, clinic, and field. *Anal Chem* 85, 451-472 (2013).
73. Mehling, M. and Tay, S. Microfluidic cell culture. *Current Opinion in Biotechnology* 25, 95-102 (2014).
74. Ong, S.E., Zhang, S., Du, H. & Fu, Y. Fundamental principles and applications of microfluidic systems. *Frontiers in bioscience : a journal and virtual library* 13, 2757-2773 (2008).
75. Merrin, J. Frontiers in Microfluidics, a Teaching Resource Review. *Bioengineering* 6, 109 (2019).
76. Reynolds, O. An experimental investigation of the circumstances which determine whether the motion of water shall be direct or sinuous, and of the law of resistance in parallel channels. *Philosophical Transactions of the Royal Society of London* 174, 935-982 (1883).
77. Shang, L., Cheng, Y. and Zhao, Y. Emerging Droplet Microfluidics. *Chemical reviews* 117, 7964-8040 (2017).
78. Washburn, E.W. The Dynamics of Capillary Flow. *Physical Review* 17, 273-283 (1921).
79. Qamar, A.Z. and Shamsi, M.H. Desktop Fabrication of Lab-On-Chip Devices on Flexible Substrates: A Brief Review. *Micromachines* 11, 126 (2020).
80. Becker, H. and Dietz, W. Microfluidic devices for u-TAS applications fabricated by polymer hot embossing, Vol. 3515. (SPIE, 1998).
81. Lee, D.-S., Yang, H., Chung, K.-H. and Pyo, H.-B. Wafer-Scale Fabrication of Polymer-Based Microdevices via Injection Molding and Photolithographic Micropatterning Protocols. *Analytical Chemistry* 77, 5414-5420 (2005).
82. Harrison, D.J. et al. Micromachining a miniaturized capillary electrophoresis-based chemical analysis system on a chip. *Science (New York, N.Y.)* 261, 895-897 (1993).

83. Belder, D., Kohler, F., Ludwig, M., Tolba, K. & Piehl, N. Coating of powder-blasted channels for high-performance microchip electrophoresis. *Electrophoresis* 27, 3277-3283 (2006).
84. Wang, L. et al. Prototyping chips in minutes: Direct Laser Plotting (DLP) of functional microfluidic structures. *Sensors and Actuators B: Chemical* 168, 214-222 (2012).
85. Jezierski, S., Gitlin, L., Nagl, S. and Belder, D. Multistep liquid-phase lithography for fast prototyping of microfluidic free-flow-electrophoresis chips. *Anal Bioanal Chem* 401, 2651-2656 (2011).
86. Ma, J. et al. A simple photolithography method for microfluidic device fabrication using sunlight as UV source. *Microfluidics and Nanofluidics* 9, 1247-1252 (2010).
87. Guijt, R.M. & Breadmore, M.C. Maskless photolithography using UV LEDs. *Lab on a Chip* 8, 1402-1404 (2008).
88. Abgrall, P., Conedera, V., Camon, H., Gue, A.M. & Nguyen, N.T. SU-8 as a structural material for labs-on-chips and microelectromechanical systems. *Electrophoresis* 28, 4539-4551 (2007).
89. Carrel, A. Pure Cultures of Cells. *Journal of Experimental Medicine* 16, 165-168 (1912).
90. Jaccard, N. et al. Automated and Online Characterization of Adherent Cell Culture Growth in a Microfabricated Bioreactor. *Journal of laboratory automation* 19, 437-443 (2014).
91. Zór, K. et al. A compact multifunctional microfluidic platform for exploring cellular dynamics in real-time using electrochemical detection. *RSC Advances* 4, 63761-63771 (2014).
92. Novo, P., Volpetti, F., Chu, V. and Conde, J.P. Control of sequential fluid delivery in a fully autonomous capillary microfluidic device. *Lab Chip* 13, 641-645 (2013).
93. Bennett, M.R. et al. Metabolic gene regulation in a dynamically changing environment. *Nature* 454, 1119-1122 (2008).
94. Chen, Y.A. et al. Generation of oxygen gradients in microfluidic devices for cell culture using spatially confined chemical reactions. *Lab Chip* 11, 3626-3633 (2011).
95. Scherber, C. et al. Epithelial cell guidance by self-generated EGF gradients. *Integrative biology : quantitative biosciences from nano to macro* 4, 259-269 (2012).

96. Polacheck, W.J., Charest, J.L. and Kamm, R.D. Interstitial flow influences direction of tumor cell migration through competing mechanisms. *Proceedings of the National Academy of Sciences of the United States of America* 108, 11115-11120 (2011).
97. Wu, C. et al. Arp2/3 is critical for lamellipodia and response to extracellular matrix cues but is dispensable for chemotaxis. *Cell* 148, 973-987 (2012).
98. Kim, S.M., Lee, S.H. and Suh, K.Y. Cell research with physically modified microfluidic channels: a review. *Lab Chip* 8, 1015-1023 (2008).
99. Toh, Y.C. et al. A novel 3D mammalian cell perfusion-culture system in microfluidic channels. *Lab Chip* 7, 302-309 (2007).
100. Vickerman, V., Blundo, J., Chung, S. & Kamm, R. Design, fabrication and implementation of a novel multi-parameter control microfluidic platform for three-dimensional cell culture and real-time imaging. *Lab Chip* 8, 1468-1477 (2008).
101. Yi, C., Li, C.-W., Ji, S. and Yang, M. Microfluidics technology for manipulation and analysis of biological cells. *Analytica chimica acta* 560, 1-23 (2006).
102. Gomez-Sjoberg, R., Leyrat, A.A., Pirone, D.M., Chen, C.S. and Quake, S.R. Versatile, fully automated, microfluidic cell culture system. *Anal Chem* 79, 8557-8563 (2007).
103. Lee, K.S., Boccazzi, P., Sinskey, A.J. and Ram, R.J. Microfluidic chemostat and turbidostat with flow rate, oxygen, and temperature control for dynamic continuous culture. *Lab Chip* 11, 1730-1739 (2011).
104. Eydelnant, I.A., Uddayasankar, U., Li, B., Liao, M.W. & Wheeler, A.R. Virtual microwells for digital microfluidic reagent dispensing and cell culture. *Lab Chip* 12, 750-757 (2012).
105. Huang, S.B. et al. An integrated microfluidic cell culture system for high-throughput perfusion three-dimensional cell culture-based assays: effect of cell culture model on the results of chemosensitivity assays. *Lab Chip* 13, 1133-1143 (2013).
106. Xu, B.Y., Hu, S.W., Qian, G.S., Xu, J.J. and Chen, H.Y. A novel microfluidic platform with stable concentration gradient for on chip cell culture and screening assays. *Lab Chip* 13, 3714-3720 (2013).
107. Munoz-Berbel, X. et al. Monolithically integrated biophotonic lab-on-a-chip for cell culture and simultaneous pH monitoring. *Lab Chip* 13, 4239-4247 (2013).



108. Shah, P. et al. Microfluidic bioreactors for culture of non-adherent cells. *Sensors and Actuators B: Chemical* 156, 1002-1008 (2011).
109. Yamazoe, H., Ichikawa, T., Hagihara, Y. and Iwasaki, Y. Generation of a patterned co-culture system composed of adherent cells and immobilized nonadherent cells. *Acta Biomaterialia* 31, 231-240 (2016).
110. Krausz, E. et al. Translation of a tumor microenvironment mimicking 3D tumor growth co-culture assay platform to high-content screening. *J Biomol Screen* 18, 54-66 (2013).
111. Lovitt, C.J., Shelper, T.B. and Avery, V.M. Advanced Cell Culture Techniques for Cancer Drug Discovery. *Biology* 3, 345-367 (2014).
112. Hubert, C.G. et al. A Three-Dimensional Organoid Culture System Derived from Human Glioblastomas Recapitulates the Hypoxic Gradients and Cancer Stem Cell Heterogeneity of Tumors Found In Vivo. *Cancer Res* 76, 2465-2477 (2016).
113. Occhetta, P. et al. High-Throughput Microfluidic Platform for 3D Cultures of Mesenchymal Stem Cells, Towards Engineering Developmental Processes. *Scientific Reports* 5, 10288 (2015).
114. Yang, K. et al. A microfluidic array for quantitative analysis of human neural stem cell self-renewal and differentiation in three-dimensional hypoxic microenvironment. *Biomaterials* 34, 6607-6614 (2013).
115. Macown, R.J., Veraitch, F.S. and Szita, N. Robust, microfabricated culture devices with improved control over the soluble microenvironment for the culture of embryonic stem cells. *Biotechnology journal* 9, 805-813 (2014).
116. Amit, M. et al. Suspension Culture of Undifferentiated Human Embryonic and Induced Pluripotent Stem Cells. *Stem Cell Reviews and Reports* 6, 248-259 (2010).
117. Marques, M.P.C. and Szita, N. Bioprocess microfluidics: applying microfluidic devices for bioprocessing. *Current Opinion in Chemical Engineering* 18, 61-68 (2017).
118. Krull, R. and Peterat, G. Analysis of reaction kinetics during chemostat cultivation of *Saccharomyces cerevisiae* using a multiphase microreactor. *Biochemical Engineering Journal* 105, 220-229 (2016).

119. Metto, E.C. et al. An integrated microfluidic device for monitoring changes in nitric oxide production in single T-lymphocyte (Jurkat) cells. *Anal Chem* 85, 10188-10195 (2013).
120. Yamazoe, H., Sugiyama, Y., El Omri, A., Hagihara, Y. and Okada, T. Facile immunostaining and labeling of nonadherent cells using a microfluidic device to entrap the cells. *Journal of Bioscience and Bioengineering* 117, 375-378 (2014).
121. Liberale, C. et al. Integrated microfluidic device for single-cell trapping and spectroscopy. *Sci Rep* 3, 1258 (2013).
122. Perozziello, G. et al. A microfluidic dialysis device for complex biological mixture SERS analysis. *Microelectronic Engineering* 144, 37-41 (2015).
123. McFaul, S.M., Lin, B.K. and Ma, H. Cell separation based on size and deformability using microfluidic funnel ratchets. *Lab Chip* 12, 2369-2376 (2012).
124. Gossett, D.R. et al. Label-free cell separation and sorting in microfluidic systems. *Anal Bioanal Chem* 397, 3249-3267 (2010).
125. Perozziello, G. et al. Microfluidics and nanotechnology: towards fully integrated analytical devices for the detection of cancer biomarkers. *RSC Advances* 4, 55590-55598 (2014).
126. Simone, G. et al. Galectin-3 coats the membrane of breast cells and makes a signature of tumours. *Molecular bioSystems* 10, 258-265 (2014).
127. Kwon, C.H. et al. Drug-eluting microarrays for cell-based screening of chemical-induced apoptosis. *Anal Chem* 83, 4118-4125 (2011).
128. Weltin, A. et al. Cell culture monitoring for drug screening and cancer research: a transparent, microfluidic, multi-sensor microsystem. *Lab Chip* 14, 138-146 (2014).
129. Breslin, S. and O'Driscoll, L. Three-dimensional cell culture: the missing link in drug discovery. *Drug Discovery Today* 18, 240-249 (2013).
130. Ju, S.M., Jang, H.J., Kim, K.B. and Kim, J. High-Throughput Cytotoxicity Testing System of Acetaminophen Using a Microfluidic Device (MFD) in HepG2 Cells. *Journal of toxicology and environmental health. Part A* 78, 1063-1072 (2015).
131. Hong, B. et al. A concentration gradient generator on a paper-based microfluidic chip coupled with cell culture microarray for high-throughput drug screening. *Biomedical microdevices* 18, 21 (2016).

132. Mathur, A. et al. Human iPSC-based Cardiac Microphysiological System For Drug Screening Applications. *Scientific Reports* 5, 8883 (2015).
133. Kondo, E., Wada, K.-I., Hosokawa, K. and Maeda, M. Cryopreservation of adhered mammalian cells on a microfluidic device: Toward ready-to-use cell-based experimental platforms. *Biotechnology and Bioengineering* 113, 237-240 (2016).
134. Lin, L. and Lin, J.-M. Development of cell metabolite analysis on microfluidic platform. *Journal of Pharmaceutical Analysis* 5, 337-347 (2015).
135. Ma, S., Murphy, T.W. and Lu, C. Microfluidics for genome-wide studies involving next generation sequencing. *Biomicrofluidics* 11, 021501-021501 (2017).
136. Herling, T.W. et al. A Microfluidic Platform for Real-Time Detection and Quantification of Protein-Ligand Interactions. *Biophys J* 110, 1957-1966 (2016).
137. Volpetti, F., Garcia-Cordero, J. and Maerkl, S.J. A microfluidic platform for high-throughput multiplexed protein quantitation. *PLoS One* 10, e0117744 (2015).
138. Mok, J., Mindrinos, M.N., Davis, R.W. and Javanmard, M. Digital microfluidic assay for protein detection. *Proceedings of the National Academy of Sciences* 111, 2110-2115 (2014).
139. Clauder, F. et al. Multifunctional coatings combining bioactive peptides and affinity-based cytokine delivery for enhanced integration of degradable vascular grafts. *Biomaterials Science* (2020).
140. de Haan, P. et al. Digestion-on-a-chip: a continuous-flow modular microsystem recreating enzymatic digestion in the gastrointestinal tract. *Lab Chip* 19, 1599-1609 (2019).
141. Sheyn, D. et al. Bone-chip system to monitor osteogenic differentiation using optical imaging. *Microfluid Nanofluidics* 23 (2019).
142. Liu, L. et al. Three-dimensional brain-on-chip model using human iPSC-derived GABAergic neurons and astrocytes: Butyrylcholinesterase post-treatment for acute malathion exposure. *PLoS One* 15, e0230335 (2020).
143. Maschmeyer, I. et al. A four-organ-chip for interconnected long-term co-culture of human intestine, liver, skin and kidney equivalents. *Lab Chip* 15, 2688-2699 (2015).

144. Lee, J. and Kim, S. Kidney-on-a-Chip: A New Technology for Predicting Drug Efficacy, Interactions, and Drug-induced Nephrotoxicity. *Current drug metabolism* 19, 577-583 (2018).
145. Perestrelo, A.R., Águas, A.C.P., Rainer, A. and Forte, G. Microfluidic Organ/Body-on-a-Chip Devices at the Convergence of Biology and Microengineering. *Sensors* 15, 31142-31170 (2015).
146. Schimek, K. et al. Integrating skin and vasculature in a Multi-Organ-Chip Platform. *BMC Proceedings* 9, P20 (2015).
147. Kato, Y., Hirai, Y., Kamei, K., Tsuchiya, T. and Tabata, O. in 2015 Transducers - 2015 18th International Conference on Solid-State Sensors, Actuators and Microsystems (TRANSDUCERS) 1549-1552 (2015).
148. Hochstetter, A. Lab-on-a-Chip Technologies for the Single Cell Level: Separation, Analysis, and Diagnostics. *Micromachines (Basel)* 11 (2020).
149. Kanton, S. et al. Organoid single-cell genomic atlas uncovers human-specific features of brain development. *Nature* 574, 418-422 (2019).
150. Fung, C.W., Chan, S.N. and Wu, A.R. Microfluidic single-cell analysis-Toward integration and total on-chip analysis. *Biomicrofluidics* 14, 021502 (2020).
151. Lo, S.J. and Yao, D.J. Get to Understand More from Single-Cells: Current Studies of Microfluidic-Based Techniques for Single-Cell Analysis. *International journal of molecular sciences* 16, 16763-16777 (2015).
152. Matula, K., Rivello, F. and Huck, W.T.S. Single-Cell Analysis Using Droplet Microfluidics. *Advanced biosystems* 4, e1900188 (2020).
153. Liu, W.W. and Zhu, Y. "Development and application of analytical detection techniques for droplet-based microfluidics"-A review. *Analytica chimica acta* 1113, 66-84 (2020).
154. Ghallab, Y. and Badawy, W. Sensing methods for dielectrophoresis phenomenon: from bulky instruments to lab-on-a-chip. *IEEE Circuits and Systems Magazine* 4, 5-15 (2004).
155. Schwarz, M.A. and Hauser, P.C. Recent developments in detection methods for microfabricated analytical devices. *Lab Chip* 1, 1-6 (2001).

156. Salimi-Moosavi, H., Jiang, Y., Lester, L., McKinnon, G. and Harrison, D.J. A multireflection cell for enhanced absorbance detection in microchip-based capillary electrophoresis devices. *Electrophoresis* 21, 1291-1299 (2000).
157. Malik, A.K. and Faubel, W. Photothermal and light emitting diodes as detectors for trace detection in capillary electrophoresis. *Chemical Society Reviews* 29, 275-282 (2000).
158. Funamoto, K. et al. A novel microfluidic platform for high-resolution imaging of a three-dimensional cell culture under a controlled hypoxic environment. *Lab on a Chip* 12, 4855-4863 (2012).
159. Perozziello, G., Candeloro, P., Coluccio, M.L. and Fabrizio, E.D. Optofluidics for handling and analysis of single living cells. 4, 18 (2017).
160. Eland, L.E., Wipat, A., Lee, S., Park, S. and Wu, L.J. in *Methods in Microbiology*, Vol. 43. (eds. C. Harwood and G.J. Jensen) 69-111 (Academic Press, 2016).
161. Turgeon, R.T. and Bowser, M.T. Micro free-flow electrophoresis: theory and applications. *Anal Bioanal Chem* 394, 187-198 (2009).
162. Yin, X.Y. et al. A simple chip free-flow electrophoresis for monosaccharide sensing via supermolecule interaction of boronic acid functionalized quencher and fluorescent dye. *Electrophoresis* 34, 2185-2192 (2013).
163. Ryu, G. et al. Highly sensitive fluorescence detection system for microfluidic lab-on-a-chip. *Lab on a Chip* 11, 1664-1670 (2011).
164. Lakowicz, J.R. *Principles of fluorescence spectroscopy*, Edn. 3. ed. (Springer, New York, NY; 2006).
165. Lentz, B.R., Moore, B.M. and Barrow, D.A. Light-scattering effects in the measurement of membrane microviscosity with diphenylhexatriene. *Biophys J* 25, 489-494 (1979).
166. Craig, D.B., Wetzl, B.K., Duerkop, A. and Wolfbeis, O.S. Determination of picomolar concentrations of proteins using novel amino reactive chameleon labels and capillary electrophoresis laser-induced fluorescence detection. *Electrophoresis* 26, 2208-2213 (2005).

167. Slais, K., Horká, M., Novácková, J. and Friedl, Z. Fluorescein-based pI markers for capillary isoelectric focusing with laser-induced fluorescence detection. *Electrophoresis* 23, 1682-1688 (2002).
168. Jablonski, A. Efficiency of Anti-Stokes Fluorescence in Dyes. *Nature* 131, 839-840 (1933).
169. Brivio, M. et al. Integrated Microfluidic System Enabling (Bio)chemical Reactions with On-Line MALDI-TOF Mass Spectrometry. *Analytical Chemistry* 74, 3972-3976 (2002).
170. Oedit, A., Vulto, P., Ramautar, R., Lindenburg, P.W. and Hankemeier, T. Lab-on-a-Chip hyphenation with mass spectrometry: strategies for bioanalytical applications. *Curr Opin Biotechnol* 31, 79-85 (2015).
171. Schwarzkopf, F., Scholl, T., Ohla, S. and Belder, D. Improving sensitivity in microchip electrophoresis coupled to ESI-MS/MS on the example of a cardiac drug mixture. *Electrophoresis* 35, 1880-1886 (2014).
172. Wink, K. et al. An integrated chip-mass spectrometry and epifluorescence approach for online monitoring of bioactive metabolites from incubated Actinobacteria in picoliter droplets. *Analytical and Bioanalytical Chemistry* 410, 7679-7687 (2018).
173. Baldwin, R.P. et al. Fully Integrated On-Chip Electrochemical Detection for Capillary Electrophoresis in a Microfabricated Device. *Analytical Chemistry* 74, 3690-3697 (2002).
174. Wang, J. Electrochemical detection for microscale analytical systems: a review. *Talanta* 56, 223-231 (2002).
175. Godino, N., Gorkin, R., Bourke, K. and Ducreé, J. Fabricating electrodes for amperometric detection in hybrid paper/polymer lab-on-a-chip devices. *Lab on a Chip* 12, 3281-3284 (2012).
176. Ansari, K., Ying, J.Y.S., Hauser, P.C., de Rooij, N.F. and Rodriguez, I. A portable lab-on-a-chip instrument based on MCE with dual top-bottom capacitive coupled contactless conductivity detector in replaceable cell cartridge. *Electrophoresis* 34, 1390-1399 (2013).
177. Tantra, R. and Manz, A. Integrated Potentiometric Detector for Use in Chip-Based Flow Cells. *Analytical Chemistry* 72, 2875-2878 (2000).

178. Zitzmann, F.D. and Jahnke, H.-G. et al. Microfluidic Free-Flow Electrophoresis Based Solvent Exchanger for Continuously Operating Lab-on-Chip Applications. *Anal Chem* 89, 13550-13558 (2017).
179. Perozziello, G. et al. Microfluidic device for continuous single cells analysis via Raman spectroscopy enhanced by integrated plasmonic nanodimers. *Opt. Express* 24, A180-A190 (2016).
180. Kohlheyer, D., Eijkel, J.C., van den Berg, A. and Schasfoort, R.B. Miniaturizing free-flow electrophoresis - a critical review. *Electrophoresis* 29, 977-993 (2008).
181. Lee, Y.H., Tan, H.T. and Chung, M.C. Subcellular fractionation methods and strategies for proteomics. *Proteomics* 10, 3935-3956 (2010).
182. Hannig, K. Die trägerfreie kontinuierliche Elektrophorese und ihre Anwendung. *Fresenius' Zeitschrift für analytische Chemie* 181, 244-254 (1961).
183. Raymond, D.E., Manz, A. and Widmer, H.M. Continuous Sample Pretreatment Using a Free-Flow Electrophoresis Device Integrated onto a Silicon Chip. *Analytical Chemistry* 66, 2858-2865 (1994).
184. Michov, B.M. and Michov, B. Elektrophorese: Theorie und Praxis. (de Gruyter, Berlin u.a.; 1996).
185. Gey, M. Instrumentelle Analytik und Bioanalytik: Biosubstanzen, Trennmethoden, Strukturanalytik, Applikationen, Edn. 2., überarb. und erw. Aufl. (Springer, Berlin; 2008).
186. Westermeier, R. and Gronau, S. Electrophoresis in practice: a guide to methods and applications of DNA and protein separations, Edn. 4., revised and enlarged edition. (Wiley-VCH, Weinheim; 2005).
187. Helmholtz, H. Studien über electriche Grenzschichten. *Annalen der Physik* 243, 337-382 (1879).
188. Bockris, J.O.m., Devanathan, M.A.V., Müller, K. and Butler, J.A.V. On the structure of charged interfaces. *Proceedings of the Royal Society of London. Series A. Mathematical and Physical Sciences* 274, 55-79 (1963).
189. Gouy, M. Sur la constitution de la charge électrique à la surface d'un électrolyte. *J. Phys. Theor. Appl.* 9, 457-468 (1910).

190. Chapman, D.L. LI. A contribution to the theory of electrocapillarity. *The London, Edinburgh, and Dublin philosophical magazine and journal of science* 25, 475-481 (1913).
191. Stern, O. Zur Theorie der elektrolytischen Doppelschicht. *Zeitschrift für Elektrochemie und angewandte physikalische Chemie* 30, 508-516 (1924).
192. Grahame, D.C. Properties of the Electrical Double Layer at a Mercury Surface. II. The Effect of Frequency on the Capacity and Resistance of Ideal Polarized Electrodes<sup>1</sup>. *Journal of the American Chemical Society* 68, 301-310 (1946).
193. Lottspeich, F. Bioanalytik, Edn. 3. Aufl. (Springer Spektrum, Berlin; 2012).
194. Belder, D. and Ludwig, M. Surface modification in microchip electrophoresis. *Electrophoresis* 24, 3595-3606 (2003).
195. Gey, M. Instrumentelle Bioanalytik: Biosubstanzen, Trennmethoden, Strukturanalytik, Applikationen ; mit 17 Tabellen. (Vieweg, Braunschweig; 1998).
196. Weinberger, R. Practical capillary electrophoresis, Edn. 2. ed. (Acad. Press, San Diego, Calif. u.a.; 2000).
197. Li, S.F. Capillary electrophoresis: principles, practice and applications. (Elsevier, Amsterdam u.a.; 1992).
198. Weber, G. and Bocek, P. Recent developments in preparative free flow isoelectric focusing. *Electrophoresis* 19, 1649-1653 (1998).
199. Gebauer, P. and Boček, P. A new type of migrating zone boundary in electrophoresis: 1. General description of boundary behavior based on electromigration dispersion velocity profiles. *Electrophoresis* 26, 453-462 (2005).
200. Fonslow, B.R. and Bowser, M.T. Optimizing Band Width and Resolution in Micro-Free Flow Electrophoresis. *Analytical Chemistry* 78, 8236-8244 (2006).
201. Kohlheyer, D., Eijkel, J.C.T., Schlautmann, S., van den Berg, A. and Schasfoort, R.B.M. Microfluidic High-Resolution Free-Flow Isoelectric Focusing. *Analytical Chemistry* 79, 8190-8198 (2007).
202. Rudisch, B.M. et al. Nonaqueous Micro Free-Flow Electrophoresis for Continuous Separation of Reaction Mixtures in Organic Media. *Anal Chem* 91, 6689-6694 (2019).



203. Fonslow, B.R. and Bowser, M.T. Free-Flow Electrophoresis on an Anodic Bonded Glass Microchip. *Analytical Chemistry* 77, 5706-5710 (2005).
204. Fonslow, B.R., Barocas, V.H. and Bowser, M.T. Using Channel Depth To Isolate and Control Flow in a Micro Free-Flow Electrophoresis Device. *Analytical Chemistry* 78, 5369-5374 (2006).
205. Kohlheyer, D., Besselink, G.A.J., Schlautmann, S. and Schasfoort, R.B.M. Free-flow zone electrophoresis and isoelectric focusing using a microfabricated glass device with ion permeable membranes. *Lab on a Chip* 6, 374-380 (2006).
206. Xu, Y., Zhang, C.-X., Janasek, D. and Manz, A. Sub-second isoelectric focusing in free flow using a microfluidic device. *Lab on a Chip* 3, 224-227 (2003).
207. Lu, H., Gaudet, S., Schmidt, M.A. and Jensen, K.F. A Microfabricated Device for Subcellular Organelle Sorting. *Analytical Chemistry* 76, 5705-5712 (2004).
208. Zhang, C.-X. and Manz, A. High-Speed Free-Flow Electrophoresis on Chip. *Analytical Chemistry* 75, 5759-5766 (2003).
209. Kuhn, R., Hoffstetter-Kuhn, S. and Wagner, H. Free-flow electrophoresis for the purification of proteins: II. Isoelectric focusing and field step electrophoresis. *Electrophoresis* 11, 942-947 (1990).
210. Wang, S. et al. Carrier ampholyte-free free-flow isoelectric focusing for separation of protein. *Electrophoresis* 40, 2610-2617 (2019).
211. Stastna, M. and Slais, K. Preparative divergent flow IEF without carrier ampholytes for separation of complex biological samples. *Electrophoresis* 31, 433-439 (2010).
212. Verheggen, T.P.E.M., Reijenga, J.C. and Everaerts, F.M. Isotachophoretic analyses of anions at high pH. *Journal of Chromatography A* 260, 471-477 (1983).
213. Everaerts, F.M., Beckers, J.L. and Verheggen, T.P.E.M. Isotachophoresis: Theory, Instrumentation and Applications. (Elsevier Science, 2011).
214. Janasek, D., Schilling, M., Manz, A. and Franzke, J. Electrostatic induction of the electric field into free-flow electrophoresis devices. *Lab on a Chip* 6, 710-713 (2006).
215. Janasek, D., Schilling, M., Franzke, J. and Manz, A. Isotachophoresis in free-flow using a miniaturized device. *Anal Chem* 78, 3815-3819 (2006).

216. Albrecht, J.W., El-Ali, J. and Jensen, K.F. Cascaded free-flow isoelectric focusing for improved focusing speed and resolution. *Anal Chem* 79, 9364-9371 (2007).
217. Albrecht, J.W. and Jensen, K.F. Micro free-flow IEF enhanced by active cooling and functionalized gels. *Electrophoresis* 27, 4960-4969 (2006).
218. Raymond, D.E., Manz, A. and Widmer, H.M. Continuous separation of high molecular weight compounds using a microliter volume free-flow electrophoresis microstructure. *Anal Chem* 68, 2515-2522 (1996).
219. Mazereeuw, M., de Best, C.M., Tjaden, U.R., Irth, H. and van der Greef, J. Free flow electrophoresis device for continuous on-line separation in analytical systems. An application in biochemical detection. *Anal Chem* 72, 3881-3886 (2000).
220. Macounova, K., Cabrera, C.R., Holl, M.R. and Yager, P. Generation of natural pH gradients in microfluidic channels for use in isoelectric focusing. *Anal Chem* 72, 3745-3751 (2000).
221. Shinohara, T. et al. Silver Ion Selective Electrode Based on Calix[4]arene Methyl Ketonic Derivative. *Analytical Sciences* 17, 889-892 (2001).
222. Spierings, G.A.C.M. Wet chemical etching of silicate glasses in hydrofluoric acid based solutions. *J Mater Sci* 28, 6261-6273 (1993).
223. Wang, T., Chen, J., Zhou, T. and Song, L. Fabricating Microstructures on Glass for Microfluidic Chips by Glass Molding Process. *Micromachines (Basel)* 9 (2018).
224. Dittrich, P.S., Tachikawa, K. and Manz, A. Micro total analysis systems. Latest advancements and trends. *Anal Chem* 78, 3887-3908 (2006).
225. McDonald, J.C. et al. Fabrication of microfluidic systems in poly(dimethylsiloxane). *Electrophoresis* 21, 27-40 (2000).
226. Khademhosseini, A. et al. Molded polyethylene glycol microstructures for capturing cells within microfluidic channels. *Lab Chip* 4, 425-430 (2004).
227. Beebe, D.J. et al. Functional hydrogel structures for autonomous flow control inside microfluidic channels. *Nature* 404, 588-590 (2000).
228. Seong, G.H., Zhan, W. and Crooks, R.M. Fabrication of microchambers defined by photopolymerized hydrogels and weirs within microfluidic systems: application to DNA hybridization. *Anal Chem* 74, 3372-3377 (2002).

229. Dikovsky, D., Bianco-Peled, H. and Seliktar, D. The effect of structural alterations of PEG-fibrinogen hydrogel scaffolds on 3-D cellular morphology and cellular migration. *Biomaterials* 27, 1496-1506 (2006).
230. Anciaux, S.K., Geiger, M. and Bowser, M.T. 3D Printed Micro Free-Flow Electrophoresis Device. *Anal Chem* 88, 7675-7682 (2016).
231. Waldbaur, A., Rapp, H., Länge, K. and Rapp, B.E. Let there be chip- towards rapid prototyping of microfluidic devices: one-step manufacturing processes. *Analytical Methods* 3, 2681-2716 (2011).
232. Sollier, E., Murray, C., Maoddi, P. and Di Carlo, D. Rapid prototyping polymers for microfluidic devices and high pressure injections. *Lab on a Chip* 11, 3752-3765 (2011).
233. Zhang, C.X. and Manz, A. High-speed free-flow electrophoresis on chip. *Anal Chem* 75, 5759-5766 (2003).
234. Macounova, K., Cabrera, C.R. and Yager, P. Concentration and separation of proteins in microfluidic channels on the basis of transverse IEF. *Anal Chem* 73, 1627-1633 (2001).
235. Kohlheyer, D., Eijkel, J.C., Schlautmann, S., van den Berg, A. and Schasfoort, R.B. Bubble-free operation of a microfluidic free-flow electrophoresis chip with integrated Pt electrodes. *Anal Chem* 80, 4111-4118 (2008).
236. Pfeiffer, S.A. et al. Continuous purification of reaction products by micro free-flow electrophoresis enabled by large area deep-UV fluorescence imaging. *Anal Bioanal Chem* 410, 853-862 (2018).
237. Fonslow, B.R. and Bowser, M.T. Fast electrophoretic separation optimization using gradient micro free-flow electrophoresis. *Anal Chem* 80, 3182-3189 (2008).
238. Turgeon, R.T. and Bowser, M.T. Improving sensitivity in micro-free flow electrophoresis using signal averaging. *Electrophoresis* 30, 1342-1348 (2009).
239. Yan, J. et al. A simple and highly stable free-flow electrophoresis device with thermoelectric cooling system. *Journal of Chromatography A* 1321, 119-126 (2013).
240. Islinger, M., Wildgruber, R. and Volkl, A. Preparative free-flow electrophoresis, a versatile technology complementing gradient centrifugation in the isolation of highly purified cell organelles. *Electrophoresis* 39, 2288-2299 (2018).

- 
241. Weber, P.J.A., Weber, G. and Eckerskorn, C. Isolation of Organelles and Prefractionation of Protein Extracts Using Free-Flow Electrophoresis. *Current Protocols in Protein Science* 32, 22.25.21-22.25.21 (2003).
242. Slais, K. Divergent flow isoelectric focusing. *Electrophoresis* 29, 2451-2457 (2008).
243. Stastna, M. and Slais, K. Single-input divergent flow IEF for preparative analysis of proteins. *Electrophoresis* 29, 4503-4507 (2008).
244. Mazanec, K., Bobalova, J. and Slais, K. Divergent flow isoelectric focusing: fast and efficient method for protein sample preparation for mass spectrometry. *Anal Bioanal Chem* 393, 1769-1778 (2009).
245. Stastna, M. and Slais, K. Continuous fast focusing in a trapezoidal void channel based on bidirectional isotachopheresis in a wide pH range. *Electrophoresis* 36, 2579-2586 (2015).
246. Chartogne, A., Tjaden, U.R. and Van der Greef, J. A free-flow electrophoresis chip device for interfacing capillary isoelectric focusing on-line with electrospray mass spectrometry. *Rapid communications in mass spectrometry : RCM* 14, 1269-1274 (2000).
247. Park, J.K. et al. Direct coupling of a free-flow isotachopheresis (FFITP) device with electrospray ionization mass spectrometry (ESI-MS). *Lab on a Chip* 15, 3495-3502 (2015).
248. Kinde, T.F., Lopez, T.D. and Dutta, D. Electrophoretic extraction of low molecular weight cationic analytes from sodium dodecyl sulfate containing sample matrices for their direct electrospray ionization mass spectrometry. *Anal Chem* 87, 2702-2709 (2015).
249. Benz, C., Boomhoff, M., Appun, J., Schneider, C. and Belder, D. Chip-based free-flow electrophoresis with integrated nanospray mass-spectrometry. *Angewandte Chemie (International ed. in English)* 54, 2766-2770 (2015).

## Chapter 2

### Research Article I

---

**A NOVEL MICROFLUIDIC MICROELECTRODE CHIP FOR A  
SIGNIFICANTLY ENHANCED MONITORING OF  
NPY-RECEPTOR ACTIVATION IN LIVE MODE**

---

Published in Lab on Chip (2017), 17: 4294-4302.

doi: 10.1039/C7LC00754J

Franziska D. Zitzmann, Heinz-Georg Jahnke, Felix Nitschke, Annette G. Beck-Sickinger,  
Bernd Abel, Detlev Belder, Andrea A. Robitzki

## 2.1 Abstract

Lab-on-a-chip devices that combine, e.g. chemical synthesis with integrated on-chip analytics and multi-compartment organ-on-a-chip approaches, are a fast and attractive evolving research area. While integration of appropriate cell models in microfluidic setups for monitoring the biological activity of synthesis products or test compounds is already in focus, the integration of label-free bioelectronic analysis techniques is still poorly realized. In this context, we investigated the capabilities of impedance spectroscopy as a non-destructive real-time monitoring technique for adherent cell models in a microfluidic setup. While an initial adaptation of a microelectrode array (MEA) layout from a static setup revealed clear restrictions in the application of impedance spectroscopy in a microfluidic chip, we could demonstrate the advantage of a FEM simulation based rational MEA layout optimization for an optimum electrical field distribution within microfluidic structures. Furthermore, FEM simulation based analysis of shear stress and time-dependent test compound distribution led to identification of an optimal flow rate. Based on the simulation derived optimized microfluidic MEA, comparable impedance spectra characteristics were achieved for HEK293A cells cultured under microfluidic and static conditions. Furthermore, HEK293A cells expressing Y1 receptors were used to successfully demonstrate the capabilities of impedimetric monitoring of cellular alterations in the microfluidic setup. More strikingly, the maximum impedimetric signal for the receptor activation was significantly increased by a factor of 2.8. Detailed investigations of cell morphology and motility led to the conclusion that cultivation under microfluidic conditions could lead to an extended and stabilized cell-electrode interface.

## 2.2 Introduction

Integrated devices with microfluidic structures have certain advantages like miniaturized and complex setups with well-defined environment control as well as the possibility of different compartments on the same chip, each with individually controlled conditions. Therefore, microfluidics-based lab-on-a-chip devices are the focus of different application fields like miniaturized chemical synthesis,<sup>1</sup> mobile diagnostics,<sup>2</sup> and cell analysis tool development<sup>3</sup> as well as more *in vivo* like screening and organ-on-a-chip approaches.<sup>4,5</sup> There are strong efforts to combine different modules on a single chip. Thus, in the field of, e.g. chemical synthesis, the combination of microfluidic synthesis and separation modules with integrated online analytics based on mass spectrometry,<sup>6,7</sup> HPLC<sup>8</sup> or other common analytical techniques<sup>9,10</sup> is intensively investigated. In contrast, the inline analysis of biological activity, especially by using complex cell models, is still a challenge. While

single microfluidic modules for cell cultivation are studied and described in detail,<sup>11,12</sup> the integration of real-time monitoring techniques into microfluidic setups for cell cultures is a challenge. Thus, approaches for adherent cell cultures in microfluidic devices are mostly limited to optical analyses of defined cell reservoirs.<sup>13</sup>

In contrast, a large variety of bioelectronic analysis techniques and approaches were described for the non-invasive real-time monitoring of cell culture and tissue models in static setups without a continuous medium supply. Despite the availability of other techniques, impedance spectroscopy based approaches are widely described to quantitatively monitor a wide range of cellular characteristics and alterations.<sup>14,15</sup> In particular, impedimetric monitoring of fast cellular reactions like activation of G-protein coupled receptors (GPCRs)<sup>16,17</sup> or ion channel activity modulation<sup>18,19</sup> would be perfectly suitable for integrated microfluidic lab-on-a-chip approaches.

In this context, we aimed at transferring these superior impedimetric monitoring capabilities that are widely used for cell culture monitoring and screening purposes under static cultivation conditions into microfluidic based devices for the monitoring of cell cultures under continuous flow conditions. In this work, we wanted to investigate if MEA layouts for impedimetric monitoring of adherent cell layers in static setups can be used in small volume cell reservoirs under microfluidic conditions and if cellular alterations like receptor activation can be sensitively and quantitatively monitored in microfluidic setups.

## 2.3 Materials and Methods

### 2.3.1 Fabrication of microelectrode arrays and microfluidic structures

Microelectrode arrays (MEAs) were produced in a clean room by a lift-off technique as previously described.<sup>20</sup> Details of the fabrication can be found in the supplementary information (page 73). Microfluidic structures with integrated MEAs were produced *via* photopolymerization of polyethylene glycol diacrylate (PEG-DA) using modifications of a procedure previously described for microfluidic chip production.<sup>21</sup> Briefly, holes at the inlet/outlet positions of the cover plates (Henneberg & Co, Manebach, Germany) were generated using a sand blaster (Barth Serienapparate, Germany) with granules of 50  $\mu\text{m}$  particle size. After the TPM coating of the cover plate and MEA, double-sided tape (3M, 468MP 200MP Adhesive) was attached for a defined distance between the glass slides. 200  $\mu\text{l}$  of PEG-DA (Sigma Aldrich, Germany; MW 258) with 1% (w/w) 2,2-dimethoxy-2-phenylacetophenone (Sigma Aldrich, Germany) was used to fill the space between the glass slides. The chip was placed in the mask aligner (Süss Micro Tec MA6, Garching,

Germany) and a light-impermeable photomask (16 000 dpi, Zitzmann GmbH, Eching, Germany) containing the cell cavity structures was aligned. Photopolymerization was carried out with a Hg lamp ( $\lambda = 350\text{--}405\text{ nm}$ ;  $P = 12\text{ mW cm}^{-2}$ ) at an illumination time of 1.7 s. Subsequently, the nonpolymerized prepolymer was removed by reduced pressure and the microfluidic structures were rinsed with ethanol (70% (v/v) in water) to remove PEG-DA residues from the microelectrodes. Finally, the chip was re-exposed to UV light for 30 s and for the connection to pumps silicon tubes were bonded at the cover plate holes.

### 2.3.2 Cell culture

HEK293A cells (Life Technologies) were grown in DMEM, supplemented with 10% fetal bovine serum, 2 mM Glutamax, 100 U ml<sup>-1</sup> penicillin and 100  $\mu\text{g ml}^{-1}$  streptomycin (all by Life Technologies) at 37 °C, 5% CO<sub>2</sub> and 95% humidity. For the experiments, MEAs and microfluidic chips were coated with 4 mg ml<sup>-1</sup> collagen I (Life Technologies, Germany) in 0.02 N acetic acid for 2 hours at 37 °C, followed by removal of the coating solution and washing with phosphate-buffered saline (Life Technologies). For static experiments 125 000 cells per well were seeded in 200  $\mu\text{l}$  medium and cultured overnight in a cell culture incubator. For microfluidic experiments, cell reservoirs were filled with a cell suspension of 10 million cells per ml. After an initial static adhesion time of 45 min at 37 °C, microfluidic chips were connected to neMESYS syringe pumps (Cetoni GmbH, Germany) and cultured using the identified optimum flow rate of 15  $\mu\text{l min}^{-1}$  overnight at 37 °C on a microscopic stage using a self-developed chip heating system. The application of a medium containing 100 nM NPY (Sigma Aldrich) was realized using a 3-way valve (Vici Jour, Switzerland).

### 2.3.3 Electrochemical impedance spectroscopy

Impedance measurements were performed using a high-precision impedance analyzer (ISX-3, ScioSpec Scientific Instruments GmbH, Germany) and a self-developed multiplexer front end. Impedance spectra were recorded with 10 mV alternating voltage in a frequency range of 500 Hz to 5 MHz using our self-developed software IMAT v2.2.5.3. The self-developed software IDAT v3.6.5.2 was used to calculate the relative impedance ( $(|Z|_{\text{covered}} - |Z|_{\text{cell-free}})/|Z|_{\text{cell-free}} \times 100\%$ ), determine the frequency of the relative impedance maximum and trace it over time. Additionally, the relative impedance traces were optionally normalized to the beginning of the experiment and the control group as stated for the experiments. For statistical analysis, only electrodes with a sufficient cell signal (>50%)



and at least 10 electrodes (replicates) per reservoir or well were used. For the analysis of the signal variance over time, we analyzed the standard deviation of each individual measurement electrode derived relative impedance trace within 60 minutes and a measurement interval of 5 minutes.

#### 2.3.4 Finite element method (FEM) simulation

Chip layouts were generated using AutoCAD 2016 (Autodesk) and imported into COMSOL Multiphysics 5.3 (Comsol Multiphysics GmbH, Germany). To simulate the electrical field, the AC/DC-module was used. The relative permittivity of the culture medium was set to  $80^{22,23}$  and the electrical conductivity to  $1.55 \text{ S m}^{-1}$ .<sup>22,24</sup> The electrode material was assigned to gold from the materials library. The counter electrode was connected to a ground and at the measurement electrode 10 mV were applied. For the electrical double layer, a contact impedance was assigned between the electrode surface and the medium with a capacitance of  $0.1 \text{ F m}^{-2}$  and a resistance of  $0.03 \text{ } \Omega \text{ m}^2$ . Both values were derived by an equivalent circuit fitting of the measured reference spectra (static well) using a self-developed LabView program. The simulation was done with the finer mesh size. Impedance magnitude spectra were obtained in the results section under “derived values”. The available admittance was transformed into the reciprocal impedance and the magnitude was derived by the calculation command “abs”. To simulate the laminar flow and the analyte distribution the module laminar flow and transport of diluted species were coupled. The dynamic viscosity for the medium was set to  $0.00078 \text{ Pa s}$ .<sup>25, 26</sup> The simulation was done with the finer mesh size.

#### 2.3.5 Statistics

Statistical analyses were performed using Graphpad Prism 5.02. All presented values are means  $\pm$  standard error of the mean (sem) unless stated otherwise. Group comparisons were done by *t*-test. Differences between two means with  $p < 0.05$  were considered significant (\*),  $p < 0.01$  very significant (\*\*) and  $p < 0.001$  highly significant (\*\*\*).

## 2.4 Results and Discussion

### 2.4.1 Microfluidic systems need optimized microelectrode array design for impedimetric cell monitoring

To investigate the cellular behavior and reaction of cell cultures under microfluidic conditions in comparison to the static culture situation, we started with an already described microelectrode array (MEA) that was optimized for the sensitive and spatially resolved impedimetric monitoring of cellular alterations.<sup>20</sup> The MEA consists of 9 separated culture units (wells) each comprising 42 measurement electrodes (100  $\mu\text{m}$  diameter) and a semi-circle like counter electrode with a distinct larger surface area (Figure 2-1A). As a cellular model, a HEK293 derived cell line was chosen, which is already well established for impedimetric monitoring of receptor<sup>16,27</sup> and ion channel activation.<sup>18,19</sup> We used HEK293A cells in combination with a collagen I coating of the MEA, resulting in a reproducible and stable monolayer 24 hours after seeding (Figure 2-1B). Live/dead staining proved the overall vitality of the cultures with only individual damaged cells, which commonly occurs in static cell cultures (Figure 2-1B). Next, impedance spectra of the MEA with and without cells were recorded to determine the accessible cell signal. The major cellular contribution to the impedance magnitude spectra was found between 10 kHz and 1 MHz with a maximum signal at around 100 kHz (Figure 2-1D), which is in line with previous observations for microelectrodes in static cultivation chambers.<sup>20,28</sup>

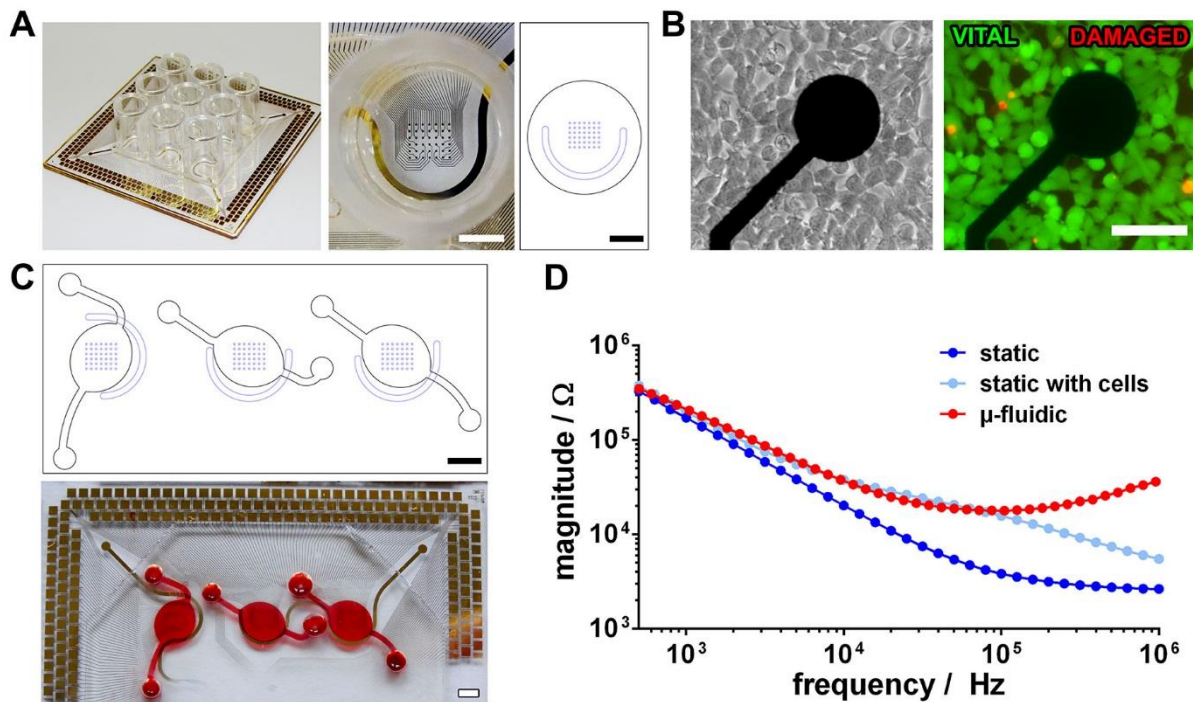


**Figure 2-1: Microelectrode array based impedimetric monitoring of adherent cells.** (A) Microelectrode array with nine static culture chambers each including 42 microelectrodes with 100  $\mu\text{m}$  in diameter and a counter electrode (semi-circle). (scale bar = 2 mm) (B) Microscopic images of the adherent HEK293A cells cultured on the microelectrode array. Live/Dead staining proved the viability of the established cell layer. (scale bar = 100  $\mu\text{m}$ ) (C) Microelectrode array with microfluidic cell culture chambers (100  $\mu\text{m}$  height). (scale bar = 2 mm) (D) Impedimetric analysis of static and microfluidic microelectrode arrays demonstrating cell signal relevant frequency and magnitude ranges.

Based on this MEA, the culture chambers were replaced by a microfluidic structure comprising three cell reservoirs that each include 42 measurement electrodes (Figure 2-1C) but reduced the accessible area by a factor of 3 (45  $\text{mm}^2$  vs. 15  $\text{mm}^2$ ). Additionally, the counter electrode is now located outside the cell reservoir within the microfluidic channel, which aimed on sufficient space within the cell reservoir for the measurement electrode positioning, the conducting paths and for imaging. Together with a design channel height of 100  $\mu\text{m}$  each cell reservoir has a volume of only 1.5  $\mu\text{l}$ , which would drastically minimize the dead volume and required space in complex lab-on-a-chip systems with the demand for inline bioanalytical monitoring. Afterwards, this microfluidic MEA was impedimetrically characterized by filling the cell reservoirs and microchannels with medium. The impedance measurement was performed without a flow. Unfortunately, the magnitude spectra of the microfluidic MEA revealed a distinct increase in impedance, especially in the frequency range between 10 kHz and 1 MHz, where the cell signal is prominent (Figure 2-1D), which means a drastically reduced sensitivity for impedimetric cell monitoring and, moreover, for sensitive detection of cellular alterations by impedance spectroscopy.

### 2.4.2 FEM simulation based design of an optimized microfluidic MEA

Although the impedance measurements were performed with an alternating potential of only 10 mV, which means minimal current flows, the reduced electrolyte filled volume seems to impair the electrical field between the measurement and the counter electrode. To analyze and optimize the MEA layout for the microfluidic integration in a rational way, finite element method (FEM) based simulations were performed (Figure 2-2). The simulation for the microelectrode with the maximum distance from the counter electrode at 100 kHz and 10 mV is shown (Figure 2-2A). The static MEA layout was simulated with a medium fill height of 5 mm for the culture chamber. Despite the potential projected on the surface, for the static layout the field current density lines were also included (red lines). Interestingly, simulated field current density lines extended several millimeters in height into the culture chamber. Based on the initial microfluidic chip layout the counter electrode was positioned in the microchannel inlet to the cell culture reservoir (Figure 2-2A, layout:  $\mu$ -fluidic). To avoid limitations by the reduced counter electrode ( $0.2 \text{ mm}^2$ ), the area was increased to  $0.75 \text{ mm}^2$  that is a hundred times bigger than the measurement electrode. The simulated potential revealed that nearly all of the culture reservoir is influenced by the 10 mV potential applied at the measurement electrode. This difference between the static and the  $\mu$ -fluidic layout is also visible in the cross section of the simulated potential field (Figure S 2.1). To validate our simulated model, we compared measurement data and simulation derived impedance magnitude spectra (Figure 2-2B), which revealed a good match for the static (blue) and the  $\mu$ -fluidic (red) layout. Based on these initial simulations we assumed that the electrical field is restricted by the small volume of the microfluidic channel and chamber. To investigate this, we calculated the current density field from the simulated model and presented it for better visualization at a logarithmic scale (Figure S 2.2). For the static layout (reference), the maximum current field density is found at the measurement electrode (2.49) as was expected. Furthermore, high current field densities extend at least up to  $500 \text{ }\mu\text{m}$  in height and lower current field densities up to 3 mm and more, which is in line with the demonstrated current density field lines (Figure 2-2, static layout). In contrast, for the initial microfluidic layout (Figure S 2.2) the current field density at the electrode is distinctly decreased (1.91), which means that the current flow at the measurement electrode is clearly restricted by an increased resistance that could be caused by the small electrolyte volume within the culture reservoir.

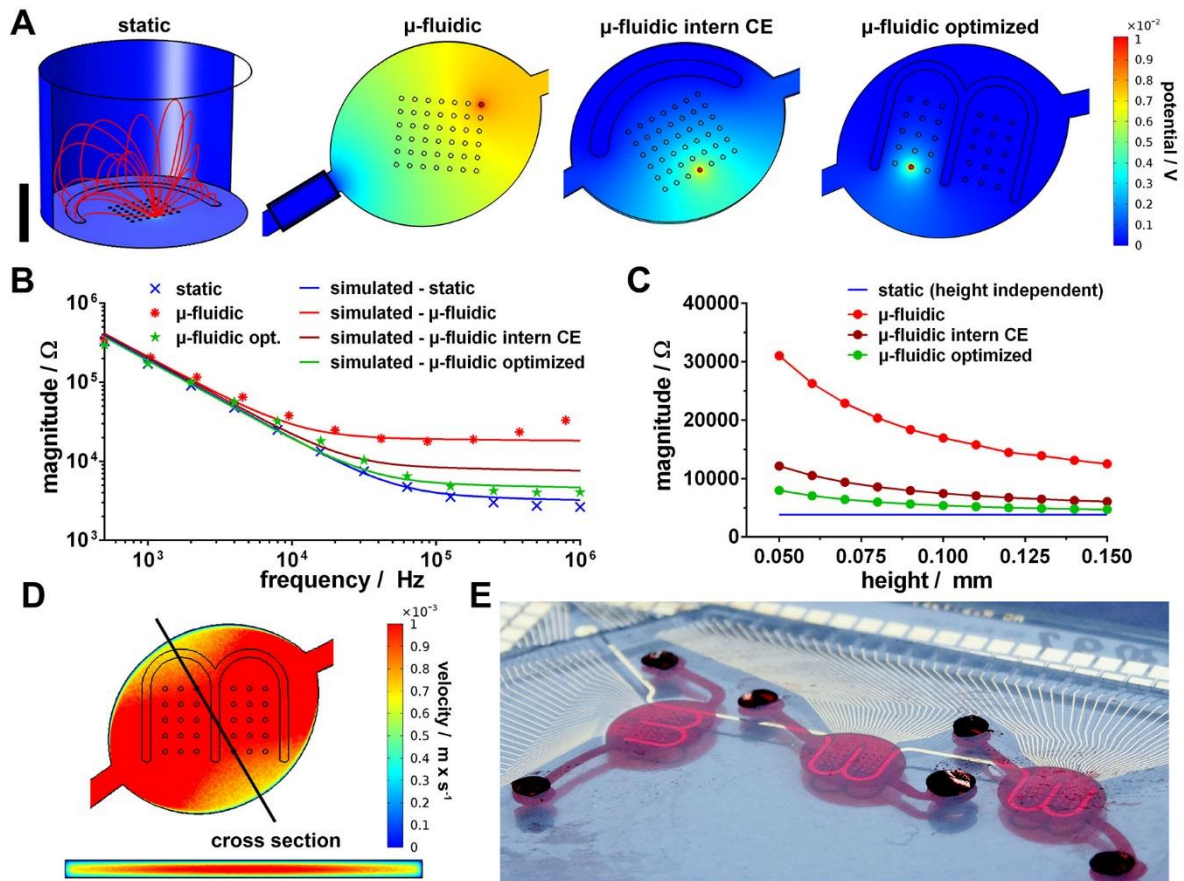


**Figure 2-2: FEM based optimization of microfluidic microelectrode array.** (A) Simulation derived potential field at the surface of the static (5 mm height) and microfluidic culture chambers (100  $\mu\text{m}$  height) for 10 mV applied potential at 100 kHz. For the static cell, current density lines are also shown (red lines). For the microfluidic chamber an counter electrode in the connected channel ( $\mu$ -fluidic), a curved counter electrode ( $\mu$ -fluidic intern CE) or a W-shaped counter electrode ( $\mu$ -fluidic optimized) was used. (scale bar for height = 2 mm) (B) Measured (symbols) and simulation (lines) derived impedance magnitude spectra. (C) Simulation derived influence of the microfluidic chamber height on the impedance magnitude at 100 kHz. (D) Simulation derived velocity within the microfluidic culture chamber for a flow rate of 15  $\mu\text{l}/\text{min}$  (cross section is stretched by factor two in height). (E) Image of optimized microfluidic microelectrode array with W-shaped counter electrode.

Therefore, we performed the simulation with an electrode layout, where the counter electrode is positioned within the culture reservoir ( $\mu$ -fluidic intern CE). The simulation revealed for the potential (Figure 2-2A and Figure S 2.2) a distinct decreased influence within the culture reservoir in comparison to the initial microfluidic layout. Moreover, the current density cross section projection (Fig. S 2.2) revealed for the maximum current density at the measurement electrode (2.26) a much more comparable situation to the static layout (2.49). This seems to be possible by an increased current flow in the electrolyte above the electrode and in the surrounding area. Finally, this results in a distinctly decreased impedance magnitude in comparison to the original microfluidic layout, which is still clearly higher than for the reference (static layout) (Figure 2-2B).

For further improvement, the distance between measurement and counter electrodes was reduced at the expense of reducing the number of measurement electrodes from 42 to 30. The simulation for this layout ( $\mu$ -fluidic optimized) revealed a further distinctly reduced influence of the potential field (Figure 2-2A and Figure S 2.1) within the culture reservoir. More strikingly, the simulation derived current density cross section projection revealed a maximum current density at the measurement electrode (2.49) that is comparable to that of the reference (static layout). Thus, this resulted in a comparable impedance magnitude spectrum to that of the reference (Figure 2-2B, simulated –  $\mu$ -fluidic optimized). For analyzing the influence of the microfluidic structure on the microelectrode array configuration, we performed FEM simulations for all electrodes within the array (Figure S 2.3). While the FEM simulation derived impedance magnitude spectra revealed no influence of the measurement–counter electrode distance for the static layout, this was not the case for the  $\mu$ -fluidic layout with the counter electrode within the microfluidic channel. This was also the case for the  $\mu$ -fluidic intern CE layout. In contrast, the  $\mu$ -fluidic optimized layout resulted in a clearly minimized influence of the measurement–counter electrode distance. The statistical analysis at 100 kHz (Figure S 2.3B) revealed standard deviations of 11  $\Omega$  (static), 1111  $\Omega$  ( $\mu$ -fluidic), 715  $\Omega$  ( $\mu$ -fluidic intern CE) and 165  $\Omega$  ( $\mu$ -fluidic optimized) that are an expression of the variance. Although the value for the  $\mu$ -fluidic optimized layout is ten times lower than that for the initial  $\mu$ -fluidic layout and still more than four times lower than that for the  $\mu$ -fluidic intern CE layout, it is still ten times higher than that for the static layout. This demonstrates the critical influence of the microfluidic structure on the electrical field. Therefore, we used the simulation models to evaluate the influence of the culture reservoir height. For comparison, the impedance magnitude at 100 kHz is shown (Figure 2-2C). As expected, the impedance magnitude increases with lowered culture reservoir height. For the initial microfluidic layout, the impedance magnitude rises about 35% when the height is reduced from 150  $\mu\text{m}$  (12.5 k $\Omega$ ) down to 100  $\mu\text{m}$  (16.9 k $\Omega$ ); moreover, it rises about 148% when the height is reduced to 50  $\mu\text{m}$  (31 k $\Omega$ ). For the optimized microfluidic layout the impedance magnitude rises about 15% when the height is reduced from 150  $\mu\text{m}$  (4.7 k $\Omega$ ) down to 100  $\mu\text{m}$  (5.4 k $\Omega$ ) and 70% (8 k $\Omega$ ) when the height is reduced to 50  $\mu\text{m}$ . When compared to the value for the static layout (3.8 k $\Omega$ ), the culture reservoir of the optimized microfluidic layout should be at least 100–120  $\mu\text{m}$  in height. If it was distinctly lower, the impedance magnitude would clearly rise in comparison to the reference (static layout). Before going into the fabrication of the optimized  $\mu$ -fluidic layout, the velocity within the culture reservoir (100  $\mu\text{m}$  height) was analyzed using simulations. With an inlet pump speed of 15  $\mu\text{l min}^{-1}$  a relatively homogenous flow rate with maximum velocities in the range of 1  $\text{mm s}^{-1}$  above the MEA are achieved (Figure 2-2D). Based on all presented

simulation derived results and findings, the optimized microfluidic MEA layout was produced with the optimized culture reservoir height of 100  $\mu\text{m}$  (Figure 2-2E). For validation of the simulation, impedance spectra from the optimized microfluidic MEA were recorded, whereas the magnitude spectrum matched perfectly with the simulation derived impedance magnitude spectrum (Figure 2-2B,  $\mu$ -fluidic optimized).

### 2.4.3 Impedimetric monitoring of cell attachment under optimized flow conditions

After optimizing the  $\mu$ -fluidic chip layout, we wanted to investigate the capabilities of culturing eukaryotic adherent cells within the cell reservoirs and to characterize the cell layer attachment by impedance spectroscopy. Because shear stress and therefore the flow rate is critical for eukaryotic cells in microfluidic devices,<sup>25,29</sup> the optimum flow rate was determined theoretically by the use of the established FEM model (Figure 2-3A). While a shear stress of 1 Pa and higher can lead to extensive cell detachment or even damaging of adherent cells, shear stress levels in the range of 0.1–1 Pa can induce distinct cell morphology alterations like cell alignment in the flow direction as well as directed cell migration in the flow direction.<sup>25,30,31</sup>

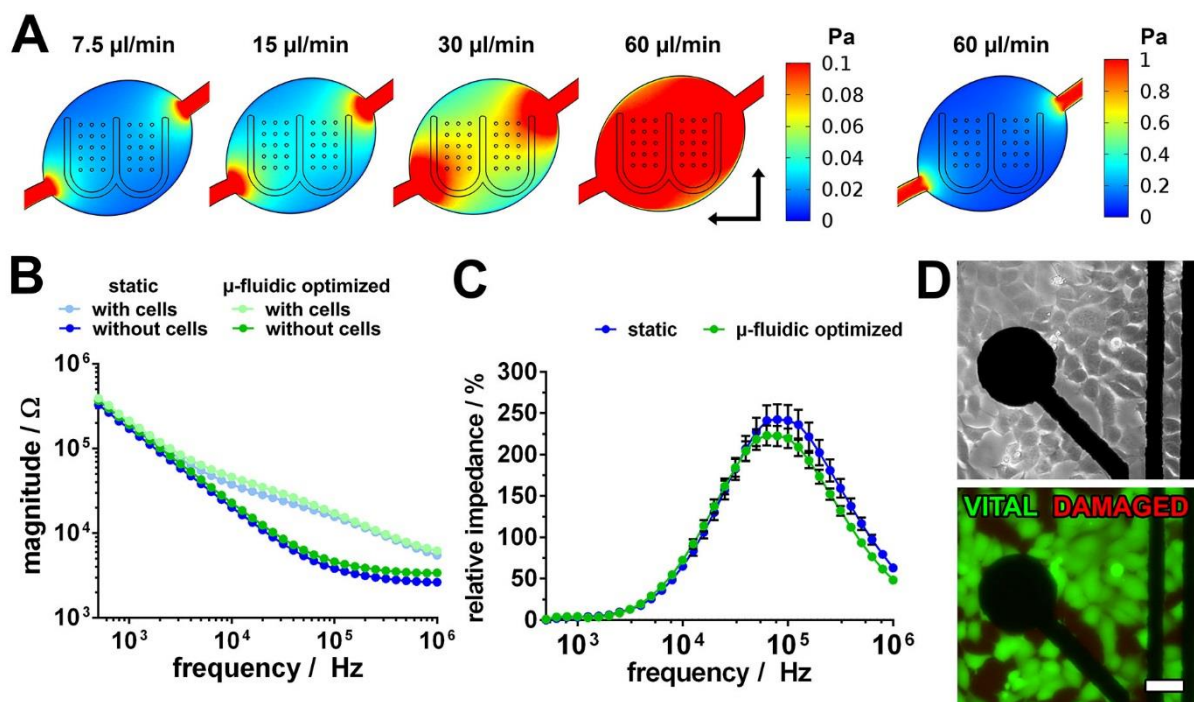


**Figure 2-3: Identification of optimum flow rate and characterization of cells cultured under microfluidic conditions.** (A) FEM simulation derived shear stress in Pascal dependent on flow rate (XY-scale = 1.5 mm). (B) Comparison of impedance magnitude spectra from static and optimized microfluidic conditions (average from 25 electrodes). (C) Comparison of relative impedance spectra from HEK-Y1 cells cultivated under static and microfluidic conditions ( $n = 25$  electrodes). (D) Microscopic images of the HEK-Y1 cells cultured under microfluidic conditions including viability proof by live/dead staining (scale bar = 50  $\mu\text{m}$ ).

Since we wanted to avoid such drastic impacts on the adhered cell layer, our aim was to stay clearly below shear stress levels of 0.1 Pa. The simulation derived shear stress revealed shear stress levels clearly below 1 Pa for flow rates up to  $120 \mu\text{l min}^{-1}$  (Figure S 2.4). Nevertheless, for staying below 0.1 Pa over the whole MEA, a flow rate of  $30 \mu\text{l min}^{-1}$  is already critical at the outer edge of the MEA (Figure 2-3A). Moreover, the simulation derived shear stress values represent the wall shear stress. In contrast, shear stress levels on cells that represent irregular surface topologies can be clearly higher in the range of 10% in comparison to the wall shear stress.<sup>32</sup> Therefore, a flow rate of  $15 \mu\text{l min}^{-1}$  is optimal because the simulated wall shear stress is in the range of 0.03–0.05 Pa for the whole MEA area.

After identification of the optimum flow rate of  $15 \mu\text{l min}^{-1}$ , the fabricated microfluidic chip with the optimized MEA layout was used to monitor the cell attachment and spreading by impedance spectroscopy. After an initial period of 45 min without an applied flow (static condition) for cell attachment, the chip was connected to the pumps and placed under a microscope to acquire a time lapse video overnight (Movie S1). In parallel, cell attachment and spreading was monitored by impedance spectroscopy (Figure S 2.5). From both the time lapse and the impedimetric time trace, it is clearly visible that during the first hours the attached cells mainly kept their spherical shape. Interestingly, for the identified optimal flow rate no directed cell migration into the flow direction could be observed. Between 4 and 8 hours, most of the cells started to flatten and spread their cell bodies over the culture area and after 10–12 hours this process was nearly finished, clearly visible in the establishment of a relative impedance plateau. To ensure that this state of a well-established cell–electrode interface with an optimum impedimetric cell signal is reached, experiments were always started after 15 hours of cultivation. For this time point, the impedance magnitude spectra (Figure 2-3B) as well as the relative impedance spectra of HEK-Y1 cells cultivated under microfluidic and static conditions were compared (Figure 2-3C). As expected by the FEM simulation derived optimization, for both conditions the cell-free magnitude spectra were comparable. More interestingly, there were no clear differences for the averaged spectra with cells. Even the relative impedance spectra revealed a maximum cell signal that was not significantly different with 223% for the microfluidic and 242% for the static cultures. The small decrease as well as the slight shift to the left of the right spectrum side could be a consequence of the slightly higher impedance magnitude of the cell free  $\mu$ -fluidic chip (Figure 2-3B) and, therefore, a slightly lower sensitivity as well as cell signal. Furthermore, we examined if the cell caused decrease of the reservoir height led to a basic impedance increase, especially in the higher



frequency range. The FEM simulation of cell heights of 5  $\mu\text{m}$  up to 50  $\mu\text{m}$  revealed no basic impedance increase (Figure S 2.6). Additionally, we proved that the Y1-receptor expression showed no alteration due to the culturing under microfluidic conditions (Figure S 2.7). Finally, we proved the viability of the microfluidic cultured HEK-Y1 cells by live/dead staining (Figure 2-3D), which revealed no damaged cells within the whole culture reservoir. In contrast to static cultures, where individual damaged cells and cell debris commonly occur, detached damaged cells and cell debris are flushed away in microfluidic setups with continuous flow through. Moreover, microscopic examination proved that the applied flow rate of 15  $\mu\text{l min}^{-1}$  is optimal to avoid detrimental effects like detachment or migration of cells into the flow direction or even extensive cell damage.

#### **2.4.4 Microfluidic based cell culturing enhances impedimetric signal for NPY-receptor activation**

After proving that the HEK-Y1 cells can be cultured in our optimized microfluidic MEA chip and sensitive impedimetric monitoring of the cell layer is possible, we wanted to analyze if the microfluidic cultivation has an influence on the bioelectronic monitoring, *e.g.* the detection of receptor activation by impedance spectroscopy. Based on the reduced culture reservoir volume (1.5  $\text{mm}^3$  vs. 225  $\text{mm}^3$  for the static layout) and the flow rate of 15  $\mu\text{l min}^{-1}$  (one complete medium exchange every 6 seconds) we assumed that time shifts between the application of biological active substances and cellular alterations as well as concentration gradients should be drastically minimized in the microfluidic chip. To prove this, a FEM simulation was performed with 100 nM compound applied at the inlet (Figure 2-4A). While it needed more than one second till substantial concentrations of the compound were observable on the first electrodes, the laminar flow led to a homogeneous distribution at the maximum concentration of 100 nM already after 10 seconds. In comparison to static setups with culture chambers comprising several 100  $\mu\text{l}$  medium and at least undefined concentration gradients for the first seconds or even minutes after application of a compound stock, the conditions in our optimized microfluidic setup are much more defined and homogenous and therefore perfectly suitable for fast cellular reaction kinetics like receptor<sup>16</sup> or ion channel<sup>19</sup> modulations. Based on the evaluated and simulation derived characteristics, the Y1-receptor activation by 100 nM NPY was monitored under static and microfluidic conditions (Figure 2-4B). For the experiment under static conditions a maximum relative impedance increase of 14% was observed 10 minutes after NPY application. This impedance increase is comparable to that of a previous study,<sup>16</sup> where the maximum effects were in the range of 10–20%. More strikingly,

the experiment under microfluidic conditions revealed a clearly increased NPY effect on the maximum impedance increase of about 57%, which was six times higher than the NPY effect within the experiment under static conditions. Surprised by the drastic increase of the impedimetrically monitored NPY effect, we reproduced the experiments several times. The statistical analysis of four independent experiments ( $n = 4$ ) (Figure 2-4C) revealed an extremely significant increase for NPY induced receptor activation on the impedance signal under microfluidic conditions ( $40.5 \pm 10.0\%$ ) in comparison to the static conditions ( $14.7 \pm 3.7\%$ ). The value for the NPY induced impedimetric effect under static conditions is again in line with previously reported values.<sup>16</sup> In contrast, we found no published studies or results that could explain the observed impedimetric signal increase by a factor of 2.8 under microfluidic conditions.

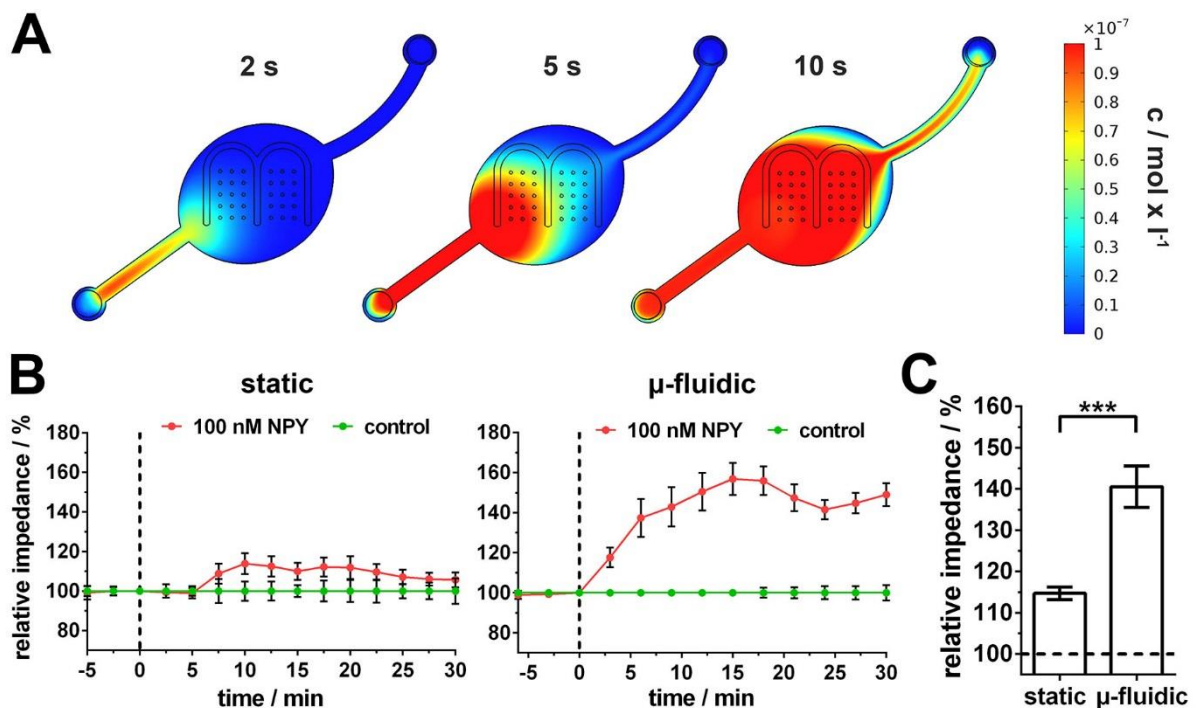


**Figure 2-4: Enhancement of impedimetric detection for Y1-receptor activation under microfluidic conditions.** (A) Simulation derived distribution of analyte for the identified optimum pump speed of  $15 \mu\text{l}/\text{min}$ . (B) Time traces of relative impedance after application of  $100 \text{ nM}$  NPY (time point  $0 \text{ min}$ ) ( $n = 10$  electrodes). Time traces were normalized to time point  $0 \text{ min}$  and control. (C) Statistical analysis of the impedimetrically detected Y1 receptor activation effect under static and microfluidic conditions ( $n = 4$  experiments).

Since the impedimetric monitoring of the NPY receptor activation is attributed to small structural and morphological changes,<sup>16,17</sup> we wanted to have a closer look at the cell morphology. The transmission light microscopy derived images were examined without any obvious NPY induced effect (Figure S 2.8). Although this is in line with a previous study, where the  $G_i$  receptor subunit mediated NPY effect could not clearly be observed

by microscopy,<sup>16</sup> a HEK293A cell line that constitutively expresses an mCherry coupled farnesyl anchor was used to label the cytoplasmic membrane. A comparison of these cells cultured under static and microfluidic conditions (Figure 2-5A) revealed slight differences in cell morphology. While cultured cells in a microfluidic environment seem to spread a little bit more on the surface with a more flattened cell periphery, the statically cultured cells have more rounded cell bodies or even pronounced vertical cell surface areas at cell–cell contacts (Figure 2-5A, arrows). Moreover, this slightly different morphology is also visible in the live/dead staining (Figure 2-1B vs. Figure 2-3D). Although the chosen microfluidic conditions do not lead to drastic morphological effects (Movie S1) like cell detachment, directed migration or cell body shape alignment in the flow direction as can occur at flow shear stress levels above 0.1 Pa, there are actually published studies in which already much lower shear stress levels in the range of 0.001–0.005 Pa can lead to mechanosensitive signaling and, as a consequence, expression pattern alterations as well as small morphological changes at the nanoscopic level.<sup>32,33</sup> Based on this, we propose that culturing HEK293A cells under microfluidic conditions could lead to an extended cell–electrode interface that could be caused by increased cell adhesion and/or increased electrode coverage leading to minimized current leakage around the cells as well as between the cells. In this context, we analyzed the signal variance (expressed by the standard deviation) of each individual measurement electrode within 60 minutes and a 5 minute measurement interval. For microelectrodes, these short signal variations over time are mainly caused by cell motility.<sup>34,35</sup> In this context, the statistical analysis (Figure 2-5B) revealed an extremely significant lower signal variance for the cells cultured under microfluidic conditions (3.6% vs. 9.8%) and, therefore, a lower cell motility. This would support our assumption of an extended and stabilized cell–electrode interface and is also in line with a study performed on endothelial cells that showed a decrease of cell velocity and motility under 0.3 Pa flow shear stress.<sup>36</sup>

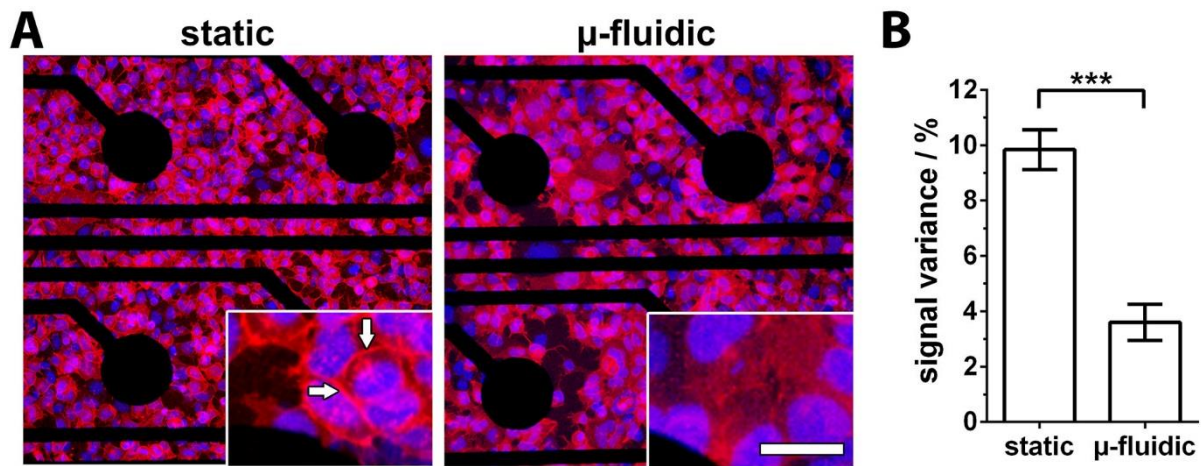


**Figure 2-5: Analysis of cell morphology and motility.** (A) Live Imaging of HEK293A cells with mCherry coupled farnesyl anchor for cell membrane labeling. In the static setup more rounded cell bodies with pronounced vertical cell surface areas at cell-cell contacts (arrows) are visible (scale bar =120  $\mu\text{m}$ , for insert 25  $\mu\text{m}$ ). (B) Analysis of cell motility based on the individual electrode signal variance (expressed by the standard deviation) within 60 minutes ( $n = 4$  experiments).

## 2.5 Conclusion

In summary, we were able to demonstrate that optimized MEA layouts for the impedance spectroscopy based cell monitoring in static culture chamber designs cannot always be directly transferred into microfluidic chip designs. In particular, when MEAs have to be included in culture reservoirs with minimized volume, the electric field can be critically restricted and therefore can drastically interfere with the impedance measurements. In contrast, we could show that FEM simulations are a suitable approach to optimize the MEA layout as well as the microfluidic chip design in a rational way. Moreover, the simulation derived theoretical impedance characteristics matched with real measurement data that were obtained for the initial MEA layout as well as the optimized MEA layout. Furthermore, using the optimized microfluidic MEA chip, the impedimetric monitoring of HEK-Y1 cells cultivated under microfluidic conditions revealed comparable impedimetric characteristics with regard to the relative impedance spectra shape and height. More strikingly, the impedimetric monitoring of the Y1-receptor activation in the microfluidic setup revealed a 2.8 times higher as well as significant impedance signal increase in comparison to the static setup. More detailed morphological analysis led to the assumption that this signal increase probably could be achieved by an extended and stabilized cell–electrode interface. Thus, our study revealed that using optimized MEAs in a microfluidic setup for the impedimetric monitoring of cellular alterations can lead to an increased signal and, therefore, to an enhanced sensitivity at least for the herein used HEK293 cell line and the

Y1-receptor. Nevertheless, this also offers the opportunity for an enhanced monitoring sensitivity of other cell lines and cellular alterations under microfluidic conditions, which will be further investigated in future studies.

## 2.6 Acknowledgment

This work was funded by the German Research Foundation [grant number: DFG, FOR RO 2652/1-1]. Impedance analyzer and confocal microscope were funded by the Free State of Saxony (SMWK) and the European Union (EFRE) [grant number: 100185265].

## 2.7 References

1. T. Rodrigues, P. Schneider and G. Schneider, *Angew Chem Int Ed Engl*, 2014, 53, 5750-5758.
2. C. Dincer, R. Bruch, A. Kling, P. S. Dittrich and G. A. Urban, *Trends in biotechnology*, 2017, DOI: 10.1016/j.tibtech.2017.03.013.
3. S. J. Lo and D. J. Yao, *Int J Mol Sci*, 2015, 16, 16763-16777.
4. C. Arrigoni, M. Gilardi, S. Bersini, C. Candrian and M. Moretti, *Stem Cell Rev*, 2017, 13, 407-417.
5. H. F. Tsai, A. Trubelja, A. Q. Shen and G. Bao, *J R Soc Interface*, 2017, 14.
6. R. J. Beulig, R. Warias, J. J. Heiland, S. Ohla, K. Zeitler and D. Belder, *Lab on a chip*, 2017, 17, 1996-2002.
7. J. J. Heiland, R. Warias, C. Lotter, L. Mauritz, P. J. Fuchs, S. Ohla, K. Zeitler and D. Belder, *Lab on a chip*, 2016, 17, 76-81.
8. C. Lotter, E. Poehler, J. J. Heiland, L. Mauritz and D. Belder, *Lab on a chip*, 2016, 16, 4648-4652.
9. C. Dietze, C. Hackl, R. Gerhardt, S. Seim and D. Belder, *Electrophoresis*, 2016, 37, 1345-1352.
10. T. A. Meier, R. J. Beulig, E. Klinge, M. Fuss, S. Ohla and D. Belder, *Chem Commun (Camb)*, 2015, 51, 8588-8591.

11. S. K. Srivastava, R. Ramaneti, M. Roelse, H. D. Tong, E. X. Vrouwe, A. G. M. Brinkman, L. C. P. M. de Smet, C. J. M. van Rijn and M. A. Jongsma, *RSC Advances*, 2015, 5, 52563-52570.
12. S. Halldorsson, E. Lucumi, R. Gomez-Sjoberg and R. M. Fleming, *Biosensors & bioelectronics*, 2015, 63, 218-231.
13. S. Jezierski, A. S. Klein, C. Benz, M. Schaefer, S. Nagl and D. Belder, *Analytical and bioanalytical chemistry*, 2013, 405, 5381-5386.
14. K. Heileman, J. Daoud and M. Tabrizian, *Biosensors & bioelectronics*, 2013, 49, 348-359.
15. Y. Xu, X. Xie, Y. Duan, L. Wang, Z. Cheng and J. Cheng, *Biosensors & bioelectronics*, 2016, 77, 824-836.
16. V. te Kamp, R. Lindner, H. G. Jahnke, D. Krinke, K. B. Kostelnik, A. G. Beck-Sickinger and A. A. Robitzki, *Biosensors & bioelectronics*, 2015, 67, 386-393.
17. C. W. Scott and M. F. Peters, *Drug Discov Today*, 2010, 15, 704-716.
18. O. Pänke, W. Weigel, S. Schmidt, A. Steude and A. A. Robitzki, *Biosensors & bioelectronics*, 2011, 26, 2376-2382.
19. M. Weyer, H. G. Jahnke, D. Krinke, F. D. Zitzmann, K. Hill, M. Schaefer and A. A. Robitzki, *Analytical and bioanalytical chemistry*, 2016, 408, 8529-8538.
20. D. Seidel, J. Obendorf, B. Englich, H. G. Jahnke, V. Semkova, S. Haupt, M. Girard, M. Peschanski, O. Brustle and A. A. Robitzki, *Biosensors & bioelectronics*, 2016, 86, 277-286.
21. S. Jezierski, L. Gitlin, S. Nagl and D. Belder, *Analytical and bioanalytical chemistry*, 2011, 401, 2651-2656.
22. N. Mittal, A. Rosenthal and J. Voldman, *Lab on a chip*, 2007, 7, 1146-1153.
23. M. G. Moisescu, M. Radu, E. Kovacs, L. M. Mir and T. Savopol, *Biochimica et biophysica acta*, 2013, 1828, 365-372.
24. A. P. Mazzoleni, B. F. Sisken and R. L. Kahler, *Bioelectromagnetics*, 1986, 7, 95-99.
25. Y. S. Sun, *Molecules*, 2016, 21.

26. M. L. Rathod, J. Ahn, N. L. Jeon and J. Lee, *Lab on a chip*, 2017, DOI: 10.1039/C7LC00340D.
27. P. Wolf, A. Rothermel, A. G. Beck-Sickinger and A. A. Robitzki, *Biosensors & bioelectronics*, 2008, 24, 253-259.
28. H. G. Jahnke, A. Rothermel, I. Sternberger, T. G. Mack, R. G. Kurz, O. Pänke, F. Striggow and A. A. Robitzki, *Lab on a chip*, 2009, 9, 1422-1428.
29. J. Hua, L. E. Erickson, T. Y. Yiin and L. A. Glasgow, *Crit Rev Biotechnol*, 1993, 13, 305-328.
30. Y. Chisti, *Crit Rev Biotechnol*, 2001, 21, 67-110.
31. A. Soghomonians, A. I. Barakat, T. L. Thirkill, T. N. Blankenship and G. C. Douglas, *Biochimica et biophysica acta*, 2002, 1589, 233-246.
32. S. H. Kim, K. Ahn and J. Y. Park, *Lab on a chip*, 2017, 17, 2115-2124.
33. H. J. Lee, M. F. Diaz, K. M. Price, J. A. Ozuna, S. Zhang, E. M. Sevick-Muraca, J. P. Hagan and P. L. Wenzel, *Nat Commun*, 2017, 8, 14122.
34. L. Ghenim, H. Kaji, Y. Hoshino, T. Ishibashi, V. Haguët, X. Gidrol and M. Nishizawa, *Lab on a chip*, 2010, 10, 2546-2550.
35. R. Szulcek, H. J. Bogaard and G. P. van Nieuw Amerongen, *J Vis Exp*, 2014, DOI: 10.3791/51300.
36. B. Wojciak-Stothard and A. J. Ridley, *J Cell Biol*, 2003, 161, 429-439.

---

## 2.8 Supplementary Information

### 2.8.1 Supplementary Materials and Methods

#### *Fabrication of microelectrode arrays and microfluidic structures*

Briefly, cleaned glass substrates (Borofloat 49/49/1.1 mm, Goettgens Industriearmaturen, Germany) were spin-coated with 3  $\mu\text{m}$  negative resist (AR-N 4340, Allresist GmbH, Germany) and baked for 90 s at 95°C. Structures were passed on the substrate via photomask (10 s UV-light, 350 nm to 425 nm) and MA6 Mask Aligner (SÜSS MicroTec, Germany) followed by development in AR 300-475 (Allresist GmbH, Germany). Electrode structures were generated by sputtering (CREAMET 500, CREAVAC GmbH, Germany) of 50 nm Ti as adhesion layer followed by 350 nm gold onto the substrate. Afterwards, remaining photoresist and metal deposition were removed in acetone. A 1  $\mu\text{m}$  thick passivation layer was generated using negative photoresist SU8-2 (Micro Resist Technology, Germany). Finally the MEA was cleaned in ultrapure water, spin-dried and plasma-cleaned at 400 mA for 7 min into the vacuum chamber (CREAMET 500, CREAVAC GmbH).



## 2.8.2 Supplementary Figures

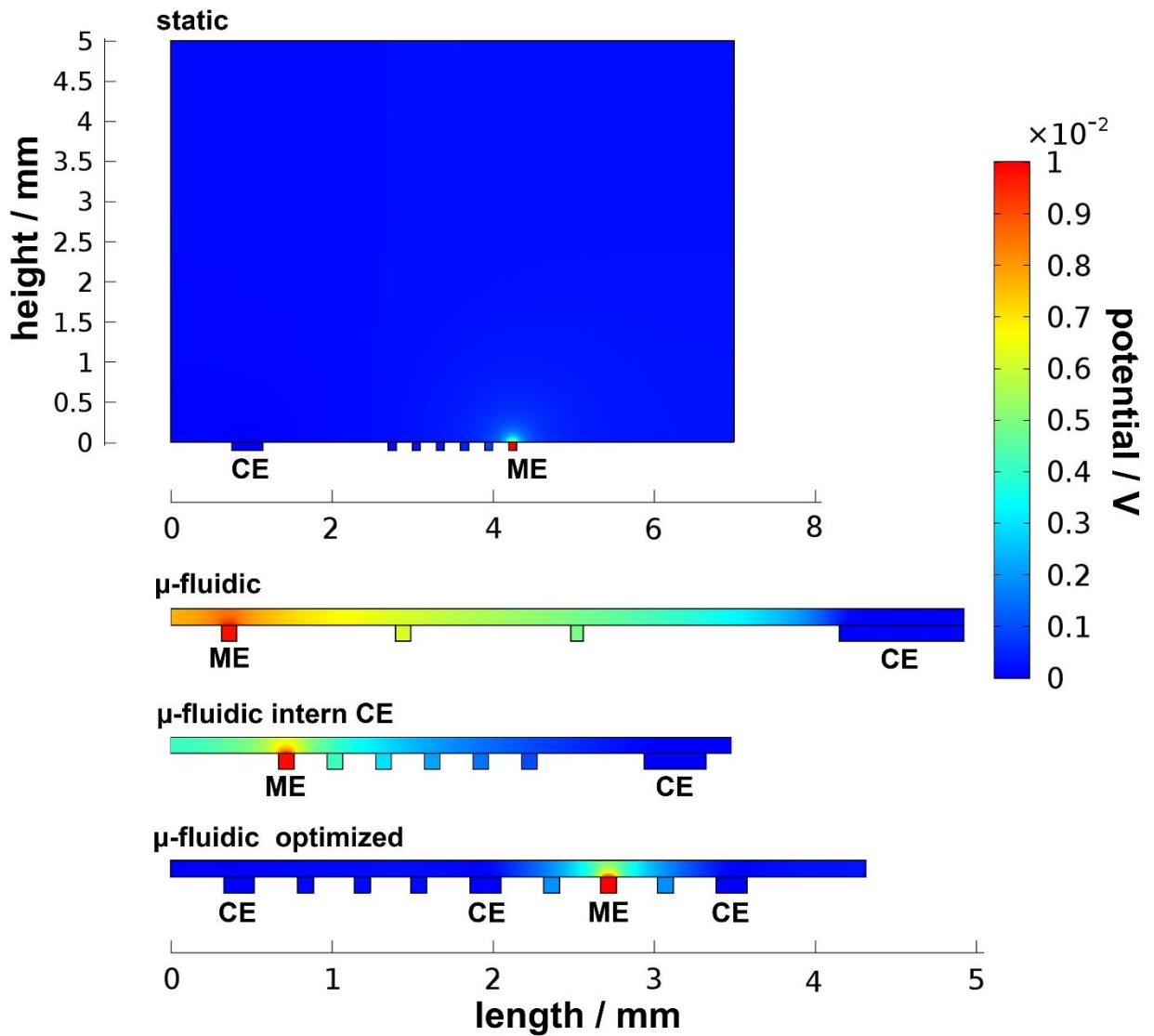


**Figure S 2.1: Cross-section of FEM simulation derived potential field.** The cross section was done through the active measurement electrode (ME) with an applied potential of 10 mV and the counter electrode (CE) that is connected to the ground. The potential field is shown for 100 kHz. The height of the microfluidic devices is 100  $\mu$ m.

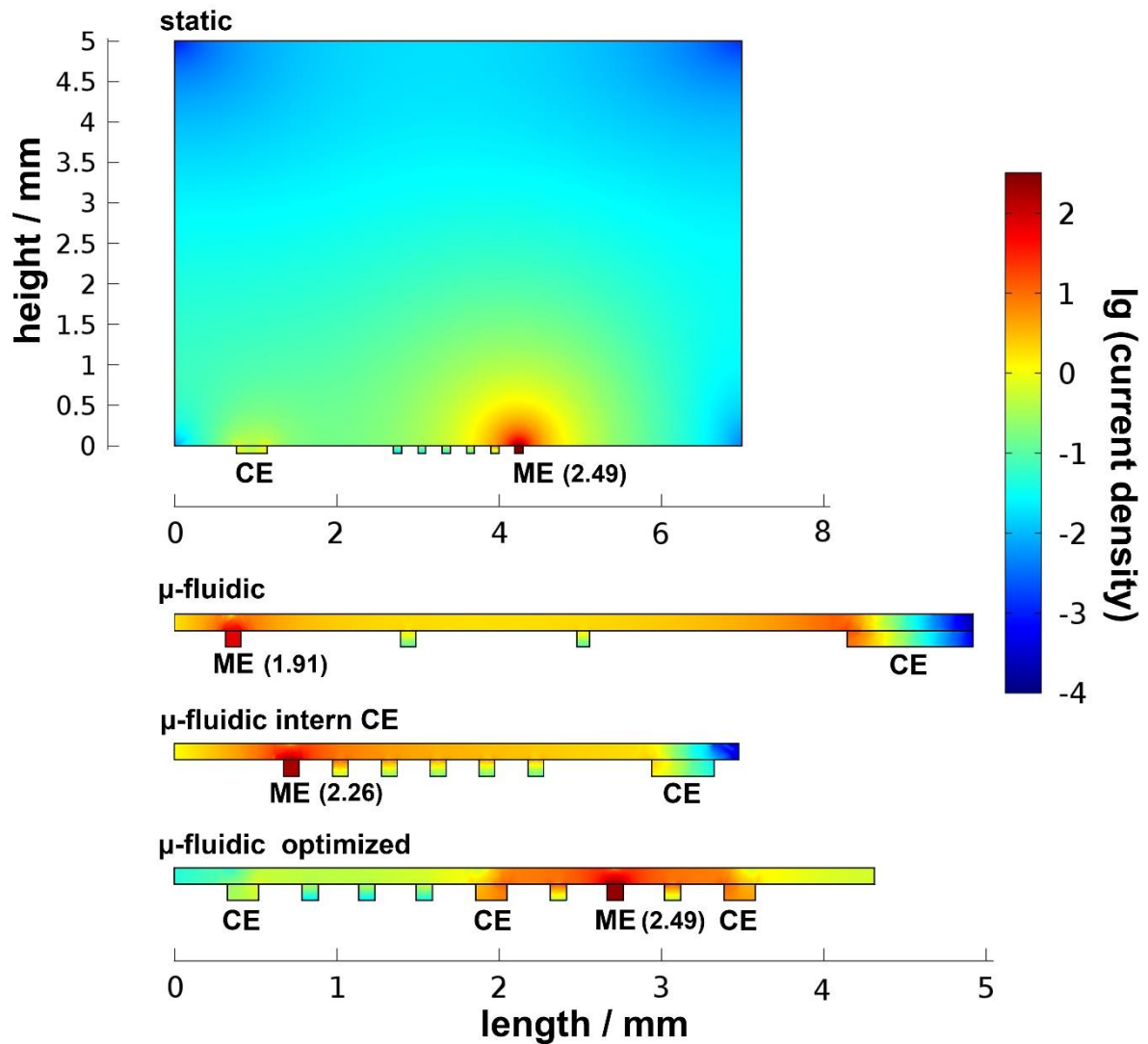


**Figure S 2.2: Cross-section of FEM simulation derived current density field.** The cross section was done through the active measurement electrode (ME) with an applied potential of 10 mV at 100 kHz and the counter electrode (CE) that is connected to the ground. For better visualization, the current density is shown on a logarithmic scale and the maximum values at the measurement electrode is given in brackets. The height of the microfluidic devices is 100  $\mu\text{m}$ .

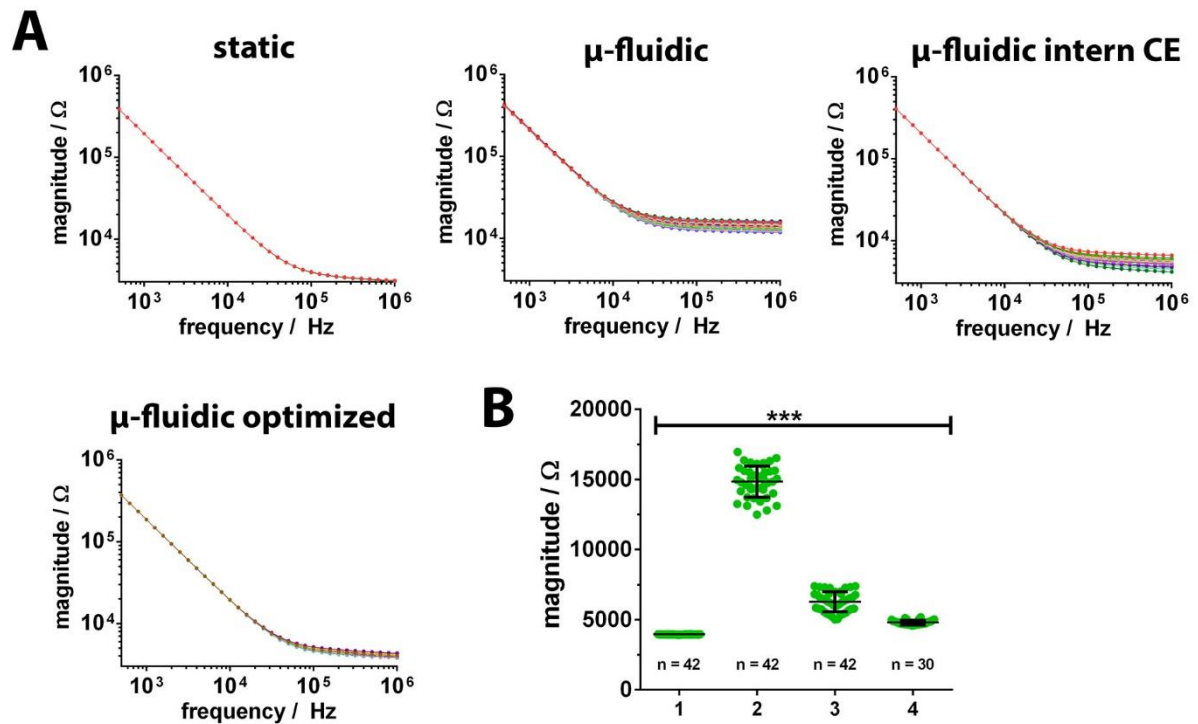


**Figure S 2.3: Influence of the microfluidic structure on the measurement-counter-electrode distance.** (A) FEM simulations were performed for all measurement electrodes within the arrays with 42 electrodes for the static, μ-fluidic and μ-fluidic intern CE layout as well as 30 electrodes for the μ-fluidic optimized layout. The simulation derived impedance magnitude spectra are shown. (B) Statistical analysis for the impedance magnitude at 100 kHz (mean ± s.d.). The test of significance for the static (1), μ-fluidic (2), μ-fluidic intern CE (3) and μ-fluidic optimized (4) layout revealed an extremely significant difference for all groups against each other ( $p < 0.001$ ).

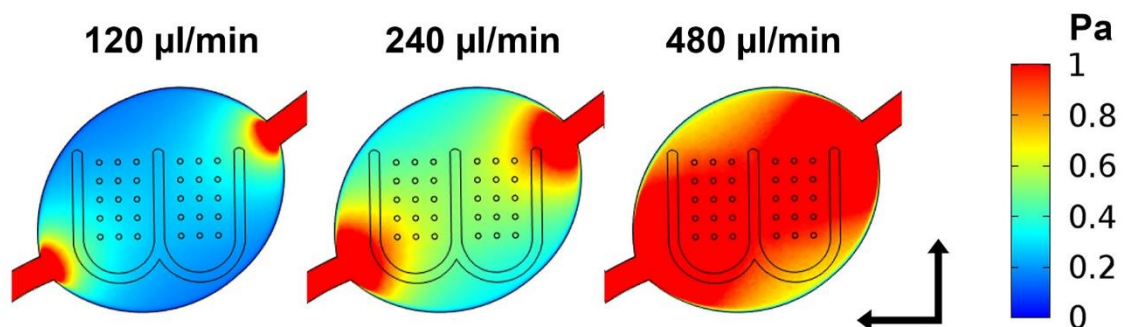


**Figure S 2.4: Influence of flow rate on shear stress.** FEM simulation derived shear stress in Pascal dependent on flow rate (XY-scale = 1.5 mm).

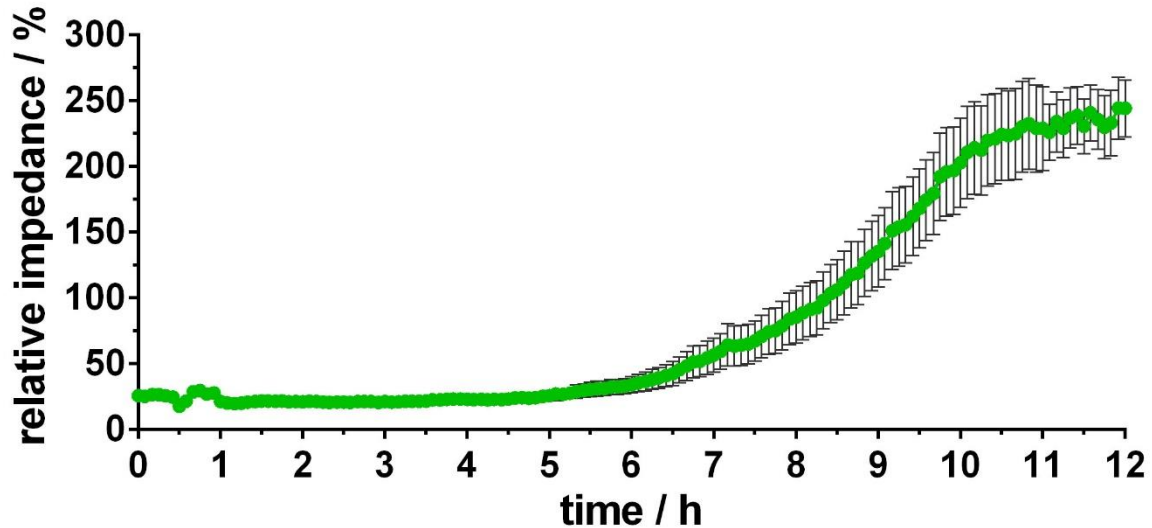


**Figure S 2.5: Relative impedance trace over time of HEK-Y1 cell cultured under microfluidic conditions.** Culturing under microfluidic condition and recording of impedance spectra was started after initial 45 minutes of HEK-Y1 cell adherence, marked as time point 0 hours ( $n = 25$  electrodes).

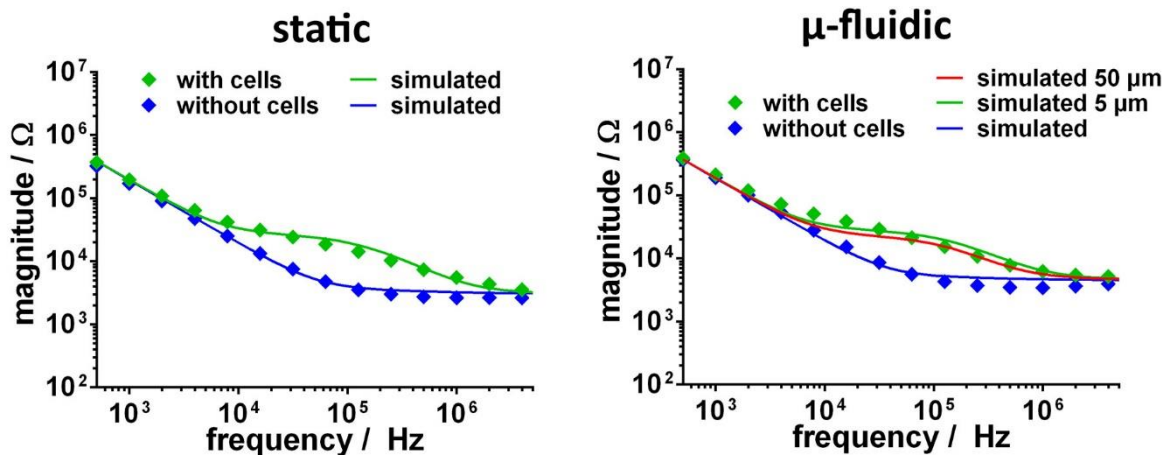


**Figure S 2.6: Influence of the cell height in the microfluidic structure on the impedance magnitude.** The impedance spectra measured in the static setup were used to determine the cell capacitance ( $0.008 \text{ F/m}^2$ ) and resistance ( $0.0002 \text{ Ohm} \times \text{m}^2$ ) by an equivalent circuit fitting. Therefore, a self-written LabView program was used. In the FEM simulation a cell layer represented by an electrode covering cylinder) with a height of  $5 \mu\text{m}$  was introduced and covered with a contact impedance with the determined cell resistance and capacitance. This represents the impedance signal dominating cell membrane. Afterwards, the cell layer height was increased to  $50 \mu\text{m}$ , which lead to a small cell impedance decrease but not to a basal impedance magnitude increase.

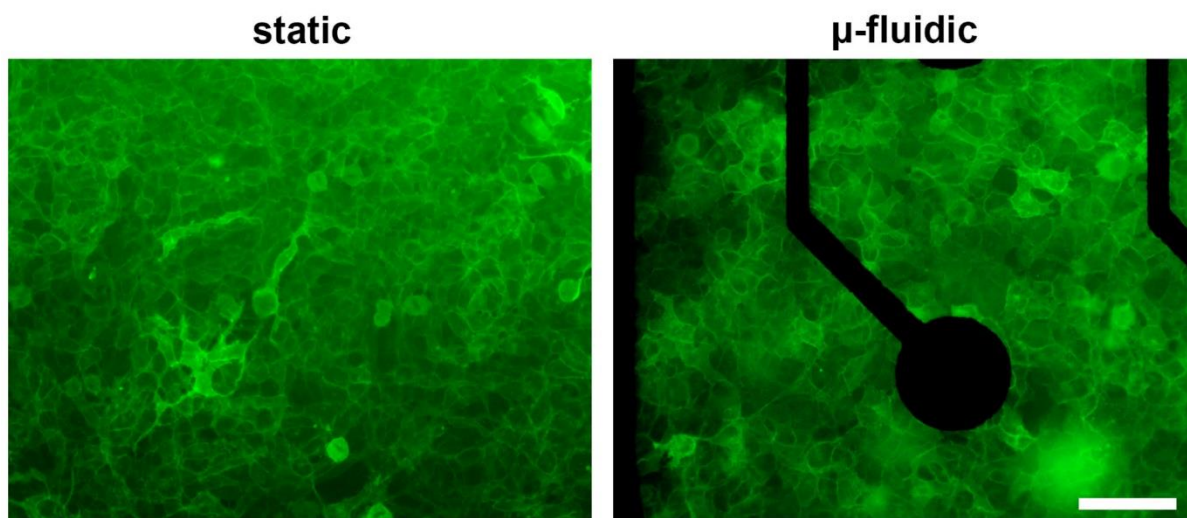


**Figure S 2.7: Recombinant Y1-receptor expression in HEKA cells under static and microfluidic conditions.** (scale bar 100  $\mu\text{m}$ ).

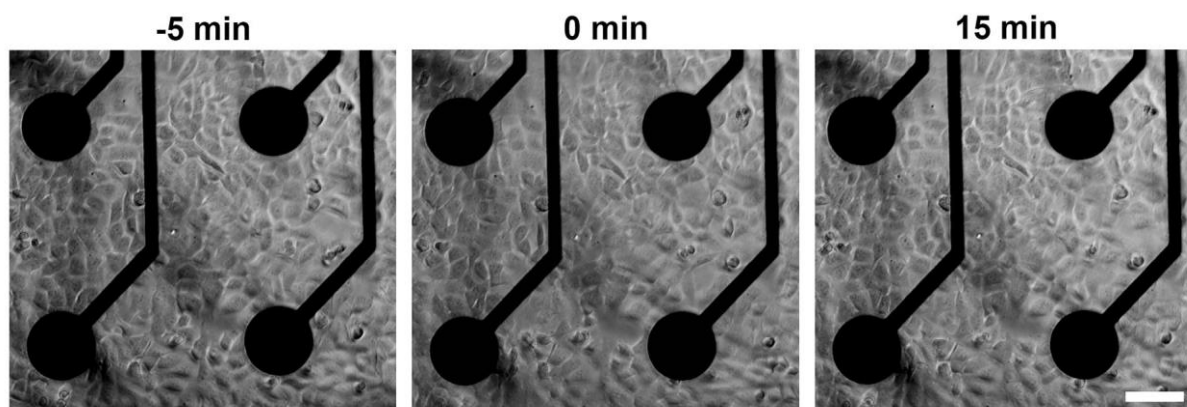


**Figure S 2.8: Microscopic images of NPY treated HEK-Y1 cells cultured under microfluidic conditions.** HEK-Y1 cells were monitored by transmission light microscopy before (-5 min), at the time point of 100 nM NPY application (0 min) and 15 min after application. (scale bar 100  $\mu\text{m}$ ).

### 2.8.3 Supplementary Movie 1

Time lapse movie (12 hours) of HEK-Y1 cells that adhere and spread over the microelectrode array within the optimized microfluidic microelectrode array chip under microfluidic cultivation conditions. Flow direction is from lower right to upper left.

## **Chapter 3**

### **Research Article II**

---

# **MICROFLUIDIC FREE-FLOW ELECTROPHORESIS BASED SOLVENT EXCHANGER FOR CONTINUOUSLY OPERATING LAB-ON-CHIP APPLICATIONS**

---

Published in *Analytical Chemistry* (2017), 89 (24), pp 13550–13558

doi: 10.1021/acs.analchem.7b03959

Franziska D. Zitzmann, Heinz-Georg Jahnke, Simon A. Pfeiffer, Ronny Frank, Felix Nitschke, Laura Mauritz, Bernd Abel, Detlev Belder, Andrea A. Robitzki

### 3.1 Abstract

For miniaturization and integration of chemical synthesis and analytics on small length scales, the development of complex lab-on-chip (LOC) systems is in the focus of many current research projects. While application specific synthesis and analytic modules and LOC devices are widely described, the combination and integration of different modules is intensively investigated. Problems for in-line processes such as solvent incompatibilities, e.g., for a multistep synthesis or the combination of an organic drug synthesis with a cell-based biological activity testing system, require a solvent exchange between serialized modules. Here, we present a continuously operating microfluidic solvent exchanger based on the principle of free-flow electrophoresis for miscible organic/aqueous fluids. We highlight a proof-of-principle and describe the working principle for the model compound fluorescein, where the organic solvent DMSO is exchanged against an aqueous buffer. The DMSO removal performance could be significantly increased to 95% by optimization of the microfluidic layout. Moreover, the optimization of the inlet flow ratio resulted in a minimized dilution factor of 5, and we were able to demonstrate that a reduction of the supporting instrumentation is possible without a significant decrease of the DMSO removal performance. Finally, the compatibility of the developed solvent exchanger for cell based downstream applications was proven. The impedimetric monitoring of HEK293A cells in a continuously operating microfluidic setup revealed no adverse effects of the residual DMSO after the solvent replacement. Our solvent exchanger device demonstrates the power of micro-free-flow electrophoresis not only as a powerful technique for separation and purification of compound mixtures but also for solvent replacement.

### 3.2 Introduction

Microfluidics has become a highly dynamic and exciting field of interdisciplinary analytical research due to the benefits of miniaturization involving speed, efficiency, and savings in solvent, reagent, and energy consumption.<sup>1</sup> Given the trend to micrototal analysis systems ( $\mu$ TAS) and lab-on-a-chip devices (LOC), research attempts to combine continuous microreactor synthesis with subsequent direct product purification, analysis, and property testing.<sup>2</sup> However, the required solvent often differs for the consecutive microfluidic modules for sequential process steps. For example, most of the chemical syntheses have to be performed in organic solvents. In contrast, the testing of microreactor products, especially in the case of biological active compounds, pharmaceutical ingredients, and in the presence of cells employing biosensors, has to be performed in aqueous buffers. While biosensor units such as optimized enzymes, antibodies, and other proteins work partly

even up to 20–30% organic cosolvent,<sup>3</sup> cell cultures typically do not tolerate organic solvents above 10%.<sup>4</sup> Another example is multistep organic synthesis reactions that often require solvent exchange to access the wide variety of established reaction conditions.<sup>5,6</sup>

In this context, there is a demand for buffer exchange devices that can be easily miniaturized and integrated in complex  $\mu$ TAS and LOC systems. To transfer a single compound between two immiscible solvents, micro-liquid–liquid extraction is widely applied, based on passive diffusion and the Nernst distribution coefficient.<sup>7,8</sup> In the case of miscible solvents, such as water/organic solvents mixture, solvent evaporation<sup>9,10</sup> and distillation methods<sup>11,12</sup> are suitable to considerably remove or separate solvents differing in their volatility. In any case, the introduced solvent removal method adds up to the modularity and complexity of microfluidic devices, and the organic solvent removal performances are partially clearly limited. Furthermore, these methods are not suitable for organic solvents with low vapor pressure like DMSO (0.06 kPa). To overcome this limitation we propose and in turn demonstrate a one-step solvent exchange procedure in a simplified microfluidic setup by the use of micro-free-flow electrophoresis ( $\mu$ FFE).  $\mu$ FFE was developed for the separation of multiple compounds in continuously operating LOC applications.<sup>13-15</sup> However, this technique has generally been optimized for the highly resolved separation of compound mixtures and is therefore complex and technically demanding with regard to space and microfluidic equipment. In contrast, the capabilities of  $\mu$ FFE for the use as a solvent exchanger have not yet been investigated or even optimized.

Thus, in the present paper we highlight the proof of principle and geometry optimization of a  $\mu$ FFE system based solvent exchanger for the active transfer of a model compound from the organic to the aqueous phase in a miscible fluid system. Moreover, this module is designed to work under continuous flow conditions and provide compatibility with downstream cell based analysis for detection of biological activity.

### **3.3 Experimental Section**

#### **3.3.1 Fabrication of Microfluidic Free-Flow Electrophoresis Chips**

$\mu$ FFE chips were fabricated by photopolymerization of polyethylene glycol diacrylate (PEG-DA) using modifications of a procedure previously described for microfluidic chip production.<sup>16</sup> Briefly, connection holes at the inlet/outlet position of the cover plates (Henneberg & Co, Manebach, Germany) were created by a sand blaster (Barth Serienapparate, Germany) with granulate of 50  $\mu$ m particle size. For a defined distance



between the glass slides, double-sided tape (468MP Adhesive, 130  $\mu\text{m}$  of thickness, 3M, Neuss, Germany) was arranged between the TPM-coated cover and base plate. PEG-DA (Sigma-Aldrich, Germany; MW 258) with 1% (w/w) 2,2-dimethoxy-2-phenylacetophenone (Sigma-Aldrich, Germany) was filled without air bubbles between the glass slides. The chip was placed in the mask aligner (Süss Micro Tec MA6, Garching, Germany), and a light-impermeable photomask (offset print, 3600 dpi, DTP-System-Studio, Leipzig, Germany) containing the microfluidic structures was aligned. The photopolymerization was carried out with a Hg lamp ( $\lambda = 350\text{--}405\text{ nm}$ ;  $P = 12\text{ mW/cm}^2$ ) at an illumination time of 1.5 s. Afterward, the nonpolymerized prepolymer was removed by reduced pressure, and the microfluidic structures were rinsed with ethanol (70%, v/v in water) to remove PEG-DA residues. Finally, the chip was re-exposed to UV-light for 30 s. Silicon tubes were bonded at the cover plate holes to connect the chip to microfluidic pumps.

### 3.3.2 Microfluidic Free-Flow Electrophoresis Device Operation

$\mu\text{FFE}$  chips were used for a continuous electrophoretic exchange of an organic solvent. To prevent electroosmotic flow, a dynamic coating of the  $\mu\text{FFE}$  chips for 10 min was applied using the following coating solution mixture: 20 mM 4-(2-hydroxyethyl)-1-piperazineethanesulfonic acid (Sigma-Aldrich, Germany), 0.2% hydroxypropyl methylcellulose (w/w, Alfa acer, Germany), and 0.1% Tween 20 (w/w, Carl Roth, Germany). For hydrodynamic injection,  $\mu\text{FFE}$  chips were connected to neMESYS syringe pumps (CETONI, Korbussen, Germany) fitted out with glass syringes (ILS, Stützerbach, Germany). Phosphate buffer (5 mM, consisting of sodium dihydrogen phosphate dihydrate and disodium hydrogen phosphate dehydrate, both Carl Roth, Karlsruhe, Germany; adjusted to pH 7.4) was used as the separation buffer. The fluorescent dyes Rhodamine B and sodium fluorescein (both 500  $\mu\text{M}$ , Sigma-Aldrich, Germany) were dissolved in dimethyl sulfoxide (DMSO, 100%, VWR, Germany).

The removal of DMSO took place using the following flow rates: For the  $\mu\text{FFE}$  chip with five inlet channels, we applied 10  $\mu\text{L}/\text{min}$  for electrode channels, 5  $\mu\text{L}/\text{min}$  for inlets for the electrode support, and 0.5–2  $\mu\text{L}/\text{min}$  for the sample inlet. For the  $\mu\text{FFE}$  chip with three inlet channels, 15  $\mu\text{L}/\text{min}$  was applied for the electrode channels, and 2  $\mu\text{L}/\text{min}$  was applied for the sample inlet. The electric field was induced by external copper electrodes connected to a voltage source (FuG Elektronik, Schechen, Germany).

The fluorescence observation was performed using a fluorescence microscope (Nikon eclipse, TE2000-U) equipped with a Hg arc lamp as light source, a 2 $\times$  objective (Nikon

PlanApo 2x/0.10, WD8.5), a camera (Andor Neo scMOS, UK), and a filter set (Nikon) for multiple excitation and emission wavelengths bands compatible for Rhodamine B ( $\lambda_{\text{exc}}$  553 nm/ $\lambda_{\text{em}}$  627 nm) and fluorescein ( $\lambda_{\text{exc}}$  460 nm/ $\lambda_{\text{em}}$  515 nm).

### 3.3.3 Determination of DMSO and Fluorescein Concentration

Fluorescein concentrations in the runoff of the  $\mu$ FFE platform were determined using spectrofluorometry. The effluent samples were diluted 1:100 (v/v) using CAPS buffer (Sigma-Aldrich, Germany; 100 mM, pH 10) in microcuvettes and placed in a spectrofluorimeter (Jasco FP-6200, Großumstadt, Germany). Fluorescence excitation was set at 485 nm, and emission spectra were collected from 500 to 600 nm. External calibration using standards was performed. A linear relationship between fluorescein concentration and fluorescence intensity was obtained for emission intensity at 512 nm. Cross sensitivity with Rhodamine B present in solution was not significant.

DMSO concentrations were determined using liquid chromatography and absorbance detection at 210 nm loosely based on a literature procedure.<sup>17</sup> The chromatograph was a Class-VP (Shimadzu, Duisburg, Germany) equipped with a ProntoSIL 100-5-CN column (120 mm  $\times$  3 mm, Knauer, Berlin, Germany) and a diode array detector (SPD-M10 AVP, Shimadzu). Samples were diluted with purified water as needed, and 5  $\mu$ L was injected into the system. The mobile phase (200  $\mu$ L/min) consisted of purified water and acetonitrile (99.9%/ 0.1%). An external calibration with standards was performed, and a linear relationship between peak area (210 nm) and DMSO concentration was obtained.

### 3.3.4 Cell Culture and Impedimetric Monitoring

HEK293A cells (Life Technologies, Germany) were grown in DMEM medium, prepared from DMEM low glucose powder (Sigma-Aldrich, Germany) by addition of 3.7 g/L D-glucose (Carl Roth, Germany) and supplemented with 10% fetal bovine serum (v/v), 2 mM Glutamax, 100 units/mL penicillin, and 100  $\mu$ g/mL streptomycin (all by Life Technologies, Germany) at 37 °C, 5% CO<sub>2</sub>, and 95% humidity. For impedimetric monitoring microelectrode arrays with integrated microfluidic structures were used as previously described.<sup>18</sup> Details of the layout and fabrication can be found in the Supporting Information (page 99). The cell reservoirs were coated with 4 mg/mL collagen I (Life Technologies, Germany) in 0.02 N acetic acid for 3 h at 37 °C, followed by removal of the coating solution and washing steps with phosphate buffered saline (Life Technologies, Germany). Cell reservoirs were filled with a cell suspension of 10 million cells per mL. After

an initial static adhesion time of 45 min at 37 °C, microfluidic chips were connected to neMESYS syringe pumps and cultured with a flow rate of 15  $\mu\text{L}/\text{min}$  overnight at 37 °C on a microscopic stage. Impedimetric monitoring was performed as previously described.<sup>19</sup> Briefly, a high-precision impedance analyzer ISX-3 (ScioSpec Scientific Instruments GmbH, Germany) and a self-developed multiplexer front end was used. Impedance spectra were recorded with 10 mV alternating voltage in a frequency range of 500 Hz to 5 MHz. The relative impedance, which represents the cell signal, was calculated  $(|Z|_{\text{covered}} - |Z|_{\text{cell-free}})/|Z|_{\text{cell-free}} \times 100\%$ , and the maximum was traced over time. To exclude effects of the solvent itself on the impedance, the appropriate cell-free spectra (0%, 0.9%, 20% DMSO) were used for the calculation of the cell signal. For statistical analysis, electrodes covered with cells/sufficient cell signal were selected, and the relative impedance traces were normalized to the beginning of the experiment.

### 3.3.5 Finite Element Method (FEM) Simulation

Microfluidic structure layouts were generated using AutoCAD 2016 (Autodesk) and imported into COMSOL Multiphysics 5.3 (Comsol Multiphysics GmbH, Germany). For simulation of the laminar flow the COMSOL module “laminar flow” was employed. Simulation of the diffusion of both miscible solvents (aqueous buffer and DMSO) was included using the COMSOL module “transport of concentrated species” with the preset “Fick’s law based diffusion model”. Diffusion coefficients were set to  $2.5\text{e-}9 \text{ m}^2/\text{s}$  (water) and  $0.8\text{e-}9 \text{ m}^2/\text{s}$  (DMSO).<sup>20</sup> The simulation was done with the mesh size “coarse” and a direct solver (PARDISO).

### 3.3.6 Software and Statistics

The photomasks of microfluidic structures were designed by Inkscape 0.48. OriginPro 2016 (OriginLab, Northampton, USA) and Graphpad Prism 5 (GraphPad Software, USA) were used for data analysis and plotting. Statistical analyses were conducted using Graphpad Prism. All presented values are means  $\pm$  standard error of mean (SEM). Significance analyses were done by ANOVA and Bonferroni post hoc test. Differences between two means with  $p < 0.05$  were considered significant (\*),  $p < 0.01$  very significant (\*\*), and  $p < 0.001$  highly significant (\*\*\*)

### 3.4 Results and Discussion

#### 3.4.1 Working Principle of the Solvent Exchanger

The solvent exchanger is based on microfluidic free-flow electrophoresis ( $\mu$ FFE). In  $\mu$ FFE samples are continuously pumped through a separation chamber flanked by appropriate buffer streams. An electrical potential is applied perpendicular to the flow direction. Charged components of the sample therefore migrate toward the respective side of the separation bed according to their electrophoretic mobility as schematically shown in Figure 3-1A.

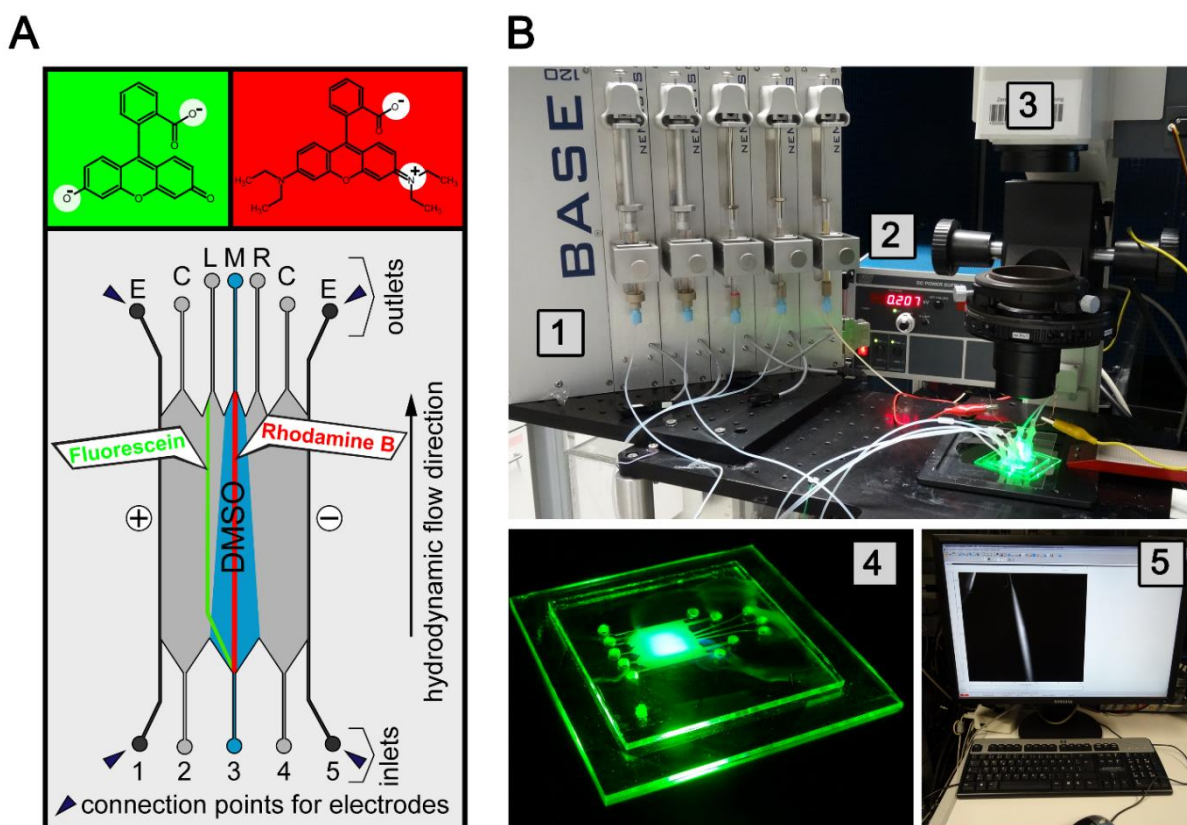


**Figure 3-1: Scheme of the solvent exchanger working principle and supporting instrumentation.** (A) Schematically representation of the  $\mu$ FFE-based device to remove organic solvents from compounds. (1) anionic electrode channel, (2) inlet for the anionic support, (3) sample inlet, (4) inlet for the cationic support, (5) cationic electrode channel, (E/C) outlet channels for sheath flows and (L/M/R) left, middle and right outlet channel for the sample collection. (B) Experimental setup for free flow electrophoresis experiments. (1) Precision low pressure pump, (2) voltage source, (3) fluorescence microscope, (4) microfluidic chip, (5) controlling device.

$\mu$ FFE is commonly used to separate and purify mixtures of charged components (e.g., protein digests). In contrast, we used this technique to extract a compound of interest from a stream of organic solvent into an aqueous medium in this way performing a “solvent exchange”.  $\mu$ FFE is ideal for this purpose, because most organic solvents are uncharged and therefore do not migrate under electrophoresis conditions. The only requirement for

the extracted species is an electrophoretic mobility under appropriate conditions, which is the case for many biologically active compounds such as drugs.<sup>21</sup> However, the separation efficiency and in turn the performance of the proposed solvent exchanger depends on the magnitude of the electrophoretic mobility, and higher charged compounds with large mobility are easier to separate from the solvent.

### 3.4.2 Development of the $\mu$ FFE Based Solvent Exchanger Module

For a proof of principle and due to its wide use as a high solubility solvent for many organic compounds and anionic salts, DMSO was selected to be exchanged. Furthermore, we used the fluorescent dye fluorescein as a model compound that can be easily detected and quantified by fluorescence microspectroscopy. To visualize the DMSO flow during the removal, we used a second fluorescence dye, Rhodamine B, because it is a neutral compound with an overall zero net charge and therefore flows with the DMSO. As exchange buffer, we selected an aqueous phosphate buffer to demonstrate the compatibility with cell-based downstream analysis. The  $pK_a$  value of sodium fluorescein is in the range of 3–4, and the fluorescence intensity of sodium fluorescein decreases strongly below a pH of 7.<sup>22</sup> Therefore, we chose a pH of 7.4 for the buffer. The removal of DMSO from fluorescein was carried out by applying an electric potential using external electrodes that can be simply integrated in the electrode buffer inlets. Depending on the charge, molecules move to the cathode or anode. In our case, fluorescein will migrate to the anode and into the aqueous buffer due to its negative charge, whereas DMSO and Rhodamine B should not be deflected due to their neutral net charge (Figure 3-1A).

For testing and analyzing the performance of the solvent exchanger module, the chip was mounted on a fluorescence microscope and was connected to a precision low pressure pump system and a voltage source (Figure 3-1B). For the quantitative analysis of the DMSO solvent removal performance, we used liquid chromatography with absorbance detection at 210 nm.<sup>17</sup> From the calibration curve (Figure 3-2A) it can be perceived that DMSO concentrations down to 0.001% were detectable by HPLC. Therefore, the method is very sensitive and feasible to determine DMSO at various concentrations.

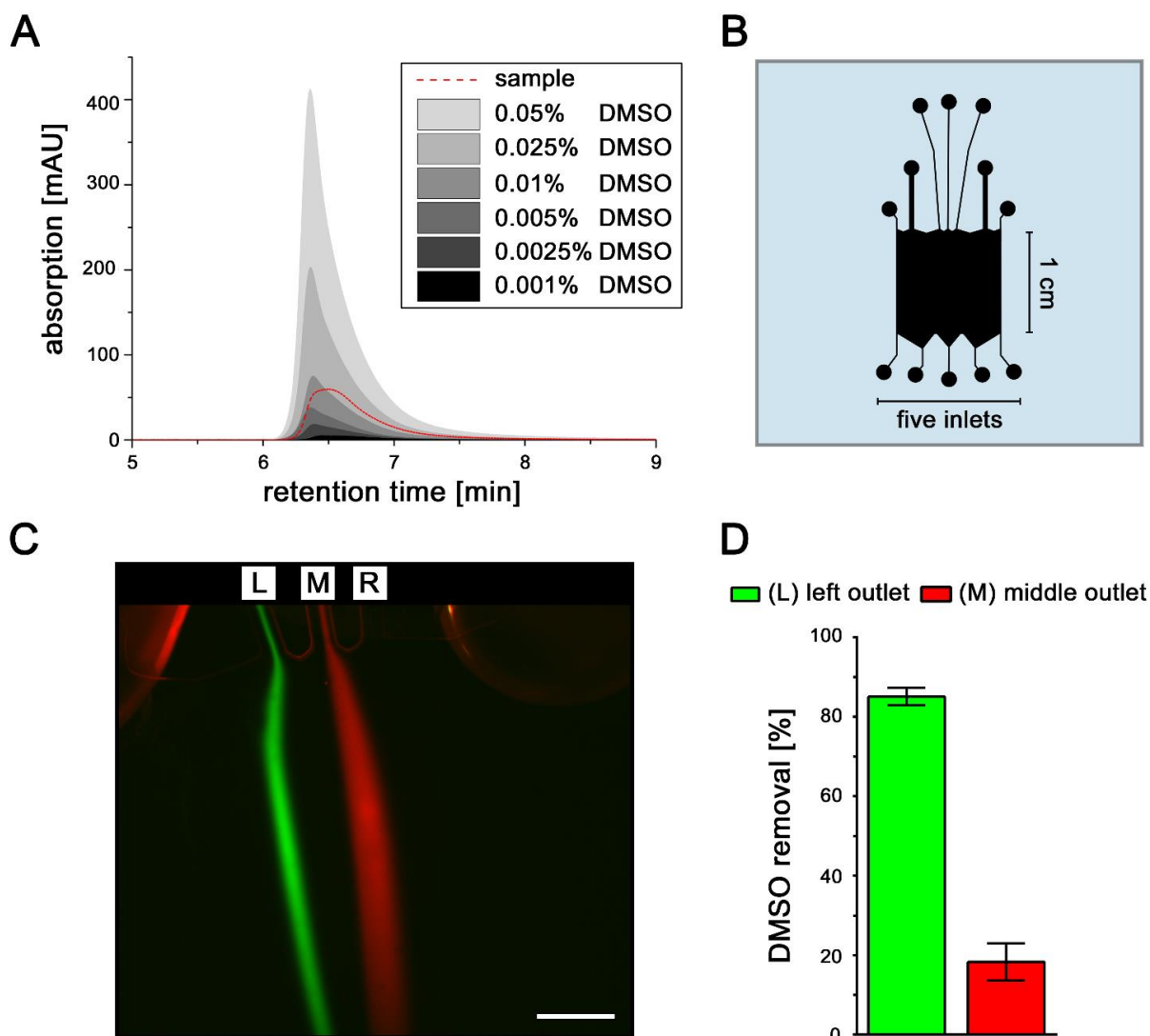


**Figure 3-2: Quantitative analysis of  $\mu$ FFE-based solvent exchange for the model compound fluorescein.** (A) DMSO calibration curve using HPLC. (B) Photomask of the  $\mu$ FFE structure with five inlets and a separation bed length of 1 cm. (C) Deflection of the model compound fluorescein (green). The organic solvent (DMSO) stream is marked by Rhodamine B (red). Flow direction is from bottom to top. (scale bar: 500  $\mu$ m) (D) Quantification of DMSO removal.

To demonstrate the solvent removal, we started with a commonly used  $\mu$ FFE structure (Figure 3-2B) which consists of five inlets for sheath flows, electrode channel flows, and the sample injection inlet in the middle for the model compound fluorescein dissolved in DMSO. The separation compartment length is commonly in the range of 1–2 cm.<sup>13-15</sup> Thus, the dimensions of the separation compartment were 1 cm  $\times$  1 cm, and the minimal channel size was 150  $\mu$ m. However, to avoid extensive dilution of the compound by the supporting sheath flow streams, the outlet channels C (see Figure 3-1A) for the sheath flows were designed with an increased width of 500  $\mu$ m.

For the experiment, a sum flow rate of 30  $\mu$ L/min and a separation potential around 300 V was applied with a resulting electrophoretic current of 200  $\mu$ A. Figure 3-2C shows the

deflection of the fluorescein out of the DMSO flow (marked by the Rhodamine B) toward the anode as expected. The Rhodamine B was slightly deflected toward the cathode, which perhaps could be explained by the incomplete deprotonation of the carboxyl group in the used buffer with a pH of 7.4 and thus a minimal positive net charge. The process was performed continuously, and the model compound in the exchanged aqueous buffer was collected on outlet L (see Figure 3-1B). As a control, we also collected the DMSO solvent flow on outlet M (see Figure 3-1B). In order to quantify the solvent removal performance, the dilution factor was first calculated based on the fluorescein concentration determined in the collected sample from outlet L and the sample inlet (500  $\mu$ M). Since the dilution was 44, the corrected DMSO proportion at outlet L was reduced by  $85.1 \pm 2.1\%$  (Figure 3-2D). As a control, we also determined the DMSO proportion at outlet M that revealed a loss of  $18.31 \pm 4.7\%$ .

Taken together, we were able to successfully demonstrate that a certain proportion (85%) of the organic solvent DMSO could be removed from the model compound fluorescein. With respect to downstream biological activity testing using cell based sensors, the residual 15% DMSO is still a critical value and should be further optimized. Additionally, using this  $\mu$ FFE layout, a dilution of the compound by the factor 44 occurs, which also should be minimized.

### 3.4.3 Optimization of the Solvent Removal Performance

Based on the results from the initial  $\mu$ FFE layout (Figure 3-2B), we aimed to increase first the DMSO removal performance and second to reduce the dilution of the model compound fluorescein. Additionally, we attempted to reduce the extensive technical supporting equipment, especially the number of precision pumps for the sheath flows, because this is a major drawback for integrating and combining  $\mu$ FFE modules on complex lab-on-chip devices.

With a first layout a 85% reduction in DMSO content was achieved at the outlet containing the compound of interest. From the experimental data, we concluded that the remaining proportion of DMSO in outlet L might originate from the lateral diffusion band broadening of the neutral species occurring during the travel through the separation bed which might effectively lead to a spillover of the DMSO band into outlet L. One way to circumvent this would have been to space the outlets further apart - however due to space constraints this was not possible. Therefore, we aimed at reducing the diffusional band broadening of the DMSO stream. As Fonslow and Bowser have shown,<sup>23</sup> the lateral band broadening

depends on the residence time of the sample in the separation bed, which can be reduced by reducing separation bed length, while keeping the same flow rates and separation potential. At the same time the reduced separation bed length also leads to a reduced resolution of the separated compounds.<sup>24</sup> While this is usually not desirable, for the solvent exchanger this was not a problem, because the resolution between the compound of interest and the neutral species DMSO was more than sufficient. Therefore, we tested different separation bed lengths down to 0.5 cm (Figure 3-3A). The fluorescence based monitoring revealed a reliable deflection and collection of the fluorescein out of the Rhodamine B labeled DMSO stream (Figure 3-3B). The statistical analysis of the collected fluorescein samples at outlet L from five independent experiments (Figure 3-3C) revealed an increased DMSO removal for 0.8 cm up to  $90.7 \pm 1.5\%$ . A further reduction of the separation bed to a length of 0.6 cm resulted in a significant higher removal up to  $92.6 \pm 1.3\%$  DMSO and, more strikingly, for 0.5 cm length up to  $95.9 \pm 1.0\%$ .



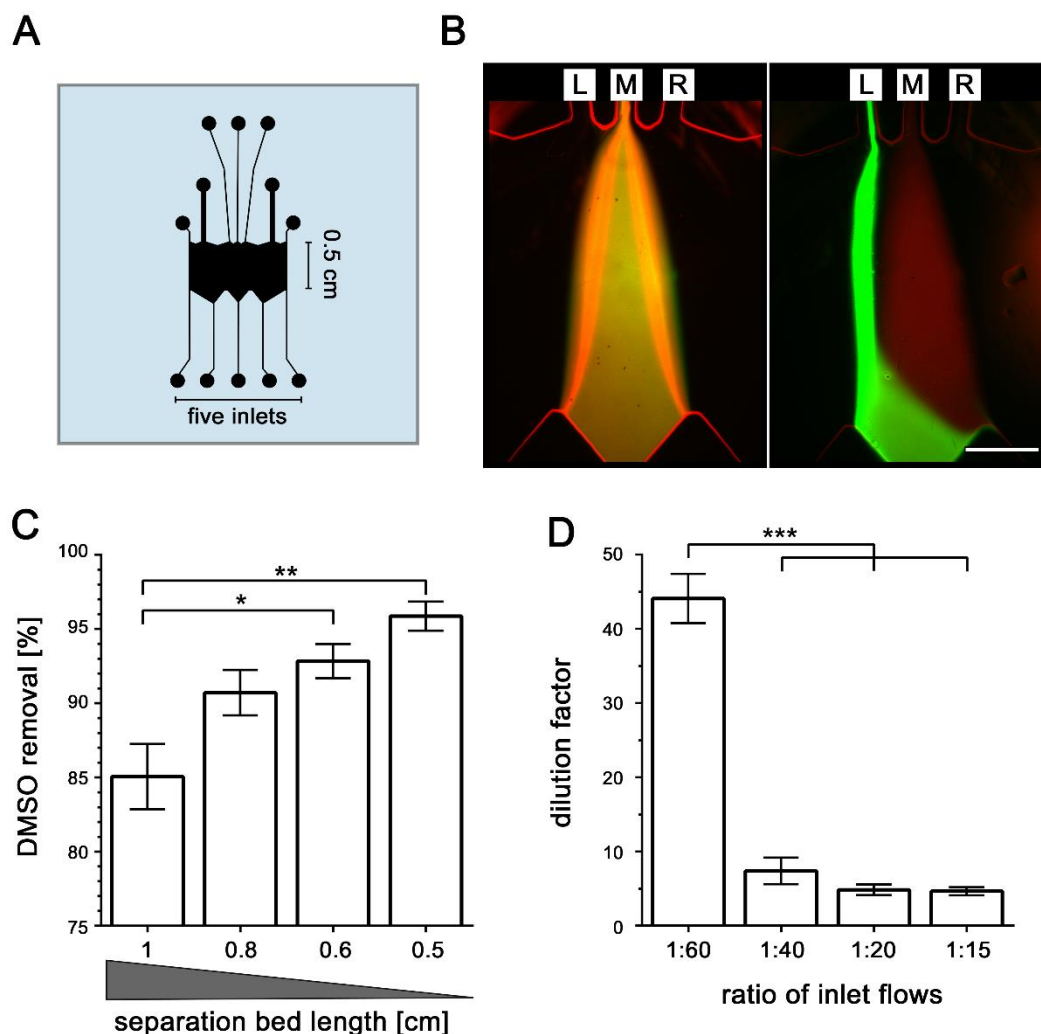


**Figure 3-3: Optimization of the solvent exchanger module for an enhanced DMSO removal performance and a minimized dilution.** (A) Layout with reduced separation bed length of 0.5 cm, adapted outlet channels and five inlet channels. (B) Fluorescence microscopic images without (left) and with (right) applied potential (200 V). The model compound fluorescein is deflected by the applied electrical field (green). The DMSO stream is marked by Rhodamine B. Flows were from bottom to top. (scale bar: 500  $\mu\text{m}$ ) (C) Quantification of the DMSO removal performance in correlation to the reduced separation bed length. (n = 5; \* p < 0.05; \*\* p < 0.01) (D) Statistical analysis of the dilution factor in correlation to the inlet flow ratio (sample flow to supporting flows). (n = 6; \*\*\* p < 0.001)

We attribute this increased removal efficiency to reduced lateral band broadening due to lateral diffusion. To investigate that, we simulated the DMSO diffusion in the microfluidic environment by finite element method based simulation (Figure 3-4), utilizing the layout of the separation bed with 1 and 0.5 cm and inlet flow rates of 1.5  $\mu\text{L}/\text{min}$  for the DMSO stream as well as 5  $\mu\text{L}/\text{min}$  and 15  $\mu\text{L}/\text{min}$  for the inner and outer sheath flow streams, respectively. The diffusion of DMSO in aqueous buffer solution under microfluidic conditions was modeled by the combination of the COMSOL module “laminar flow” and “transport of concentrated species” that allowed the diffusion simulation of two miscible fluids. The resulting DMSO mass fraction distribution within the separation bed clearly

showed the increased lateral diffusion of the highly concentrated DMSO (100% at the central inlet) depending on the separation bed length (Figure 3-4A). In line with this, the XZ-cross section in front of the outlets (Figure 3-4B) showed the clearly broadened DMSO lateral diffusion for the separation bed with 1 cm length vs 0.5 cm length. As a result, the DMSO mass fraction at the compound outlet (L) is found to be clearly increased for the separation bed with 1 cm length vs 0.5 cm length (Figure 3-4C). This effect could be quantitatively modeled and understood employing COMSOL modeling.

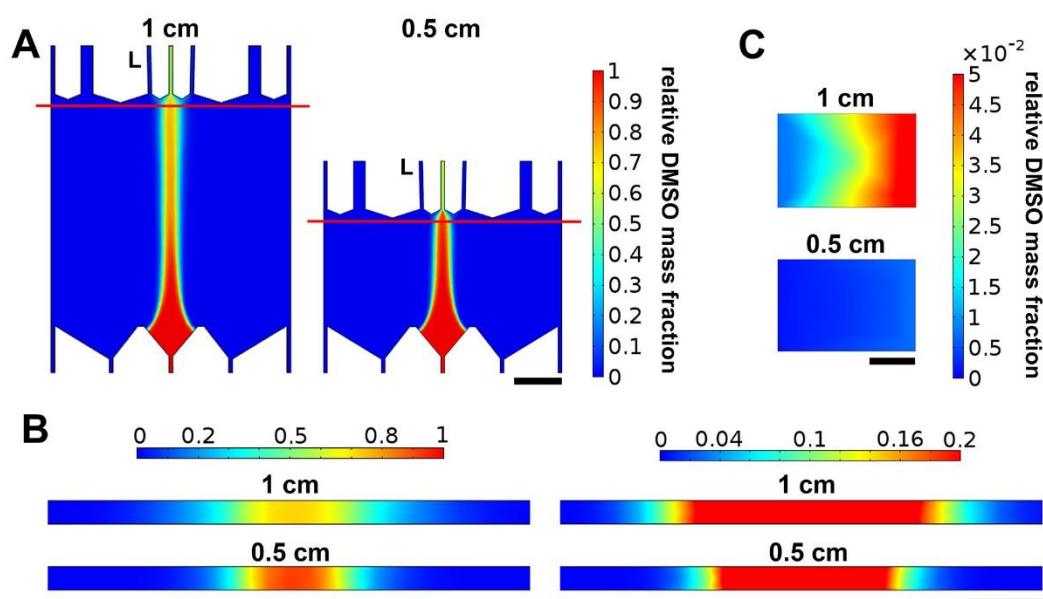


**Figure 3-4: Finite element method based simulation of DMSO lateral diffusion.** (A) XY-cross section of the separation bed at 50  $\mu\text{m}$  height. The color scale shows the relative DMSO mass fraction (color scale maximum 100%, scale bar = 2 mm). At the red line a cross section was defined in front of the outlets. (B) XZ-cross section in front of the outlets showing the lateral diffusion of DMSO at different scale (left: color scale maximum 100%; right: color scale maximum 20%, scale bar = 300  $\mu\text{m}$ ). (C) XZ-cross section at outlet L (color scale maximum 5%, scale bar = 50  $\mu\text{m}$ ).

Next, we aimed to reduce the dilution during the buffer exchange, because this could be unfavorable e.g. if the compound is already considerably diluted within the initial solvent. Since the dilution is caused by the sheath flow rate in correlation with the sample flow rate, we decreased this ratio that was 1:60 for the initial experiments. We tested different flow ratios by increasing the sample inlet flow rate from 0.5  $\mu\text{L}/\text{min}$  to 2  $\mu\text{L}/\text{min}$  and statistically analyzed the dilution factor for six independent experiments (Figure 3-3D). While for the initial ratio of 1:60 the dilution factor was  $44.1 \pm 3.3\%$ , this was significantly reduced down to  $7.4 \pm 1.8\%$  for the ratio of 1:40 and, moreover, down to  $5.5\% \pm 0.6\%$  for the ratio of 1:20 and  $4.6 \pm 0.6\%$  for the ratio of 1:15. Thus, by reducing the inlet flow ratio of the sample

and sheath flows below 1:40, dilution factors in the range of five can be achieved, which is an improvement of more than a factor of 8.

Taken together, the reduction of the separation bed length as well as the reduction of the inlet flow ratio resulted in a significantly improved solvent removal performance with more than 95% and a minimized dilution factor of 5 for the model compound.

With regard to cell-based applications e.g. biological activity tests, the residual DMSO proportion of less than 5% is considered as uncritical as demonstrated in various *in vitro* toxicity studies.<sup>25,26</sup> Although recent studies, in particular on sensitive cell types such as neurons and immune cells, have revealed cytotoxic effects at DMSO concentrations above 1%,<sup>25,4</sup> the achieved DMSO removal performance is clearly uncritical when the minimized dilution factor is taken into account, which results in a final DMSO proportion of less than 1%. To the best of our knowledge, a solvent exchanger for miscible organic/aqueous systems providing the demonstrated performance as shown herein has not been described in the literature so far.

#### **3.4.4 Reduction of $\mu$ -Fluidic Supporting Instrumentation**

Beyond the solvent removal performance, we also wanted to minimize the instrumental effort, especially with regard for implementation in complex lab-on-chip systems e.g. chemical synthesis in combination with (bio) analytical monitoring.

In this context, we adapted the optimized layout of the solvent exchange module (see Figure 3-3A) by reducing the number of sheath flow inlets from four to two (Figure 3-5A). Consequently, only two instead of four precision pumps would be required for the supporting sheath flows. Based on the results of the solvent exchanger module optimization a comparable deflection of the model compound fluorescein could be achieved with the reduced sheath flow inlets as visualized by the fluorescence monitoring (Figure 3-5B). More strikingly, the statistical analysis of the DMSO removal performance from five independent experiments revealed a value of  $92.1 \pm 1.8\%$  (Figure 3-5C) that was significantly higher in comparison with the initial separation bed length and without a significant difference in comparison to the minimized separation bed length (see Figure 3-3C). Additionally, the dilution factor was determined to be  $6.9 \pm 0.8\%$  that was highly significantly lower in comparison to the initial determined dilution factor and comparable to the minimized dilution factors that were achieved by optimization of the inlet flow ratio (see Figure 3-3D).

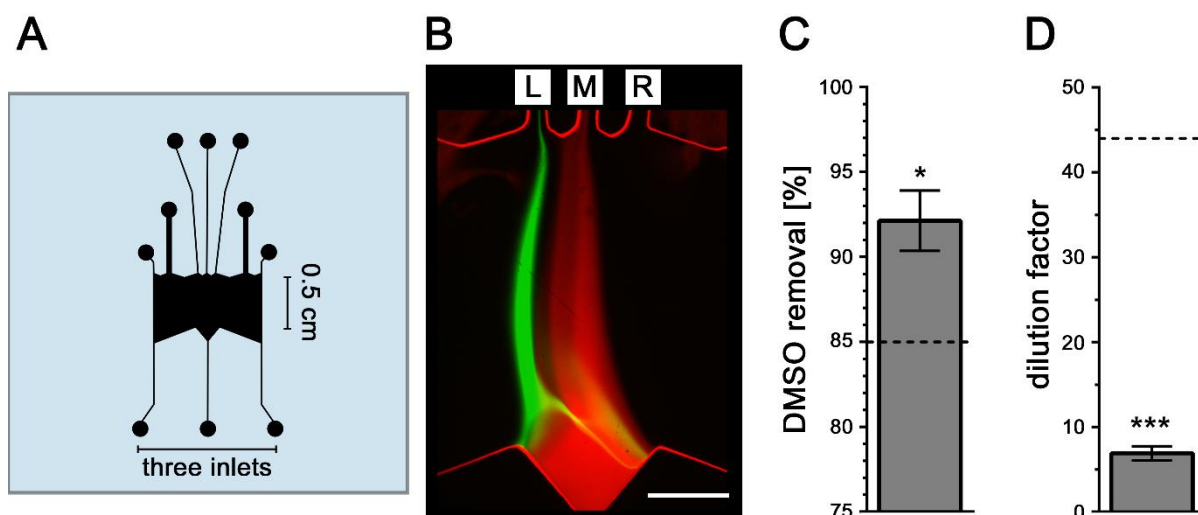


**Figure 3-5: Minimization of supporting instrumentation.** (A) Microfluidic photomask for  $\mu$ FFE with reduced sheath flow inlets (two instead of four). (B) Fluorescence microscopic images with deflected model compound fluorescein (green). The DMSO stream is marked by Rhodamine B. Flow direction is from bottom to top. (scale bar: 500  $\mu$ m) (C) Quantification of the DMSO removal performance for the optimized layout with reduced number of sheath flow inlets and 0.5 cm separation bed length (dashed line = value for initial layout with 5 inlets and separation bed length of 1 cm). (n = 5; \* p < 0.05) (D) Statistical analysis of the dilution factor for the optimized layout (dashed lines = initial experiments with 5 inlets and an inlet flow ratio of 1:60). (n = 5; \*\*\* p < 0.001)

The successful reduction of instrumental efforts without reducing the DMSO removal performance clearly increases the wide applicability of our buffer exchange module and simplifies the integration in complex LOC and  $\mu$ TAS systems.

### 3.4.5 Solvent Exchanger Performance for Cell Based Detection Systems

While the achieved performance of our optimized  $\mu$ FFE based solvent exchanger module with residual DMSO concentrations below 1% is quite uncritical concerning cytotoxic effects,<sup>27,25,26</sup> organic solvents such as DMSO can also influence cell adhesion and cell-cell contacts. Using a sensitive technique such as the multielectrode array based impedimetric monitoring, even small changes in cellular adhesion and cell contacts can be detected. Thus, small impedance changes in the range of 1–5% can occur even for DMSO concentrations of 0.1%.<sup>19</sup> With regard to cell adhesion, which is critical in a continuous operating microfluidic setup, we wanted to demonstrate that our optimized  $\mu$ FFE based solvent exchanger module is suitable for a direct downstream cell based analysis in a microfluidic system. Therefore, we tested the maximum resulting DMSO concentration that could occur for our optimized solvent exchanger module (0.9%). Since a minimized dilution of factor five occurs during the buffer exchange, we also analyzed the effect of 20% DMSO, since this would be the concentration of the solely diluted sample inlet solution without the buffer exchange. To analyze the influence of these concentrations we used a

microelectrode array with integrated microfluidic structures that consisted of three cell cavities with 30 gold electrodes (diameter of 100  $\mu\text{m}$ ) that allows the parallel testing of both concentrations and a control (Figure S 3.1). As a cell culture model we used the human embryonic kidney cell line HEK293A that was used in several studies for the sensitive impedimetric detection of biological activity.<sup>28,29,19</sup> Moreover, these cells were already used in a microfluidic setup without problems.<sup>30</sup> The HEK293A cell layers were cultivated under microfluidic conditions with 15  $\mu\text{L}/\text{min}$  until sufficient electrodes were covered by cells. For the DMSO containing sample addition the flow rate was kept constant. Since the used phosphate buffer had a low osmolality (5 mM), the test solutions were mixed continuously at the inlet of the chip with a 2-fold concentrated cell culture medium in a 1:1 ratio. This means that a further dilution is introduced within the cell-based analytic chip resulting in final DMSO concentrations on the cells of 0.45% for the sample that represents the outlet of our buffer exchange module and 10% for the control sample. While low proportions of organic solvents in the per mill and low percentage range have no distinct influence on the impedance spectra, higher proportions influence the impedance (Figure 3-2). To exclude the influence of the solvent itself on the impedimetric cell signal, appropriate blank values containing the different DMSO proportions were used for calculating the relative impedance traces that represents the cell signal. The relative impedimetric time trace derived from 13 electrodes (Figure 3-6A) revealed a drastic decrease of the relative impedance down to  $12.9 \pm 2.7\%$  for the DMSO control sample (20% DMSO) already after 5 min, which never recovered within the monitored time range of 60 min. In parallel, microscopic images were collected that revealed a distinct loss of cell–cell and cell–substrate adhesion after 5 min reflected by the rounded cell shapes (Figure 3-6B). Hereafter, all cells were completely detached and flushed away by the microfluidic flow as it is shown for the 60 min time point. In contrast, the sample representing the outlet of our buffer exchanger with a concentration of 0.9% DMSO revealed only a slight initial relative impedance decrease after 5 min down to  $96.0 \pm 1.3\%$ , which is comparable to previous observed solvent control effects on HEK293A cells.<sup>19</sup> More strikingly, after 15 min of continuous application the impedimetric time trace for the 0.9% sample was not distinguishable from the untreated control. The microscopic monitoring supports the impedimetric results. During the whole experiment, no morphological alterations of the cells were observed. Thus, the compatibility of our optimized  $\mu\text{FFE}$  based solvent exchanger module with a direct connected downstream cell-based bioanalytic unit could be successfully demonstrated.

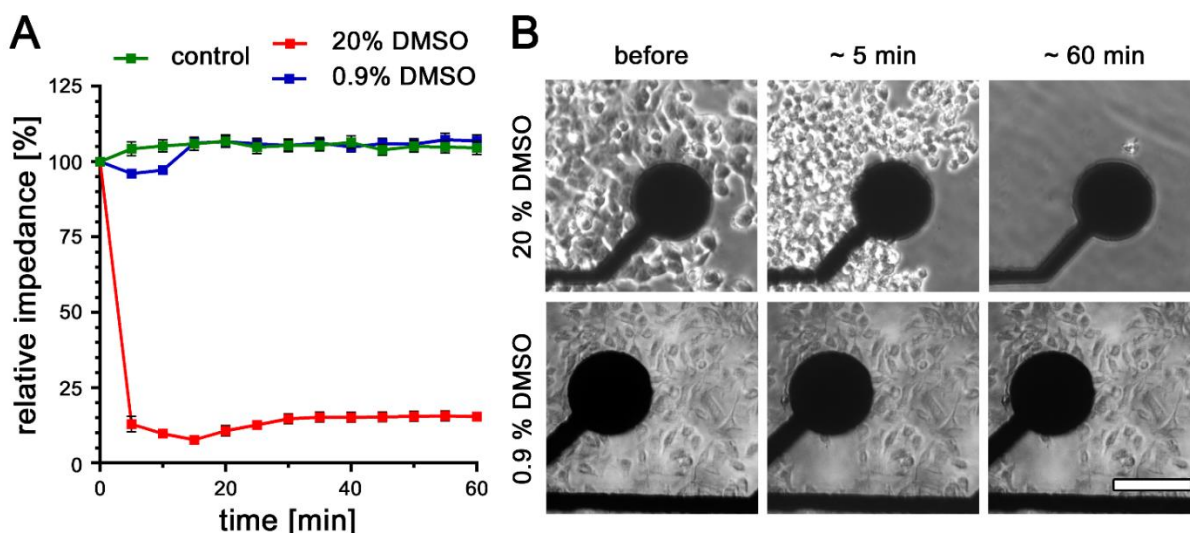


**Figure 3-6: Validation of compatibility with cell based downstream applications in a microfluidic setup.** (A) Time traces of relative impedance derived from HEK293A cells that were cultured under continuous flow conditions. At time point 0 minutes, DMSO samples with different concentrations (as marked) were continuously applied. ( $n = 13$  electrodes). (B) Microscopic images of HEK293A cells cultured under microfluidic conditions at different time points after continuous DMSO addition (scale bar: 100  $\mu\text{m}$ ).

### 3.5 Conclusions

Using free-flow electrophoresis in a microfluidic setup, we successfully demonstrated for the model compound fluorescein the buffer exchange from the organic solvent DMSO to an aqueous solution. The performance as well as mechanistic insight has been highlighted. We could significantly increase the performance of our solvent exchanger module (95% DMSO removal) and minimize the supporting instrumentation by optimization of the layout and flow rates. Subject to the condition of good miscibility of the organic and aqueous solvent, our approach could be suitable for other organic solvents e.g. methanol, ethanol, isopropyl alcohol, *tert*-butyl alcohol, acetone, acetonitrile, dimethylformamide, and tetrahydrofuran. However, it has to be taken into account that the solvent exchanger is based on free-flow electrophoresis, and therefore, only works for charged compounds. Although this offers already a wide spectrum of compounds for the conditions used in this study, this could be additionally expanded by adaption of the used buffer conditions. Thus, by adjusting e.g. the pH of the target buffer, compounds could be deflected in the electrical fields that are not charged under the actual tested conditions. Moreover, derivatization techniques, that were already developed for capillary electrophoresis,<sup>31</sup> for expanding the field of application could also be introduced. Taken together, our  $\mu\text{FFE}$  based solvent exchanger offers a great opportunity for complex LOC and  $\mu\text{TAS}$  systems to integrate and combine downstream applications, such as cell-based bioanalytical modules as well as multistep synthesis where a solvent exchange is necessary.

### 3.6 Acknowledgments

This work was funded by the German Research Foundation [grant number: DFG, FOR 2177, RO 2652/1-1]. Impedance analyzer was funded by the Free State of Saxony (SMWK) and the European Union (EFRE) [grant number: 100185265].

### 3.7 References

1. Wang, J.; Pumera, M. *Anal. Chem.* 2003, 75, 341– 345 DOI: 10.1021/ac0205210
2. Temiz, Y.; Lovchik, R. D.; Kaigala, G. V.; Delamarche, E. *Microelectron. Eng.* 2015, 132, 156– 175 DOI: 10.1016/j.mee.2014.10.013
3. Wong, T. S.; Arnold, F. H.; Schwaneberg, U. *Biotechnol. Bioeng.* 2004, 85, 351– 358 DOI: 10.1002/bit.10896
4. Timm, M.; Saaby, L.; Moesby, L.; Hansen, E. W. *Cytotechnology* 2013, 65, 887– 894 DOI: 10.1007/s10616-012-9530-6
5. Hartman, R. L.; Naber, J. R.; Buchwald, S. L.; Jensen, K. F. *Angew. Chem., Int. Ed.* 2010, 49, 899– 903 DOI: 10.1002/anie.200904634
6. Noël, T.; Kuhn, S.; Musacchio, A. J.; Jensen, K. F.; Buchwald, S. L. *Angew. Chem., Int. Ed.* 2011, 50, 5943– 5946 DOI: 10.1002/anie.201101480
7. Castell, O. K.; Allender, C. J.; Barrow, D. A. *Lab Chip* 2009, 9, 388– 396 DOI: 10.1039/B806946H
8. Kolar, E.; Catthoor, R. P. R.; Kriel, F. H.; Sedev, R.; Middlemas, S.; Klier, E.; Hatch, G.; Priest, C. *Chem. Eng. Sci.* 2016, 148, 212– 218 DOI: 10.1016/j.ces.2016.04.009
9. Cvetkovic, B. Z.; Lade, O.; Marra, L.; Arima, V.; Rinaldi, R.; Dittrich, P. S. *RSC Adv.* 2012, 2, 11117– 11122 DOI: 10.1039/c2ra21876c
10. Timmer, B. H.; van Delft, K. M.; Olthuis, W.; Bergveld, P.; van den Berg, A. *Sens. Actuators, B* 2003, 91, 342– 346 DOI: 10.1016/S0925-4005(03)00108-4
11. Hibara, A.; Toshin, K.; Tsukahara, T.; Mawatari, K.; Kitamori, T. *Chem. Lett.* 2008, 37, 1064– 1065 DOI: 10.1246/cl.2008.1064
12. Lam, K. F.; Cao, E.; Sorensen, E.; Gavriilidis, A. *Lab Chip* 2011, 11, 1311– 1317 DOI: 10.1039/c0lc00428f

13. Benz, C.; Boomhoff, M.; Appun, J.; Schneider, C.; Belder, D. *Angew. Chem., Int. Ed.* 2015, 54, 2766– 2770 DOI: 10.1002/anie.201409663
14. Kohlheyer, D.; Besselink, G. A. J.; Schlautmann, S.; Schasfoort, R. B. M. *Lab Chip* 2006, 6, 374– 380 DOI: 10.1039/b514731j
15. Zhang, C.-X.; Manz, A. *Anal. Chem.* 2003, 75, 5759– 5766 DOI: 10.1021/ac0345190
16. Jezierski, S.; Gitlin, L.; Nagl, S.; Belder, D. *Anal. Bioanal. Chem.* 2011, 401, 2651– 2656 DOI: 10.1007/s00216-011-5351-2
17. Herzler, M.; Witteweg, M.; Pragst, F. *Toxichem. Krimtech.* 2002, 69, 13– 22
18. Zitzmann, F. D.; Jahnke, H.-G.; Nitschke, F.; Beck-Sickingler, A. G.; Abel, B.; Belder, D.; Robitzki, A. A. *Lab Chip* 2017, DOI: 10.1039/C7LC00754J
19. Weyer, M.; Jahnke, H.-G.; Krinke, D.; Zitzmann, F. D.; Hill, K.; Schaefer, M.; Robitzki, A. A. *Anal. Bioanal. Chem.* 2016, 408, 8529– 8538 DOI: 10.1007/s00216-016-9978-x
20. Bordallo, H. N.; Herwig, K. W.; Luther, B. M.; Levinger, N. E. *J. Chem. Phys.* 2004, 121, 12457– 12464 DOI: 10.1063/1.1823391
21. Henchoz, Y.; Bard, B.; Guilleme, D.; Carrupt, P.-A.; Veuthey, J.-L.; Martel, S. *Anal. Bioanal. Chem.* 2009, 394, 707– 729 DOI: 10.1007/s00216-009-2634-y
22. Doughty, M. J. *Ophthalmic Physiol. Opt.* 2010, 30, 167– 174 DOI: 10.1111/j.1475-1313.2009.00703.x
23. Fonslow, B. R.; Bowser, M. T. *Anal. Chem.* 2006, 78, 8236– 8244 DOI: 10.1021/ac0609778
24. Kohlheyer, D.; Eijkel, J. C. T.; van den Berg, A.; Schasfoort, R. B. M. *Electrophoresis* 2008, 29, 977– 993 DOI: 10.1002/elps.200700725
25. Galvao, J.; Davis, B.; Tilley, M.; Normando, E.; Duchon, M. R.; Cordeiro, M. F. *FASEB J.* 2014, 28, 1317– 1330 DOI: 10.1096/fj.13-235440
26. de Menorval, M.-A.; Mir, L. M.; Fernandez, M. L.; Reigada, R. *PLoS One* 2012, 7, e41733 DOI: 10.1371/journal.pone.0041733
27. Forman, S.; Kas, J.; Fini, F.; Steinberg, M.; Ruml, T. *J. Biochem. Mol. Toxicol.* 1999, 13, 11– 15 DOI: 10.1002/(SICI)1099-0461(1999)13:1<11::AID-JBT2>3.0.CO;2-R



- 
28. Pänke, O.; Weigel, W.; Schmidt, S.; Steude, A.; Robitzki, A. A. *Biosens. Bioelectron.* 2011, 26, 2376– 2382 DOI: 10.1016/j.bios.2010.10.015
  29. te Kamp, V.; Lindner, R.; Jahnke, H.-G.; Krinke, D.; Kostelnik, K. B.; Beck-Sickinger, A. G.; Robitzki, A. A. *Biosens. Bioelectron.* 2015, 67, 386– 393 DOI: 10.1016/j.bios.2014.08.066
  30. Jezierski, S.; Klein, A. S.; Benz, C.; Schaefer, M.; Nagl, S.; Belder, D. *Anal. Bioanal. Chem.* 2013, 405, 5381– 5386 DOI: 10.1007/s00216-013-6945-7
  31. Underberg, W. J M; Waterval, J. C M. *Electrophoresis* 2002, 23, 3922– 3933 DOI: 10.1002/elps.200290010

### 3.8 Supporting information

#### Fabrication of microelectrode arrays with integrated microfluidic structures

Microelectrode arrays (MEAs) were produced in a clean room by lift-off technique. In detail, cleaned glass substrates (Borofloat 49/49/1.1 mm, Goettgens Industriearmaturen, Germany) were spin-coated with 3  $\mu\text{m}$  negative resist (AR-N 4340, Allresist, Germany). After baking for 90 s at 95°C, the MEA layout was transferred to the substrate via photomask structure (10 s UV-light, 350 nm to 425 nm) and MA6 Mask Aligner (SÜSS MicroTec, Germany) and developed in AR 300-475 (Allresist GmbH, Germany). Electrodes were generated by direct current sputtering (CREAMET 500, CREAVAC GmbH, Germany) of 50 nm ITO ( $\text{In}_2\text{O}_3:\text{SnO}_2$ ) followed by 350 nm gold as adhesion layer. Subsequently remaining photoresist and metal deposition were removed and the MEA were passivated by a 1  $\mu\text{m}$  thick layer using negative photoresist SU8-2 (Micro Resist Technology, Germany). Finally MEAs were plasma-cleaned at 400 mA for 7 min in a vacuum chamber (CREAMET 500, CREAVAC GmbH).

The microfluidic structures on the MEAs were produced in the same manner like microfluidic free-flow electrophoresis ( $\mu\text{FFE}$ ) chips, whereby MEAs presented the basis plate. Light-impermeable photomasks (16000 dpi, Zitzmann GmbH, Eching, Germany) were used for structuring. The photopolymerization of PEG-DA was executed with an illumination time of 1.7 s.

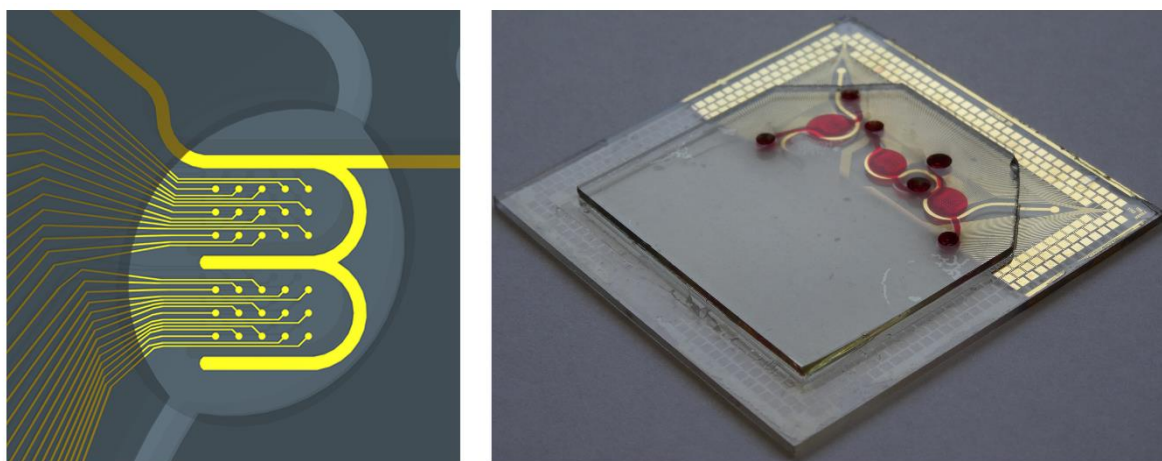


**Figure S 3.1: Microelectrode array with integrated microfluidic structures for impedimetric monitoring of cells.** The MEA comprises three cell cavities and 30 measurement electrodes (100  $\mu\text{m}$  diameter) and a W-shaped counter electrode per cavity. Cell cavities are marked red (filled with food coloring).

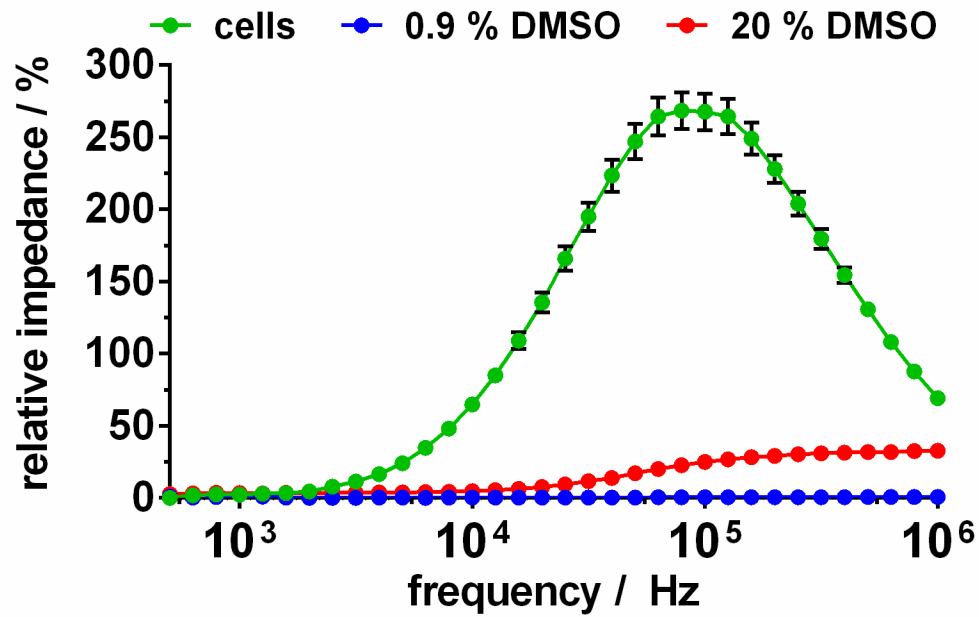


**Figure S 3.2: Relative impedance spectra of cells and solvent dilutions.** The calculation of the relative impedance from impedance spectra with cells relative to impedance spectra of cell culture medium reveals typical cell signal spectra with a maximum relative impedance in the range of 250-300%. Additionally, the relative impedance spectra for cell culture medium containing the investigated DMSO proportions revealed are shown. (n = 20 electrodes)

## Selbstständigkeitserklärung

Hiermit erkläre ich, dass ich die vorliegende Arbeit selbstständig und ohne unzulässige Hilfe oder Benutzung anderer als der angegebenen Hilfsmittel angefertigt habe und dass ich die aus fremden Quellen direkt oder indirekt übernommenen Gedanken in der Arbeit als solche kenntlich gemacht habe.

Ich versichere, dass Dritte von mir weder unmittelbar noch mittelbar geldwerte Leistungen für Arbeiten erhalten haben, die im Zusammenhang mit dem Inhalt der vorgelegten Dissertation stehen und dass die vorgelegte Arbeit weder im Inland noch im Ausland in gleicher oder ähnlicher Form einer anderen Prüfungsbehörde zum Zweck einer Promotion oder eines anderen Prüfungsverfahrens vorgelegt wurde.

Alles aus anderen Quellen und von anderen Personen übernommene Material, das in der Arbeit verwendet wurde oder auf das direkt Bezug genommen wird, wurde als solches kenntlich gemacht.

Leipzig, den 10.11.2020

.....

Franziska D. Zitzmann

## Danksagung

Ein Lab-on-a-Chip ist ein miniaturisiertes Gerät, das laut Definition in einem einzigen Chip die gesamte Funktionalität eines makroskopischen Labors inklusive Zulaufkanälen, Reaktionsbereichen und Detektionssensoren auf nur einem kreditkartengroßen Substrat unterbringt. Aber auch ein so in sich abgestimmtes analytisches System kann dabei nur durch den Support externer Prozesse erfolgreich sein. Auch diese Dissertation ist erst durch die Unterstützung zahlreicher Personen zu Stande gekommen. All denen möchte ich an dieser Stelle meinen Dank aussprechen.

Mit großer Liebe möchte ich mich bei meiner Familie bedanken - für das Verständnis wenig Zeit zu haben, für die ständige Unterstützung und die Kraft, für das immer wieder nach Hause kommen können um dort neue Energie zu tanken. Meinen Großeltern Klaus und Ingrid danke ich sehr dafür, dass sie mir bereits in jungen Jahren die Bedeutung von Bildung gelehrt haben und mich auf meinen persönlichen Bildungsweg immer unterstützt haben- sei es finanziell oder durch ein selbstgekochtes Mittagessen. Ich danke meinen Eltern von Herzen, dass ich bei euch die Ausdauer und Geduld gelernt habe, schwierige Projekte in Angriff zu nehmen und dabei das exakte Arbeiten (auch im Millimeterbereich) nicht zu vergessen.

Einen Dank der ganz besonderen Art widme ich Sabina Kanton, meiner langjährigen Wegbegleiterin während des Studiums und der Promotion. Ich danke dir für die zahlreichen wissenschaftlichen Diskussionen und den gemeinsamen Ideenaustausch, für deinen vorgelebten Ehrgeiz und für die gemeinsame Zeit. Darüber hinaus möchte ich mich bei Antje Opitz für die Korrekturen meiner deutschen Texte und die gute Freundschaft bedanken. Ein letztes Dankeschön gilt Max Vollmering für die neu entdeckte Kraft zum Fertigstellen meiner Promotion und für seine zahlreichen Korrekturhinweise.

Nicht zuletzt möchte ich den Menschen der Arbeitsgruppe „Molekularbiologisch-biochemische Prozesstechnik“ für die vielen Anregungen, fachkundigen Gespräche und die gute Zeit innerhalb und außerhalb des Labors danken. In der ereignisreichen Zeit sind Kollegen auch zu Freunden geworden. Besonderer Dank gilt Dr. Heinz-Georg Jahnke für seine stete Unterstützung bei wissenschaftlichen Fragestellungen, seinen fachlichen Ratschlägen jeglicher Art und sein zwischenmenschliches Feingefühl. Für die technische Unterstützung im Reinraum und für den einen oder anderen Ratschlag danke ich Sabine Schmidt. Ein spezieller Dank gilt meinen Bachelor- und Masterstudenten, die mir im Rahmen ihrer Abschlussarbeiten wertvolle Hilfe bei der Bearbeitung der wissenschaftlichen Fragestellungen geleistet haben.

Des Weiteren danke ich Prof. Dr. Detlev Belder und seinen Mitarbeitern, vor allem Dr. Simon Pfeiffer und Petra Gläser, für die gute Zusammenarbeit im DFG-Projekt.

Abschließend möchte ich mich bei Prof. Dr. Andrea A. Robitzki für die Betreuung dieser Dissertation bedanken. Erst durch die hervorragenden Arbeits- und Laborbedingungen konnte ich zahlreiche Methoden erlernen und damit wichtige wissenschaftliche Erfahrungen sammeln. Ebenso möchte ich mich bei ihr und Prof. Dr. Andreas Schober für die Übernahme der Gutachten bedanken.

## Author Contribution Statement I

**Free-flow electrophoresis and impedance spectroscopy of small molecular compounds in a microfluidic device**

---

**Titel: Cell-based biosensors for analyzing active compounds, their basics and conditions for miniaturization and the principles of miniaturized free-flow electrophoresis as new opportunities to remove solvents in cellular detection systems**

**Journal: Unpublished.**

**Autoren: Franziska D. Zitzmann**

---

### **Franziska D. Zitzmann**

- development of the idea and conception
- literature research
- wrote the review



---

Franziska D. Zitzmann

## Author Contribution Statement II

### Free-flow electrophoresis and impedance spectroscopy of small molecular compounds in a microfluidic device

---

**Titel:** A novel microfluidic microelectrode chip for a significantly enhanced monitoring of NPY receptor activation in live mode

**Journal:** Lab on Chip (2017), 17: 4294-4302.

**Autoren:** Franziska D. Zitzmann\*, Heinz-Georg Jahnke\*, Felix Nitschke, Annette G. Beck-Sickinger, Bernd Abel, Detlev Belder, Andrea A. Robitzki

\* contributed equally

---

#### **Franziska D. Zitzmann**

- design and fabrication of the microfluidic chips
- performed cell culture, microfluidic, fluorescence and impedance spectroscopy experiments
- analyzed, evaluated and interpreted the data
- wrote the publication

#### **Heinz-Georg Jahnke**

- performed FEM simulations
- developed software control for impedance spectroscopy
- analyzed data
- wrote and revised the manuscript

#### **Felix Nitschke**

- technical support for microfluidic chip fabrication and cell culture experiments

#### **Annette G. Beck-Sickinger**

- provided the Y1-vector for HEK293A cells
- revised the manuscript



**Bernd Abel:**

- support by FEM simulations
- revised the manuscript

**Detlev Belder:**

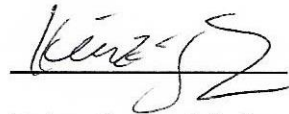
- project idea and work conception
- revised the manuscript

**Andrea A. Robitzki:**

- project idea and work conception
- project funding
- revised the manuscript



Franziska D. Zitzmann



Heinz-Georg Jahnke



Annette G. Beck-Sickinger



Bernd Abel



Detlev Belder



Andrea A. Robitzki

## Author Contribution Statement III

### Free-flow electrophoresis and impedance spectroscopy of small molecular compounds in a microfluidic device

---

**Titel: Microfluidic Free-Flow Electrophoresis Based Solvent Exchanger for Continuously Operating Lab-on-Chip Applications**

**Journal:** Analytical Chemistry (2017), 89 (24), pp 13550–13558

**Autoren:** Franziska D. Zitzmann\*, Heinz-Georg Jahnke\*, Simon A. Pfeiffer, Ronny Frank, Felix Nitschke, Laura Mauritz, Bernd Abel, Detlev Belder, Andrea A. Robitzki

\* contributed equally

---

#### **Franziska D. Zitzmann**

- development of methodology
- designed, planned and performed experiments
- fabrication of the microfluidic free-flow electrophoresis chips and the impedimetric chips
- performed cell culture, microfluidic and impedance spectroscopy experiments
- analyzed, evaluated and interpreted the data with statistic
- wrote the publication

#### **Heinz-Georg Jahnke**

- performed FEM simulations
- developed software control for impedance spectroscopy
- analyzed data
- revised the manuscript

#### **Simon A. Pfeiffer**

- performed fluorescein concentration determination
- revised the manuscript

#### **Ronny Frank**

- literature research for introduction
- revised the manuscript

**Felix Nitschke**

- technical support for microfluidic chip fabrication and cell culture experiments

**Laura Mauritz**

- performed DMSO concentration determination

**Bernd Abel:**

- support by FEM simulations
- revised the manuscript

**Detlev Belder:**

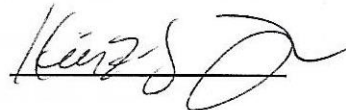
- project idea and work conception
- revised the manuscript

**Andrea A. Robitzki:**

- project idea and work conception
- project funding
- revised the manuscript



Franziska D. Zitzmann



Heinz-Georg Jahnke



Bernd Abel



Detlev Belder



Andrea A. Robitzki